5-2017

Total N-nitrosamine Precursor Adsorption with Carbon Nanotubes: Elucidating Controlling Physiochemical Properties and Developing a Size-Resolved Precursor Surrogate

Erin Needham
University of Arkansas, Fayetteville

Total *N*-nitrosamine Precursor Adsorption with Carbon Nanotubes: Elucidating Controlling Physiochemical Properties and Developing a Size-Resolved Precursor Surrogate

A dissertation submitted in partial fulfillment
of the requirements for the degree of
Doctorate of Philosophy in Civil Engineering

by

Erin Michelle Needham
University of Arkansas
Bachelor of Science in Civil Engineering, 2013

May 2017
University of Arkansas

This dissertation is approved for recommendation to the Graduate Council.

_____
Dr. Julian Fairey
Dissertation Director

_____
Dr. Wen Zhang
Committee Member

_____
Dr. David Miller
Committee Member

_____
Dr. Justin Chimka
Committee Member

Abstract

As drinking water sources become increasingly impaired with nutrients and wastewater treatment plant (WWTP) effluent, formation of disinfection byproducts (DBPs) – such as trihalomethanes (THMs), dihaloacetonitriles (DHANs), and *N*-nitrosamines – during water treatment may also increase. *N*-nitrosamines may comprise the bulk of the chronic toxicity in treated drinking waters despite forming at low ng/L levels. This research seeks to elucidate physicochemical properties of carbon nanotubes (CNTs) for removal of DBP precursors, with an emphasis on total *N*-nitrosamines (TONO).

Batch experiments with CNTs were completed to assess adsorption of THM, DHAN, and TONO precursors; physiochemical properties of CNTs were quantified through gas adsorption isotherms and x-ray photoelectron spectroscopy. Numerical modeling was used to elucidate characteristics of CNTs controlling DBP precursor adsorption. Multivariate models developed with unmodified CNTs revealed that surface carboxyl groups and, for TONO precursors, cumulative pore volume (CPV), controlled DBP precursor adsorption. Models developed with modified CNTs revealed that specific surface area controlled adsorption of THM and DHAN precursors while CPV and surface oxygen content were significant for adsorption of TONO precursors.

While surrogates of THM and DHAN precursors leverage metrics from UV absorbance and fluorescence spectroscopy, a TONO precursor surrogate has proved elusive. This is important as measurements of TONO formation potential (TONOFP) require large sample volumes and long processing times, which impairs development of treatment processes. TONO precursor surrogates were developed using samples that had undergone oxidative or sorption treatments. Precursors were analyzed with asymmetric flow field-flow fractionation (AF4) with

inline fluorescence detection (FLD) and whole water fluorescence excitation-emission matrices (EEMs). TONO precursor surrogates were discovered, capable of predicting changes in TONOFP in WWTP samples that have undergone oxidation ($R^2 = 0.996$) and sorption ($R^2 = 0.576$). Importantly, both surrogates only require just 2 mL of sample volume to measure and take only 1 hour. Application of the sorption precursor surrogate revealed that DBP precursor adsorption was feasible with freeform CNT microstructures with various dimensions and surface chemistries, establishing a framework for development of this novel CNT application for drinking water treatment.

Acknowledgements

I would like to thank my husband along with my family and friends for their encouragement and unwavering support. I would also like to acknowledge my dissertation director and committee members for their guidance. Financial support from the National Science Foundation (CBET #1254350 to Julian Fairey) and the University of Arkansas Graduate School Doctoral Academy Fellowship is gratefully acknowledged.

Table of Contents

Chapter 1: Introduction 1

1. Problem Statement 2

2. Objectives and Approach 5

    2.1. Objective 1 5

    2.2. Objective 2 5

    2.3. Objective 3 6

3. Document Organization 6

4. References 8

Chapter 2: Trihalomethane, Dihaloacetonitrile, and Total *N*-nitrosamine Precursor Adsorption by Carbon Nanotubes: The Importance of Surface Oxides and Pore Volume 10

Abstract 11

1. Introduction 12

2. Materials and Methods 15

    2.1. Site Description and Sample Collection 15

    2.2. Experimental Procedures 16

        2.2.1. Bottle-Point Isotherms 16

        2.2.2. DBPFP 17

        2.2.3. CNT Characterization 18

        2.2.4. Data Modeling 19

3. Results and Discussion 20

    3.1. DBP Precursor Adsorption by CNTs 20

    3.2. CNT Characterization 22

3.3. Impacts of Physiochemical CNT Properties on DBP Precursor Adsorption.....23
3.4. Fluorescence Metrics as DBP Precursor Surrogates 26
3.5. Implications 27
4. Conclusions.....28
5. Associated Content 30
6. Figures and Tables 31
7. References.....37
Appendix 1: Supplementary Information for "Trihalomethane, Dihaloacetonitrile, and Total *N*-nitrosamine Precursor Adsorption by Carbon Nanotubes: The Importance of Surface Oxides and Pore Volume".....45
Chapter 3: Revealing a Size-Resolved Fluorescence-Based Metric to Track Oxidative Treatment of Total *N*-nitrosamine Precursors in Wastewater-Derived Waters.....76
Abstract.....77
1. Introduction.....78
2. Materials and Methods.....79
2.1. Sample Description and Water Quality Measurements.....79
2.2. Experimental Procedures.....80
2.2.1. DBPFP.....80
2.2.2. AF4-FLD Fractograms.....81
2.3. AF4-FLD Processing.....82
2.4. Model Development 82
3. Results and Discussion 83
3.1. AF4-FLD 83

3.2. Model Development 84
3.3. Implications 86
4. Associated Content 87
5. Figures and Tables 88
6. References 91
Appendix 2: Supplementary Information for "Revealing a Size-Resolved Fluorescence-Based Metric to Track Oxidative Treatment of Total *N*-nitrosamine Precursors in Wastewater-Derived Waters" 94
Chapter 4: Trihalomethane, Dihaloacetonitrile, and Total *N*-nitrosamine Precursor Adsorption by Modified Carbon Nanotubes (CNTs) and Freeform CNT Microstructures....115
Abstract 116
1. Introduction 117
2. Materials and Methods 120
2.1. Site Description and Sample Collection 120
2.2. Batch Adsorbent Selection 120
2.3. Characterizations of Pattered CNT Forests 121
2.4. Experimental Procedures 122
2.4.1. Bottle-point Isotherms 122
2.4.2. DBPFP 122
2.4.3. Continuous Flow Experiments with CNT Mats 123
2.4.4. AF4-FLD 123
2.4.5. Fluorescence EEMs 124
2.5. Data Modeling 124

3. Results and Discussion 125

3.1. Batch Adsorption Models 125

3.2. TONO Precursor Surrogate Development 128

3.3. Continuous Flow CNT Mat Testing 129

4. Conclusions 131

5. Associated Content 133

6. Figures and Tables 134

7. References 141

Appendix 3: Supplementary Information for "Trihalomethane, Dihaloacetonitrile, and Total *N*-nitrosamine Precursor Adsorption by Modified Carbon Nanotubes (CNTs) and Freeform CNT Microstructures" 144

Chapter 5: Conclusion 155

1. Summary 156

2. Significance and Future Work 157

List of Published Papers

Chapter 2

Needham, E. M., Sidney, S. M., Chimka, J. R., and Fairey, J. L., 2016. Trihalomethane, dihaloacetonitrile, and total *N*-nitrosamine precursor adsorption by carbon nanotubes: the importance of surface oxides and pore volume. Environmental Science: Water Research and Technology, 2 (6), 1004-1013.

Chapter 3

Needham, E. M., A. M. Fernandez de Luis, J. R. Chimka, and J. L. Fairey, 2017. Revealing a size-resolved fluorescence-based metric to track oxidative treatment of total *N*-nitrosamine precursors in wastewater-derived waters. Environmental Science & Technology Letters, In Revision.

Chapter 4

Needham, E. M., J. R. Chimka, and J. L. Fairey, 2017. Trihalomethane, dihaloacetonitrile, and total *N*-nitrosamine precursor adsorption by modified carbon nanotubes (CNTs) and freeform CNT microstructures. Environmental Science: Water Research and Technology, In Progress.

Chapter 1

Introduction

1. Problem Statement

The formation of disinfection byproducts (DBPs) in drinking water systems has been studied since the 1970s but remains an ongoing regulatory compliance issue throughout the United States. For example, in 2014, the Beaver Water District (Lowell, AR) switched primary disinfectants primarily for DBP control – the capital cost of this project cost was $5.2 million and the operating cost is $1.0 million annually (HagenBurger, 2017). Halogenated DBPs such as trihalomethanes (THMs) and dihaloacetonitriles (DHANs) form through reactions between natural organic matter (NOM) present in the source water and disinfectants, such as free chlorine or chloramines. THMs are regulated under the Stage 2 Disinfectants/Disinfection Byproduct (D/DBP) Rule because of widespread occurrence in chlorinated or chloraminated drinking water and potential carcinogenicity. While DHANs are not regulated, their formation is also widespread and these DBPs are more toxic than some regulated DBPs (Muellner et al., 2007). As a result, the control of many non-regulated DBPs is an active area of research, in particular for compounds with high toxicity and widespread occurrence.

DBP formation upon disinfection can be fomented by source water impairment. For instance, drinking water sources enriched with nutrients (nitrogen and phosphorus) can undergo eutrophication (Schindler, 1974), which leads to the formation of algal organic matter (AOM); similarly, wastewater treatment plant (WWTP) effluents contain effluent organic matter (EfOM) (Sirivedhin and Gray, 2005). AOM and EfOM contain labile chemical moieties which, upon chloramination, can result in the formation of THMs, DHANs, and *N*-Nitrosamines (Krasner et al., 2013), the latter being a non-regulated group of DBPs that form at low $ng \cdot L^{-1}$ levels but may nevertheless comprise the bulk of the chronic toxicity exerted by treated drinking waters (Hrudey and Charrois, 2012). Although *N*-Nitrosodimethylamine (NDMA) is the most commonly

occurring *N*-nitrosamine in drinking water systems (Russell et al., 2012), Dai and Mitch (2013) showed that NDMA comprised just 5% of total *N*-Nitrosamines (TONO). As source waters become less pristine (i.e., continued enrichment with AOM and EfOM), development of processes for enhanced DBP precursor removal could help drinking water treatment plants (DWTPs) continue to meet regulatory requirements and decrease the toxicity of their finished water.

Carbon nanotubes (CNTs) have not been used in conventional DWTPs but have the potential to be used for adsorption of DBP precursors. CNTs have a structure similar to a rolled graphene sheet and possess high specific surface area. Because of the lack of bulk carbon in CNTs, their surface properties such as size, shape, texture, defects, and functionalities can be manipulated for desired applications. Others have observed that CNTs show an affinity for various NOM fractions in water (Wang et al., 2009; Yang and Xing, 2009), but these investigations were intended to minimize NOM uptake by CNTs in favor of adsorption of other target compounds. No existing work to date has explored the ability of CNTs to simultaneously remove THM, DHAN, and TONO precursors from natural waters.

Though CNT toxicity (Liu et al., 2013; Das et al., 2014) is a concern in drinking water treatment, particularly with respect to fate and transport of toxic substances related to CNTs (Yang and Xing, 2009), several attached growth technologies now exist to grow CNTs on various substrates or to incorporate CNTs into membrane filtration systems (De Volder et al., 2014). These options could be valuable in addressing issues with CNT toxicity. In particular, freeform CNT microstructures can be grown on silicon substrates in various shapes and sizes. Provided the physical and chemical properties of CNTs can be tuned to make CNTs a promising

sorbent for DBP precursors, these application methods can be developed to further the goal of enhanced DBP precursor removal in DWTPs.

TONO formation in drinking water systems is of particular interest as formation of these compounds is expected to increase in the coming years as source waters become less pristine and more utilities switch to chloramines to comply with the Stage 2 D/DBP rule to achieve adequate control of regulated DBPs. Additionally, drinking water TONO research was initiated relatively recently (i.e., the first publication on the subject appeared in 2010 by Mitch and colleagues), so strategies to curb TONO formation and measure TONO itself are in the developmental stage.

Spectroscopic DBP precursor surrogates provide estimates of precursor concentrations and are often developed in conjunction with DBP formation potential (DBPFP) tests. Such surrogates can be used to assess the effectiveness of treatment processes targeting removal of DBP precursors and can reduce (or even eliminate) the need for time-consuming DBPFP measurements. Metrics from fluorescence excitation-emission matrices (EEMs) have been shown to be strong precursor surrogates for total THMs (TTHMs) (Pifer and Fairey, 2014) and dihaloacetonitriles (DHANs) (Do et al., 2015). One goal of this study is to expand on past analysis techniques such as parallel factor analysis (PARAFAC) for fluorescence EEMs (Stedmon and Bro, 2008) and use asymmetric flow-field flow fractionation (AF4) with inline fluorescence detection (AF4-FLD) to develop a precursor surrogate for TONO. The use of AF4 allows for size-based separation of natural organic matter (NOM) prior to fluorescence measurement and is potentially useful for a higher resolution characterization of protein-like (i.e., organic nitrogen containing) DBP precursors that may be obscured in traditional fluorescence EEMs. Notably, the AF4-FLD measurement utilizes small sample volumes (i.e., 0.5 mL), which allows for flexibility in the design of lab-scale treatment processes.

This dissertation focuses on (1) methodological improvements to the TONO quantification procedure and data analysis techniques (2) development of a novel characterization technique for TONO precursors, (3) assessment of TONO precursor removal by CNTs in competitive adsorption systems with concomitant THM- and DHAN precursor removal, and (4) elucidation of physicochemical CNTs properties that control DBP precursor adsorption.

2. Objectives and Approach

2.1. Objective 1

The first objective of this research is to assess multiple types of CNTs for DBP precursor adsorption and identify the controlling physicochemical CNT properties. Nine types of CNTs were selected with a wide range of physicochemical characteristics and used in batch experiments to assess adsorption of TTHM, DHAN, and TONO precursors. In separate experiments, each CNT type was characterized physically by gas adsorption isotherms and chemically by x-ray photoelectron spectroscopy (XPS). Thus, the performance of the nine CNT types relative to each other and relative to other common adsorbents (such as activated carbon) can be established. The controlling physicochemical CNT properties identified will be used to guide rational selection of CNT types to maximize DBP precursor adsorption in continuous flow packed-bed column experiments.

2.2. Objective 2

The second objective of this research is to develop a TONO precursor surrogate using fluorescence EEMs and AF4-FLD. The focus of TONO method development will be on improved QA/QC practices that account for NDMA recovery in the standard curve and reaction chamber degradation over the course of a sample set. The goal of the AF4-FLD method development is to establish a procedure to separate and size (i.e., determine the approximate

molecular weight) protein-like organics in waters containing EfOM and AOM. Metrics from fluorescence EEMs and AF4-FLD will be assessed as a TONO precursor surrogate in waters treated by oxidation (i.e., chlorine, ozone, and UV disinfection) and sorption (i.e., CNTs and activated carbon).

2.3. Objective 3

The third objective of this research is to assess CNTs selected based on desirable physicochemical properties identified in Objective 1 for enhanced removal of TONO precursors. Assessments occurred in batch reactors and CNTs were characterized by gas adsorption isotherms and XPS. Hypotheses regarding physicochemical CNT properties and DBP precursor adsorption will be developed further to formulate a rational framework for optimizing CNTs. Additionally, to address fate and toxicity concerns regarding CNTs, freeform CNT microstructures grown on a silicon substrate were assessed in continuous flow studies in terms of sorption of THM, DHAN, and TONO precursors.

3. Document Organization

Chapter 2 addresses Objective 1 and details the batch application of nine types of CNTs for DBP precursor removal. These results demonstrated that CNTs have natural affinity for TTHM, DHAN, and TONO precursors. Unexpectedly, CNTs had the highest affinity for TONO precursors, which were thought to be the least hydrophobic, a result that is encouraging for targeted removal for these compounds. Chapter 2 also includes results from the physical and chemical CNT analyses and numerical models aimed at identifying control CNT properties for DBP precursor adsorption.

Chapter 3 addresses Objective 2. An AF4-FLD method was developed that can distinguish between water types enriched with EfOM in terms of NOM size and chemistry.

Metrics from this novel AF4-FLD method were used in conjunction with corresponding TONOFP data and to develop a TONO precursor surrogate. The resultant surrogate can be leveraged to develop and optimize treatment processes to curb *N*-nitrosamines in drinking water systems. Additionally, several improvements were made to TONO measurement QA/QC practices including the application of the solid phase extraction process to the standard curve (i.e., the same process as applied to the samples) and progress in accounting for degradation of the TONO reaction chamber.

Chapter 4 addresses Objective 3, which leveraged the controlling physical and chemical CNT characteristics identified in Chapter 2 to select several types of CNTs for enhanced TTHM, DHAN, and TONO precursor removal. Batch experiments with CNTs were analyzed and numerical models were developed to assess the impact of sorbent physical and chemical properties on the sorption of DBP precursors, with an emphasis on TONO. A separate TONO precursor surrogate was developed using the data from batch sorption tests in combination with the novel AF4-FLD method developed in Chapter 3 and applied to assess the performance of CNT microstructures grown on mats (De Volder et al., 2014) in a continuous flow setting.

4. References

Dai, N. and Mitch, W. A., 2013. Relative importance of N-nitrosodimethylamine compared to total N-nitrosamines in drinking waters. Environmental Science & Technology 47 (8), 3648-3656.

Das, R., Hamid, S. B. A., Ali, M. E., Ismail, A. F., Annuar, M. S. M. and Ramakrishna, S., 2014. Multifunctional carbon nanotubes in water treatment: The present, past and future. Desalination 354, 160-179.

De Volder, M., Park, S., Tawfick, S. and Hart, A. J., 2014. Strain-engineered manufacturing of freeform carbon nanotube microstructures. Nature Communications 5.

Do, T. D., Chimka, J. R. and Fairey, J. L., 2015. Improved (and singular) disinfectant protocol for indirectly assessing organic precursor concentrations of trihalomethanes and dihaloacetonitriles. Environmental Science & Technology 49 (16), 9858-9865.

HagenBurger, B. (2017). Personal Communication with J. L. Fairey on Cost of chlorine dioxide feed system at the Beaver Water District.

Hrudey, S. E. and Charrois, J. W. A., Eds. (2012). Disinfection by-products and human health. IWA Publishing and Australian Water Association, London.

Krasner, S. W., Mitch, W. A., McCurry, D. L., Hanigan, D. and Westerhoff, P., 2013. Formation, precursors, control, and occurrence of nitrosamines in drinking water: A review. Water Research 47 (13), 4433-4450.

Liu, Y., Zhao, Y., Sun, B. and Chen, C., 2013. Understanding the toxicity of carbon nanotubes. Accounts of Chemical Research 46 (3), 702-713.

Muellner, M. G., Wagner, E. D., McCalla, K., Richardson, S. D., Woo, Y. T. and Plewa, M. J., 2007. Haloacetonitriles vs. regulated haloacetic acids: are nitrogen-containing DBPs more toxic? Environmental Science & Technology 41 (2), 645-651.

Pifer, A. D. and Fairey, J. L., 2014. Suitability of organic matter surrogates to predict trihalomethane formation in drinking water sources. Environmental Engineering Science 31 (3), 117-126.

Russell, C. G., Blute, N. K., Via, S., Wu, X. and Chowdhury, Z., 2012. National assessment of nitrosamine occurrence and trends. Journal American Water Works Association 104 (3), E205-E217.

Schindler, D. W., 1974. Eutrophication and recovery in experimental lake - Implications for lake management. Science 184 (4139), 897-899.

Sirivedhin, T. and Gray, K. A., 2005. 2. Comparison of the disinfection by-product formation potentials between a wastewater effluent and surface waters. Water Research 39 (6), 1025-1036.

Stedmon, C. A. and Bro, R., 2008. Characterizing dissolved organic matter fluorescence with parallel factor analysis: a tutorial. Limnology and Oceanography-Methods 6, 572-579.

Wang, X., Tao, S. and Xing, B., 2009. Sorption and competition of aromatic compounds and humic acid on multiwalled carbon nanotubes. Environmental Science & Technology 43 (16), 6214-6219.

Yang, K. and Xing, B., 2009. Adsorption of fulvic acid by carbon nanotubes from water. Environmental Pollution 157 (4), 1095-1100.

Chapter 2

Trihalomethane, Dihaloacetonitrile, and Total *N*-nitrosamine Precursor Adsorption by Carbon Nanotubes: The Importance of Surface Oxides and Pore Volume

Abstract

As drinking water sources become increasingly impaired, enhanced removal of natural organic matter (NOM) may be required to curb formation of disinfection byproducts (DBPs) upon chlor(am)ination. While carbon nanotubes (CNTs) can adsorb NOM, their properties for DBP precursor adsorption have not been elucidated. Nine types of CNTs were assessed for trihalomethane (THM), dihaloacetonitrile (DHAN), and total *N*-nitrosamine (TONO) precursor adsorption. Batch isotherm experiments were completed with lake water and, to simulate an impaired condition, effluent from a wastewater treatment plant (WWTP). Adsorption varied with CNT type and dose, with TONO precursors having the highest percent removals from WWTP effluent (up to 97%). Physicochemical properties of CNTs were characterized by gas adsorption isotherms and x-ray photoelectron spectroscopy and numerical models were developed to identify CNT properties driving DBP precursor adsorption. The models fits were strong ($R^2 > 0.92$) and indicated removal of the three precursor types increased with percent carboxyl groups ($p < 0.01$) and, for TONO precursors only, cumulative pore volume (CPV, $p = 0.001$). A multicollinearity analysis suggested surface oxides – particularly carboxyl groups – on the CNTs increased CPV, presumably by increasing electrostatic repulsive forces, which enhanced microporosity sufficiently to overshadow any repulsion of DBP precursors from negatively charged surface oxides. A size exclusion analysis revealed all CNT pores were accessible to TONO precursors, while THM and DHAN precursors had limited access to the smaller micropores. These findings provide a framework to modify CNTs to optimize adsorption of DBP precursors and demonstrate the potential of CNTs for TONO precursor removal.

1. Introduction

The tunable physicochemical properties of carbon nanotubes (CNTs) (Tawfick et al., 2012; De Volder et al., 2014) have the potential to be exploited in drinking water treatment plants (DWTPs) to adsorb organic precursors of disinfection byproducts (DBPs). While CNT toxicity (Liu et al., 2013; Das et al., 2014) is a concern in water treatment, the technology is now available to grow CNTs on various substrates as well as to incorporate CNTs into membrane filtration systems (De Volder et al., 2014). This may alleviate problems associated with fate and transport of toxic substances related to CNTs (Yang and Xing, 2009) in drinking waters. However, before CNT-based attached growth or membrane applications can be developed specifically to enhance DBP precursor removal, fundamental investigations are needed to quantify the affinity of CNTs for important groups of DBP precursors and elucidate the physiochemical properties primarily responsible for their adsorption.

It is well known that natural organic matter (NOM) in source water reacts with disinfectants (i.e., free chlorine or chloramines) to form DBPs at low $\mu g \cdot L^{-1}$ levels, such as trihalomethanes (THMs) (Rook, 1976) and dihaloacetonitriles (DHANs) (Krasner et al., 2006). In waters enriched with algal organic matter or impacted by wastewater treatment plant (WWTP) effluents, *N*-nitrosamines can also form, albeit at low $ng \cdot L^{-1}$ levels (Krasner et al., 2013). *N*-nitrosamines are a non-halogenated group of DBPs under consideration for regulation in drinking waters due to their high toxicity (Hrudey and Charrois, 2012). While the majority of *N*-nitrosamine research to date has focused on *N*-nitrosodimethylamine (NDMA) due to its prevalence in drinking water systems (Russell et al., 2012), recent studies have demonstrated NDMA may only comprise ~5% of total *N*-nitrosamines (TONO) in chloramine systems (Dai and Mitch, 2013). As such, relatively little is known about the removal of TONO precursors by

engineered sorbents, although a recent study demonstrated that they have some affinity for activated carbon (Dai et al., 2012). Further, the authors are aware of no studies that have assessed the concomitant removal of THM, DHAN, and TONO precursors in sorption processes. With respect to CNTs, other researchers have demonstrated their affinity for various NOM fractions in water (Wang et al., 2009; Yang and Xing, 2009), although these investigations were geared towards minimizing NOM uptake by CNTs to maximize adsorption of other target compounds. Regardless, development of novel sorbents with enhanced affinities for organic DBP precursors could potentially be leveraged to curb DBP formation in finished drinking waters, regardless of the disinfection scheme used.

As DBP measurements are time- and labor-intensive, reliable DBP precursor surrogate measures can be valuable screening tools to assess treatment. Previous studies by this research group have demonstrated metrics from fluorescence excitation-emission matrices (EEMs) collected before and after treatment but prior to chlor(am)ination were strong total THM (TTHM) precursor surrogates (Pifer and Fairey, 2014). In these studies, the EEMs were decomposed by parallel factor analysis (PARAFAC) to identify principal fluorophore groups (Stedmon and Bro, 2008). The corresponding maximum intensity values, F_{MAX}, of humic- and fulvic-like fluorophores correlated strongly with TTHM precursor concentrations. A more recent study found strong correlations between fluorescence intensity values from peak-picking (i.e., excitation-emission pairs, $I_{Ex/Em}$) and removal of TTHM and DHAN precursors (Do et al., 2015). There is, however, a strong basis for why fluorescence may be useful as a TONO precursor surrogate. For example, in contrast to EPA Method 521 *N*-nitrosamines, algal-derived organic matter is a strong precursor to uncharacterized *N*-nitrosamines measured by the TONO assay (Krasner et al., 2013). Additionally, Liao and colleagues found strong correlations between the

removal of NA9FP – the sum of the FP of the six N-nitrosamines regulated under the UCMR2 along with *N*-nitrosomorpholine, *N*-nitrosopiperidine, and *N*-nitrosodiphenylamine – and the regions of a fluorescence EEM associated with aromatic proteins (R = 0.88) and soluble microbial products (R = 0.90) (Liao et al., 2014). Aromatic proteins are nitrogen-containing and *N*-nitrosamine precursors can be present as functional groups, while soluble microbial products have been identified as an NDMA precursor (Krasner et al., 2013). In essence, secondary, tertiary, and quaternary amines may not fluoresce themselves but may be associated with compounds that do so. Coupled with the labor-intensive nature of TONOFP tests, a fluorescence-based TONO precursor surrogate would advance development of control measures for these DBPs.

Given that the structure of CNTs is equivalent to that of a rolled graphene sheet, their physicochemical properties dictate their functionality. CNTs can be produced in single-walled (SW) and multi-walled (MW) varieties, both of which have high specific surface area and range in hydrophobicity (Wang et al., 2009; Yang and Xing, 2009), size (Balasubramanian and Burghard, 2005), shape (De Volder et al., 2014), texture (Birch et al., 2013), defects (Shih and Li, 2008), and functionalities (Cho et al., 2008), all of which can be manipulated for their intended application. The ability to fine-tune CNT properties is an attractive option for use as a sorbent in drinking water treatment, but it is not yet known what properties are desirable for DBP precursor removal. Adsorption by CNTs is based on accessible surface area, which includes aggregated pores and large external surface area, in contrast to activated carbon, which preferentially adsorbs lower molecular weight compounds due to size exclusion from micropores. CNTs have been shown to have high adsorption capacities for organic contaminants (Ren et al., 2011) and to

outperform other microporous adsorbents in competitive adsorption systems (Upadhyayula et al., 2009).

The objective of this study is to assess physicochemical CNT properties for enhanced TTHM-, DHAN-, and TONO-precursor adsorption. Nine commercially available CNTs were selected with a variety of characteristics and used in batch isotherm tests with two diverse water sources – a well-characterized lake water (Sen et al., 2007) that serves as a drinking water source and an effluent from a conventional WWTP. The TTHM-, DHAN-, and TONO-precursor concentrations in the raw and CNT-treated waters were indirectly measured using a recently verified DBP formation potential (DBPFP) test (Do et al., 2015), modified from Standard Methods 5710-B and D (Eaton, 2005). Each CNT type was characterized physically by gas adsorption isotherms to determine their specific surface area and pore volume distributions, and chemically by x-ray photoelectron spectroscopy (XPS) to determine the relative composition of surface functional groups. These physicochemical properties were used as primary variables in models to assess the adsorption of TTHM-, DHAN-, and TONO-precursors. Modeling results revealed strong correlations between CNT properties and removal of all three DBP precursor types. The findings of this study provide guidance for selective modification of CNTs for enhanced DBP precursor adsorption.

2. Materials and Methods

2.1. Site Description and Sample Collection

Waters used for the isotherm experiments originated from Beaver Lake, the drinking water source for Northwest Arkansas, and the West Side Wastewater Treatment Plant (WS-EFF) in Fayetteville, AR. Beaver Lake water (BL-RAW) was collected at the intake structure of the Beaver Water District DWTP (Lowell, AR) on July 7, 2014. Details on the land use and nutrient

inputs in the Beaver Lake watershed can be found elsewhere (Sen et al., 2007). WS-EFF samples were collected June 6, 2014 from the WWTP effluent. The plant utilizes biological nutrient removal, depth filtration, and ultraviolet disinfection with effluent aeration prior to discharge. Raw water characteristics are detailed in Table S1. Both waters were stored in 50-L low-density polyethylene carboys at 4 °C in the dark prior to use in the isotherm experiments.

2.2. Experimental Procedures

2.2.1. Bottle-Point Isotherms

Bottle-point isotherms were conducted with nine types of commercially available CNTs, selected to cover a range of wall type (SW and MW), diameter, and length (Table S2). CNTs were added to the sample waters at doses of 0-, 25- and 50 $mg \cdot L^{-1}$, in triplicate, in 1.25 L headspace-free amber glass bottles and were tumbled end-over-end for 3 days. Lu et al. (2007) showed that 4 hours was sufficient to reach equilibrium in a bottle-point isotherm study with MWCNTs and NOM-spiked waters. An equilibrium time of 3 days (i.e., 18 times longer) was chosen in this study and assumed to be a sufficient equilibration period for all precursors given the diversity of DBP precursors in the sample waters, including those for TONO for which little characterization information exists. The pH drift during the 3 days of tumbling was less than 0.1 pH unit from the initial values reported in Table S1. CNT doses were chosen to achieve less than 100% removal based on preliminary TTHMFP and DHANFP removal tests, the results of which are detailed in Table S3. It is important to note that the goal of this study does not include determination of the required CNT doses at a DWTP; rather, this study is intended identify CNT properties for enhanced DBP precursor adsorption and future studies will focus on development of an optimized CNT type and application mode. Following tumbling, BL-RAW samples were filtered through pre-rinsed 0.45-μm polyethersulfone (PES) membranes (Karanfil et al., 2003).

The WS-EFF samples were passed through pre-rinsed 0.7-µm glass fiber filters prior to 0.45-µm PES filtration, as direct filtration with the PES membranes was impractically slow. In both cases, filtration removed all CNTs from the water samples, which was confirmed by the lower chlorine residuals (or higher demand) of the blank relative to the CNT-treated waters (Table S4). Methods used for measuring dissolved organic carbon (DOC) and fluorescence EEMs, and performing PARAFAC analysis are in the Supplementary Information (SI) in Appendix 1.

2.2.2. DBPFP

The procedure developed by Do et al. (2015) was used to assess the DBPFP of untreated waters (i.e., samples not exposed to CNTs) and CNT-treated waters and is detailed in the SI. EPA Method 551.1 with modifications (Pifer and Fairey, 2012) was used to extract TTHMs and DHANs into *n*-pentane. A gas chromatograph equipped with an electron capture detector (GC-ECD, Shimadzu 2010) was used to quantify TTHMFP (the sum of trichloromethane, dichlorobromomethane, dibromochloromethane, and tribromomethane formation potential) and DHANFP (the sum of dichloroacetonitrile, bromochloroacetonitrile, and dibromoacetonitrile formation potential). Details regarding the GC standard curve are provided in the SI. Blanks and check standards complied with EPA Method 551.1.

Assessment of total *N*-nitrosamine formation potential (TONOFP) began with a modified SPE procedure from EPA Method 521, adapted from Kulshrestha et al. (2010). SPE columns were conditioned with methanol and Milli-Q water, and then 500 mL sample aliquots were pulled through the columns at a flow rate of 5 $mL \cdot min^{-1}$. Following 10 minutes of column aspiration, *N*-nitrosamines were eluted from the SPE columns using 12 mL of methanol. All remaining water was removed from the column extracts using a sodium sulfate drying column rinsed with an additional 3 mL of methanol; leached sodium sulfate was subsequently removed

with a 0.2 μm nominal pore size polytetrafluoroethylene syringe filter. Samples were concentrated to 1 mL in a 37 °C water bath using an evaporator with ultra high purity nitrogen gas and stored at -20 °C. To eliminate potential interferences, *S*-nitrosothiols and nitrite, if present, were quenched immediately before TONO measurement from sample extracts with 20 $g \cdot L^{-1}$ mercuric chloride in Milli-Q water and 50 $g \cdot L^{-1}$ sulfanilamide in 1 N HCl, respectively. Notably, ion chromatography results (Table S1) indicated no nitrite in raw waters (method detection limit, MDL = 0.008 $mg \cdot L^{-1}$). An Eco Physics CLD 88sp chemiluminescence NO detector was used to quantify *N*-nitrosamines in purified samples, as detailed in Mitch and Dai. (2012) TONO concentrations were determined using a five-point NDMA standard curve, which was rerun after every four samples to account for sample mass recoveries. To prevent sample carryover, blank spike samples were run between each sample. As untreated BL-RAW samples had average TONO concentrations of 33 $ng \cdot L^{-1}$ as NDMA, just above the MDL of this procedure, TONO was not measured for these CNT-treated samples.

2.2.3. CNT Characterization

CNT physical characteristics were measured rather than relying on manufacturer specifications (Table S2). The pore volume distribution and Brunauer-Emmett-Teller (BET) surface area of the CNTs were measured using a Quantachrome Nova 2200e Surface Area and Pore Size Analyzer using N_2 and CO_2 gas adsorption at 77 K and 273 K, respectively. Adsorption isotherms (Figure S1) were collected at partial pressures of 0.005-0.99 using step sizes of 0.011-0.095. Pore volume distributions (Figure S2) were calculated from the isotherms using a hybrid density functional theory model that assumed slit pore geometry for micropores and slit or cylindrical pore geometry for mesopores (Zhu et al., 2011). The BET surface area (S_{BET}) was calculated using the N_2 adsorption isotherm in the linear relative pressure range from

0.05-0.30. However, it should be noted that S_{BET} is calculated without regard for the information given about micropores by the CO_2 adsorption isotherm. As such, S_{BET} is more suitable for comparing the amount of specific surface area individual CNT types have relative to each other, rather than their absolute specific surface area (Zhu et al., 2011).

XPS measurements were performed on pristine CNTs using a PHI 5000 VersaProbe spectrometer with an AlKα source, and a vacuum of 10^{-8} Torr was maintained during analysis. Methods for the XPS data analysis are detailed in the SI and carbon spectra deconvolutions are shown in Figure S3.

2.2.4. Data Modeling

To assess the impact of physicochemical CNT characteristics on DBP precursor adsorption, a multivariate analysis was performed for the three groups of DBPs. DBPFP was expressed as a ratio, as the median of each triplicate sample to the median of each untreated sample – either BL-RAW or WS-EFF, as appropriate. The median was utilized, rather than the mean, due to its relative insensitivity to outliers. The potential undue influence on the mean caused by outliers in the data is exacerbated by small sample sizes (e.g., n=3) for a given CNT type and dose. The following independent variables are associated with each group of DBPs: DOC ratio, UV_{254} ratio, CNT dose, carbon-carbon bonds, alcohol groups, carbonyl groups, carboxyl groups, S_{BET}, and cumulative pore volume (CPV). A binary variable (called Water Type) distinguishing between water types was also included in models of TTHM and DHAN Ratio. A binary variable was deemed more appropriate than including water quality characteristics as individual independent variables because these characteristics do not vary among the samples of a given water type. This variable was only used for TTHM and DHAN Ratio because TONO Ratio does not include samples of BL-RAW that were below the MDL.

DOC and UV_{254} ratio were calculated using procedures analogous to DBP ratio and were incorporated into the numerical models to assess their usefulness as DBP precursor surrogates, as opposed to the other independent variables related to CNT properties. An additional binary variable distinguishing single- and multi-walled CNTs is explored in the SI. Analysis of variance was used to study associations between DBP ratios and independent variables, or explanatory factors; equivalent linear regression was used to test hypotheses about factor levels while controlling for other factors. Models were estimated using STATA/IC 11.2 statistical software (StataCorp, 2009) which leverages principles of applied regression analysis as detailed by Draper and Smith (1998).

3. Results and Discussion

3.1. DBP Precursor Adsorption by CNTs

Figure 1 shows percent removals of TTHMFP and DHANFP from BL-RAW (Figure 1A) and of TTHMFP, DHANFP, and TONOFP from WS-EFF (Figure 1B) attributed to each of the nine CNT types. Removal of TONOFP is only provided for WS-EFF because the concentration was below the MDL in BL-RAW. DBPFP removal is assumed to be due to adsorption of DBP precursors by the CNTs. As expected, increasing the CNT dose from 25- to 50 $mg \cdot L^{-1}$ resulted in an increase in percent removal for each DBP precursor for all nine CNT types. For TTHM precursor removal, the CNT types assessed performed similarly or better on a percent basis than the activated carbons used by Najm and colleagues (1991) and Iriarte-Velasco et al. (2008). Additionally, Iriarte-Velasco and colleagues reported removal of DOC (a commonly used as a TTHM precursor surrogate) as 27.6 and 2.2 mg DOC g^{-1} GAC for two types of GAC tested. In comparison, the removal of DOC from BL-RAW ranged from 8.5-24.2 mg DOC g^{-1} CNT, while the removal from WS-EFF was 11.4-57.1 mg DOC g^{-1} CNT, depending on the CNT type.

DHAN can be formed through two pathways utilizing different reactants, which include: (1) the decarboxylation pathway, in which chloramine (and/or free chlorine) reacts with amine-containing moieties of NOM and (2) the aldehyde pathway, where an aldehyde incorporates chloramine-nitrogen (Shah and Mitch, 2012). For BL-RAW samples, the percent removals of DHAN precursors were less than that of TTHM precursors for all nine CNT types; in contrast, for WS-EFF samples, removal of DHAN precursors by CNT Types 1, 2, and 8 surpassed removal of TTHM precursors. Though other precursors in natural waters may contribute to DHANFP in an unknown degree, this relative difference in precursor removal between BL-RAW and WS-EFF suggests the possibility either the amine- or aldehyde-based precursors are more prevalent in WS-EFF and have a greater affinity for CNTs than the less abundant precursors.

Average percent removal of TONO precursors reached a maximum of 93% (Type 9) at a CNT dose of 25 $mg \cdot L^{-1}$ and 97% at the higher CNT dose. Because of a lack of similar studies involving CNTs and TONO precursors, direct comparisons to the literature are not possible. However, using linear interpolation, we compared these results to Hanigan et al. (2012) who quantified NDMA precursor adsorption in batch studies with activated carbon and found that 6 of the 9 CNT types achieved approximately the same or higher percent removals of TONO precursors on a mass sorbent basis. It is important to note that NDMA may only comprise ~5% of TONO formed following chloramination of wastewater effluent organic matter (Dai and Mitch, 2013) and little is known about the physicochemical properties of TONO precursors relative to NDMA precursors. Additionally, the average percent removal of TONO precursors at the 50 $mg \cdot L^{-1}$ CNT dose was 31% greater than either TTHM or DHAN precursor removal. Hydrophilic base fractions of organic matter are considered the most likely *N*-nitrosamine precursors in DWTPs (Wang et al., 2013) and WWTP effluent (Pehlivanoglu-Mantas and Sedlak,

2008). Taken together, this may indicate that CNTs can sorb both hydrophobic and hydrophilic NOM fractions from natural waters although additional testing is required to support such an assertion. Regardless, the results in Figure 1B illustrate that many CNT types have high affinities for TONO precursors, the underlying reasons for which are discussed further in Section 3.3.

3.2. CNT Characterization

The physical and chemical characteristics of each CNT type are summarized in Table 1. The shape of the gas adsorption isotherms (Figure S1) indicated the nitrogen adsorption isotherms were IUPAC Type II and the carbon dioxide adsorption isotherms were Type I (Sing et al., 1985; Zhang et al., 2010; Adeniran and Mokaya, 2015). CPV varied almost one order of magnitude, from 0.135 $cm^3 \cdot g^{-1}$ (Type 7) to 1.267 $cm^3 \cdot g^{-1}$ (Type 2). The CPV measurements of all CNT types fell within the range of values reported in the literature (0.104-2.46 $cm^3 \cdot g^{-1}$), which vary based on CNT dimensions and the number of walls and are associated with both pristine and modified CNTs (Zhang et al., 2010; Adeniran and Mokaya, 2015; Apul and Karanfil, 2015). Pore volume distributions were bimodal (Figure S2), with microporosity assumed to be associated with the interstitial space within CNT bundles and mesoporosity associated with the space within individual tubes (Yang et al., 2005). S_{BET} measurements (Table 1) were within 55% of supplier specifications (Table S2) in all cases with the exception of Type 2, which was 106% greater. In fact, S_{BET} for Type 2 (837 $m^2 \cdot g^{-1}$) was higher than the range reported in the literature for SWCNTs (22-662 $m^2 \cdot g^{-1}$) (Zhang et al., 2010; Birch et al., 2013). However, S_{BET} can vary based on CNT dimensions and the methods of synthesis and purification, and thus, values outside the ranges reported in the literature are not unexpected. For all MWCNT types, S_{BET} fell within the range reported in the literature (58-653 $m^2 \cdot g^{-1}$) (Cho et al., 2008; Zhang et al., 2010; Birch et al., 2013; Apul and Karanfil, 2015). Elemental composition data from deconvolution of

carbon spectra from XPS measurements (Figure S3) indicated that surface oxides (i.e., the sum of C-O, C=O, and COO functional groups) comprised 11% (Type 7) to 14% (Type 2) of the CNTs (Table 1), which falls into the range (6-32%) reported by others (Ago et al., 1999; Komarova et al., 2015). In Section 3.3, we explore relationships between CNT properties and DBP precursor adsorption.

3.3. Impacts of Physicochemical CNT Properties on DBP Precursor Adsorption

Multivariate analysis for each DBP type yielded regression coefficients and p-values (Table 2) for TTHM (n = 36), DHAN (n = 36) and TONO (n = 18). Coefficients with $p < 0.05$ are assumed to be nonzero and indicate a significant effect on DBP ratio (i.e., influent-normalized effluent concentration), controlling for other variables in the model. Significance of an independent variable in the negative direction indicates that an increase in the magnitude of that variable resulted in a decrease in DBP ratio, otherwise stated as an increase in the removal of that DBP precursor by the nine CNT types. A scatterplot of residuals versus fitted values suggested constant error variance (Figures 2A, B, and C). R-squared values indicated strong correlations between fitted values and observed values of DBP ratio for TTHM ($R^2 = 0.92$, Figure 2D), DHAN ($R^2 = 0.92$, Figure 2E) and TONO ($R^2 = 0.96$, Figure 2F). In essence, the model has no discernible bias to the magnitude of DBP ratio and at least 92% of the variation is explained by the measured CNT properties.

The regression coefficients and p-values in Table 2 indicate several notable trends. Opposing signs of significance for the Water Type binary variable for TTHM Ratio and DHAN Ratio indicate that in comparing DBP precursor removal from the two waters, there was greater removal of (1) TTHM precursors from BL-RAW and (2) DHAN precursors from WS-EFF samples when controlling for all other variables in the model. Also, across all three DBP

groups, an increase in either CNT dose or the amount of carboxyl groups resulted in greater removal of precursors. That CNT dose shows this trend only confirms the effect of these particular dosages illustrated in Figure 1. However, the relationship between DBP ratio and the percent of carboxyl groups is intriguing due to the significance of that variable across all DBP groups and suggests that CNT surface chemistry is important for DBP precursor adsorption. For TONO Ratio only, a positive correlation with the percent of alcohol functional groups indicates a decrease in the amount of those surface oxides increased adsorption of TONO precursors. Additionally, for TONO Ratio alone, there was a significant relationship with CPV, indicating that an increase in CPV resulted in enhanced TONO precursor removal. Notably, true relationships between DBP precursor removal and CNT surface chemistry would be obscured by large errors in XPS carbon spectra deconvolution or any other independent variable. The risk of accidentally or randomly observing a relationship that is untrue is kept low by the choice of significance level (alpha = 0.05). Therefore, we have confidence in the importance of significant chemical characteristics in the models.

Surface oxides are generally considered to inhibit sorption of NOM (i.e., DBP precursors) to activated carbon due to repulsion caused by their negative surface charge (Karanfil et al., 2007). However, the results of the multivariate model (Table 2) indicate that an increase in carboxyl groups increases adsorption of all three groups of DBP precursors. Zhang et al. (2015) postulated a link between chemical and physical CNT characteristics that may be relevant here: repulsive forces created by negatively charged oxygen-containing functional groups enlarge spaces between individual CNTs in bundles thereby increasing CPV and S_{BET}. Additionally, functional groups generally form at defect sites in the CNT walls which are also locations that allow access inner microporosity or mesoporosity (depending on the inner diameter of the CNT)

(Yang et al., 2005). It has also been shown that the presence of surface oxides increases the hydrophilicity of CNT surfaces, which could enhance the adsorption of hydrophilic DBP precursors, such as those that react with chloramines to form *N*-nitrosamines (Zhang et al., 2015). Additionally, amine-based groups serving as *N*-nitrosamine precursors are positively charged at circumneutral pH. Thus, these groups would experience electrostatic attractions to the negatively charged carboxylic acid functionalities on the CNTs, which may explain the high removal of TONO precursors relative to TTHM and DHAN precursors. Hydrogen bonding may also be an important adsorption mechanism, which would be consistent with our results, as increases in oxygen groups will increase adsorption when hydrogen bonding is important (Pan and Xing, 2008). However, application of CNTs in the water produces hydrophobic interactions that could obscure the contribution of hydrogen bonding as an adsorption mechanism. The multicollinearity of the physical and chemical properties indicates that both CPV and oxygen-containing functional groups are important to CNT performance for DBP precursor removal.

To explore the concept of DBP precursor size exclusion from the CNT pore networks, linear regression models were refit for all DBP types by arbitrarily increasing minimum pore widths used for the computation of pore volume while all other variables remained unchanged (Figure 3). For TTHM, CPV p-values were large ($p > 0.5$) at low pore widths (< 5 nm) and only came close to significance ($p = 0.079$) above 15 nm. For DHAN, CPV p-values decreased from ~0.15 and became significant ($p = 0.05$) near a minimum pore width of 7 nm and remained significant throughout. For TONOFP, pore volume had a negative effect (i.e. more precursor adsorption occurred as pore volume increased) and pore width had relatively little impact on the importance of pore volume. On balance, the results in Figure 3 indicate that size exclusion effects by the CNT pores could impact adsorption of TTHM and DHAN precursors, but not

TONO precursors. The trends in Figure 3 could indicate that TONO precursors are generally smaller in size (or more accessible to the smaller CNT pores) than TTHM and DHAN precursors. At smaller pore widths, TONO precursors may not have much competition for adsorption sites; as pore width increases toward pores in excess of 15 nm, larger and more abundant TTHM and DHAN precursors could utilize a greater portion of the adsorption capacity. Others have shown that larger molecules at relatively high concentrations (such as TTHM precursors) can block CNT pores and limit further adsorption, while small molecules at trace concentrations (such as TONO precursors) experience little competition for adsorption sites (Hanigan et al., 2015).

3.4. Fluorescence Metrics as DBP Precursor Surrogates

Fluorescence EEMs were measured on untreated and CNT-treated (but not chloraminated) waters to evaluate its usefulness as a precursor surrogate and perhaps limit time-consuming DBPFP analyses in upcoming studies. Fluorescence intensities at all wavelength pairs measured were regressed against the DBP data to identify pairs for which strong correlations exist. Figure 4 shows the correlation coefficients presented on axes equivalent to the EEMs for TTHMFP (Panel A, $R_{MAX}^2 = 0.86$), DHANFP (Panel B, $R_{MAX}^2 = 0.88$), and TONOFP (Panel C, $R_{MAX}^2 = 0.50$) in WS-EFF, and TTHMFP (Panel D, $R_{MAX}^2 = 0.78$) and DHANFP (Panel E, $R_{MAX}^2 = 0.80$) in BL-RAW. These correlations represent relationships between DBP precursors remaining after treatment with CNTs and DBP concentrations formed following FP tests, performed using a recently developed method (Do et al., 2015). As expected, correlations are strong for TTHMFP and DHANFP in both waters. However, the moderate correlation coefficients for TONOFP indicate that fluorescence is unlikely to be a suitable precursor surrogate for total *N*-nitrosamine precursor concentrations when applied in this manner. Interestingly, samples from WS-EFF (Figures 4A, 4B, and 4C) show a large region of

wavelength pairs that give high correlation coefficients. In contrast, high R_{MAX}^2 values for BL-RAW (Figures 4D and 4E) are more localized and are centered near $I_{275/480}$. The insensitivity in R^2 values shown in Figures 4A, 4B, and 4C was unexpected in light of several studies attributing the various regions of EEMs to distinct fluorophore groups (i.e., humic-, fulvic-, tryptophan-, and tyrosine-like), each with its unique chemistry (Hudson et al., 2007). The results presented in Figure 4 suggest strong relationships among virtually all wavelength pairs, and thus imply interdependence (i.e. an increase in a particular fluorophore group could impact other regions of the EEM). Fluorescence EEMs were also analyzed by PARAFAC analysis. A detailed discussion of the removal of the PARAFAC components by the CNTs and correlations between PARAFAC components (Table S5) is provided in the SI. This analysis advances our assertion of fluorophore interdependence, which prevents valid conclusions regarding the affinity of CNTs for discrete humic-, fulvic- and protein-like fluorophores. The interdependence observed in both EEM correlations and PARAFAC components may be indicative of interferences on the protein-like fluorophores and preclude the use of fluorescence EEMs alone as a surrogate for TONO precursors. However, the nature of these precursors suggests that fluorescence may be utilized following elimination of interfering humics (Wang et al., 2015), in applications such as asymmetric flow field-flow fractionation where proteins can be physically separated from humics prior to fluorescence measurements.

3.5. Implications

Based on the importance of surface oxides and CPV for DBP precursor removal, future studies are needed to enhance these CNT characteristics and test their impact in sorption systems. Oxidative treatment with a mixture of nitric and sulfuric acid has been shown to result in formation of oxygen-containing groups on SWCNTs (Balasubramanian and Burghard, 2005;

Komarova et al., 2015) and MWCNTs (Ago et al., 1999). Additionally, KOH treatment can increase surface area and pore volume, specifically in mesopores (Niu et al., 2007). Based on the size exclusion results (Figure 3), this may be particularly important to improve sorption of DHAN and TTHM precursors. Furthermore, future studies of CNT modification should be paired with a reliable system for CNT integration into DWTP treatment processes. A large range of possibilities now exists regarding design of freeform CNT microstructures grown on substrates that could be adapted into current treatment processes. These microstructures can be grown to exacting specifications of size, shape, and porosity, and conformal coating can be applied to manipulate chemical properties (De Volder et al., 2014). Additionally, incorporation of CNTs into hollow fiber membranes has been shown to increase membrane flux, fouling resistance, thermal stability, porosity, and electrochemically regenerative capability with minimal CNT leaching (Huang et al., 2014; Wei et al., 2014; Jafari et al., 2015).

4. Conclusions

With no modification, CNTs have natural affinity for THM-, DHAN, and TONO precursors. The breadth of applications discovered for CNTs due to their unique set of physiochemical properties speak to their potential for further commercial availability. Though CNTs are a novel sorbent with higher costs than standard sorbents, higher performance levels – particularly with regard to TONO precursor adsorption – give CNTs an advantage that warrants future study. As production costs decrease and the body of research regarding their applications increases, CNTs gain potential for feasibility of application in conventional water treatment systems. Manipulation of physicochemical properties to enhance DBP precursor adsorption in concert with reliable methods of integration into water treatment processes could provide DWTPs with a new technique for meeting the increasingly rigorous water quality standards for

DBP control.

5. Associated Content

Notes

The authors declare no competing financial interests.

Acknowledgements

Financial support from the National Science Foundation (CBET #1254350 to JLF) and the University of Arkansas Doctoral Academy Fellowship (to EMN) is gratefully acknowledged. The authors thank Thien Do and Huong Pham (PhD students, University of Arkansas) and two anonymous reviewers for their constructive comments on previous versions of this manuscript.

6. Figures and Tables

Table 1. Physical and Chemical Characteristics of the selected CNTs

CNT Type	Physical Characteristics from SAA[1]		Relative Amount of Chemical Bonds from XPS[2]			
	CPV[3] ($cm^3\ g^{-1}$)	S_{BET}[4] ($m^2\ g^{-1}$)	C=C or C-C[5]	C-O[6]	C=O[7]	COO[8]
1	0.598	446	77.75	8.56	2.70	1.83
2	1.267	837	73.83	10.25	2.90	1.09
3	0.163	104	78.55	7.07	2.98	1.45
4	0.627	426	75.09	8.53	3.90	2.23
5	0.296	171	76.89	7.86	2.65	2.11
6	0.541	298	78.17	7.72	2.88	1.73
7	0.135	92	80.85	6.76	1.81	1.97
8	0.442	265	78.40	7.80	2.18	1.98
9	0.471	262	77.13	7.45	3.00	1.91

[1]Quantachrome Nova 2200e Surface Area and Pore Size Analyzer;
[2]PHI 5000 VersaProbe x-ray photoelectron spectrometer, reported as the percent of total carbon bond types present and does not include shake-up features
[3]Cumulative Pore Volume;
[4]Surface area calculated using the Brunauer-Emmett-Teller (BET) model; [5]Analyzed as total of C=C, C-C, and C-H bonds;
[6]Alcohol bonds;
[7]Carbonyl bonds;
[8]Carboxyl bonds

Table 2. Linear regression models of DBP ratio for TTHMFP, DHANFP and TONOFP

Independent Variables[1]	TTHMFP Ratio		DHANFP Ratio		TONOFP Ratio	
	Coeff.[2]	p-value	Coeff.	p-value	Coeff.	p-value
DOC Ratio	0.618*	0.000	0.427*	0.005	1.667	0.097
UV_{254} Ratio	0.039	0.731	0.384*	0.003	-1.900**	0.016
Water Type[3]	-0.099**	0.000	0.050*	0.009	-	-
CNT Dose (mg/L)	-0.004**	0.000	-0.003**	0.006	-0.011**	0.001
Carbon-Carbon Bonds	0.018	0.441	0.002	0.918	-0.014	0.823
Alcohol Groups (%)	0.028	0.682	-0.081	0.264	0.445*	0.016
Carbonyl Groups (%)	-0.007	0.859	0.026	0.537	-0.089	0.462
Carboxyl Groups (%)	-0.112**	0.002	-0.212**	0.000	-0.246**	0.010
BET Surface Area (m^2	-0.000	0.837	0.001	0.239	0.000	0.798
CPV[4] (mL g^{-1})	-0.096	0.679	-0.376	0.140	-2.246**	0.001
Constant	-1.034	0.666	0.919	0.710	-0.042	0.994

*Positive significance ($p < 0.05$)

**Negative significance ($p < 0.05$)

[1]Independent variables all represent terms in regression equations

[2]Regression coefficients

[3]Binary variable distinguishing between BL-RAW and WS-EFF samples, not applicable to TONO ratio

[4]Cumulative Pore Volume.

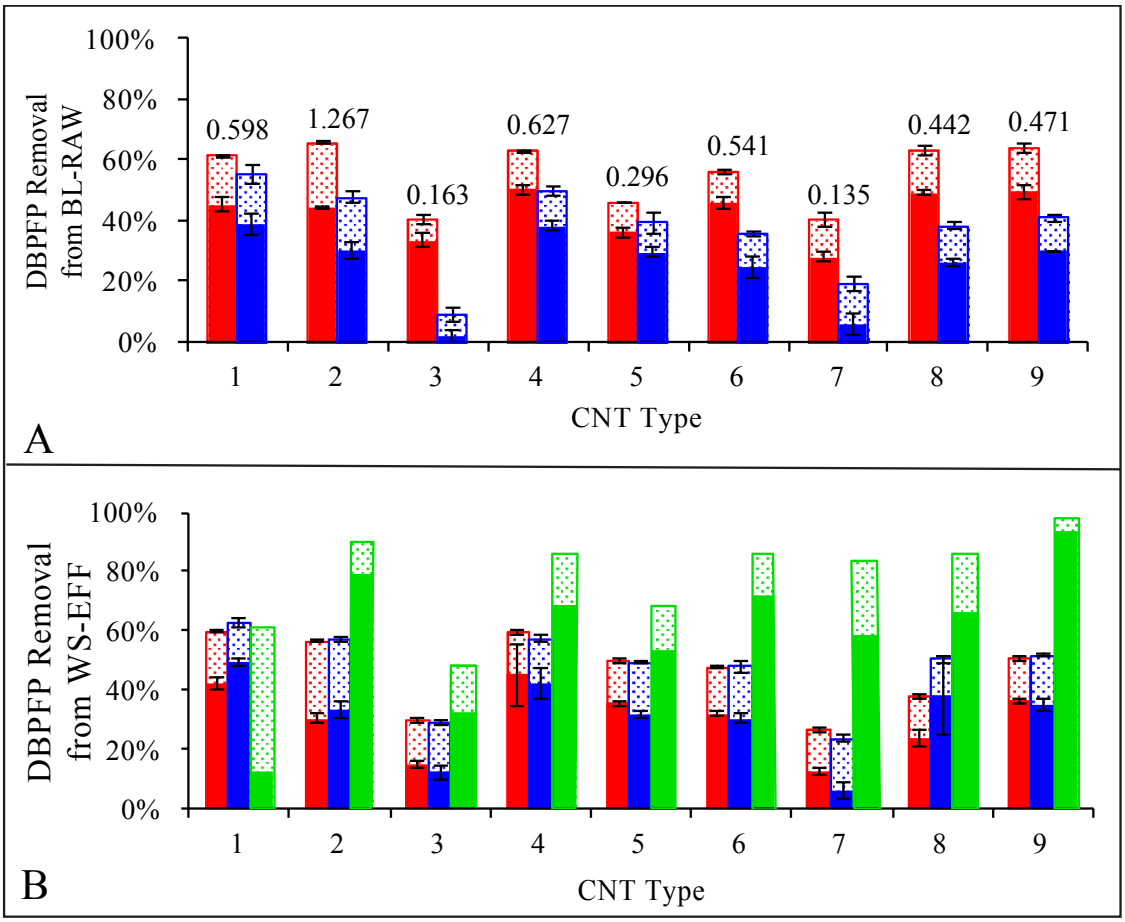

Figure 1. Percent removal of TTHMFP (■ 25 mg•L^{-1} CNT dose, □ 50 mg•L^{-1} CNT dose), DHANFP (■ 25 mg•L^{-1} CNT dose, □ 50 mg•L^{-1} CNT dose) and TONOFP (■25 mg•L^{-1} CNT dose, □ 50 mg•L^{-1} CNT dose) by nine CNT types from Beaver Lake raw water (BL-RAW, Figure 1A) and West Side wastewater treatment plant effluent (WS-EFF, Figure 1B). Values above bars in Figure 1A correspond to the CPV (cm^3•g^{-1}) of each CNT Type and hold true in Figure 1B as well. For TTHMFP and DHANFP, 95% confidence intervals are shown based on triplicate samples on a molar basis. Average FP for untreated BL-RAW samples was 0.095- and 0.022 µmol•L^{-1} for TTHMs and DHANs respectively and 0.250- and 0.086 µmol•L^{-1} respectively in WS-EFF. TONOFP was measured for WS-EFF only in mass-based units as NDMA with an average concentration of 400 ng•L^{-1} as NDMA for untreated samples.

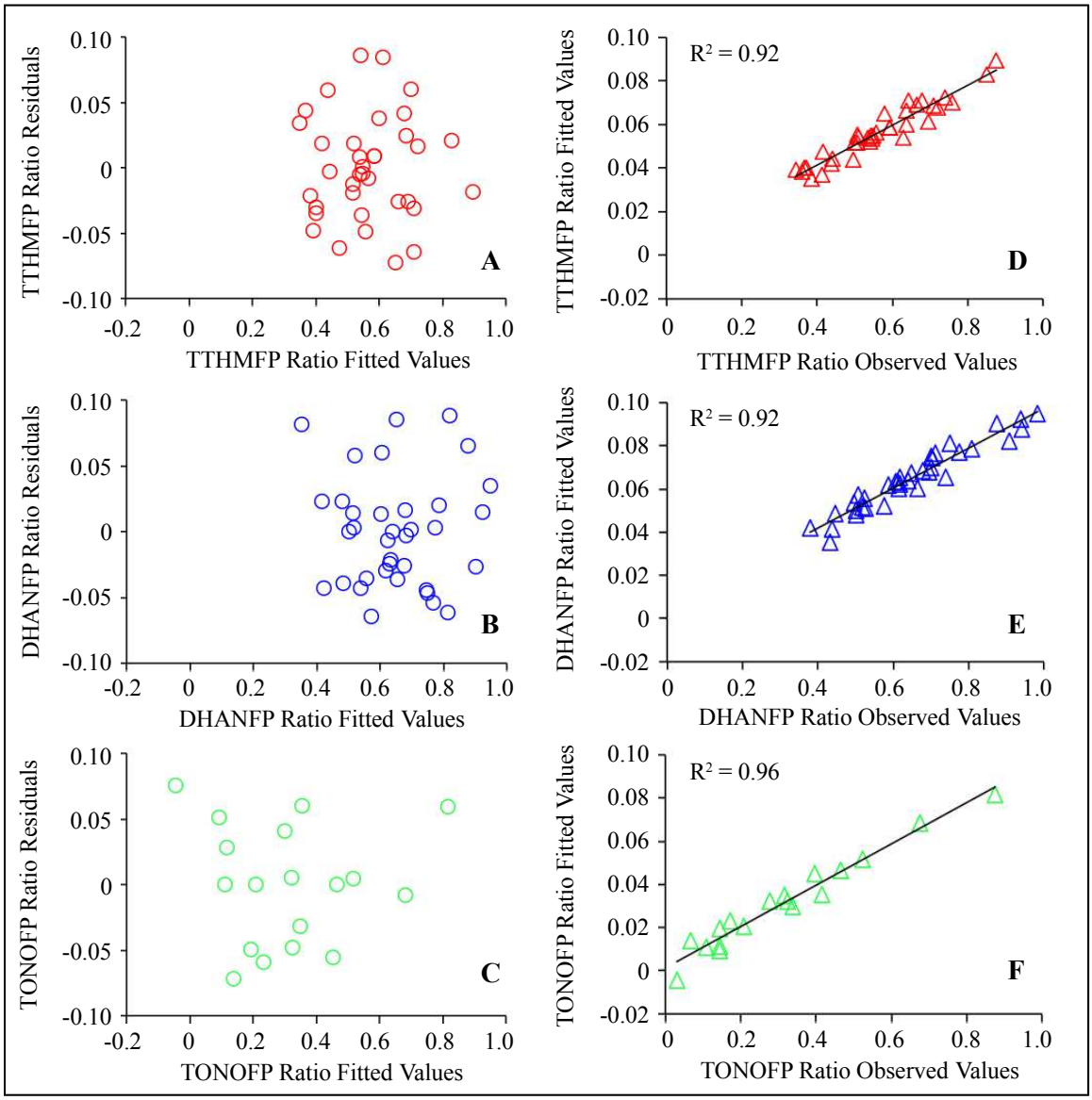

Figure 2. Error variance of models for TTHMFP Ratio (Figure 2A), DHANFP Ratio (Figure 2B) and TONOFP (Figure 2C) and representations of model correlations with observed values of TTHMFP, DHANFP and TONOFP Ratios (Figures 2D-2F). Independent variables used to fit models of TTHMFP, DHANFP, and TONOFP Ratio are detailed in Table 2.

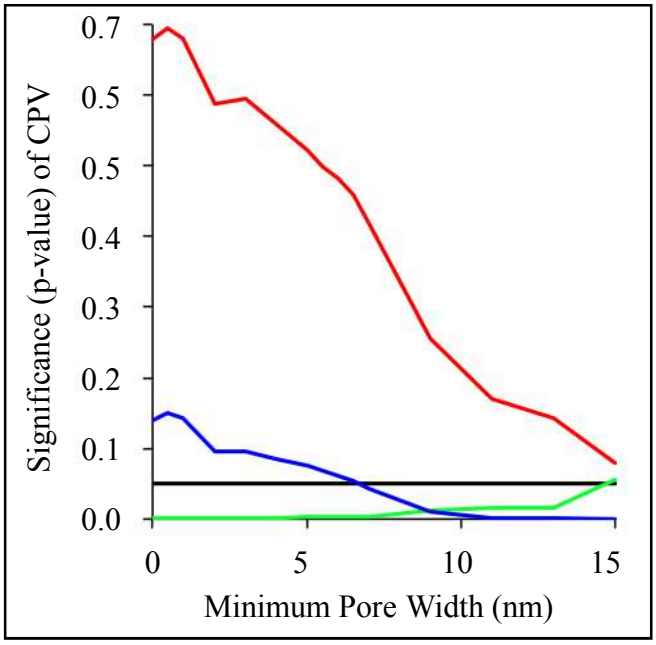

Figure 3. Significance of Cumulative Pore Volume (CPV) in linear regression models (see Table 2) of TTHMFP ratio (–), DHANFP ratio (–) and TONOFP ratio (–) as calculated by arbitrarily increasing the minimum pore widths used to calculate CPV for all nine types of carbon nanotubes. A p-value of 0.05 is included to illustrate the point below which CPV is statistically significant.

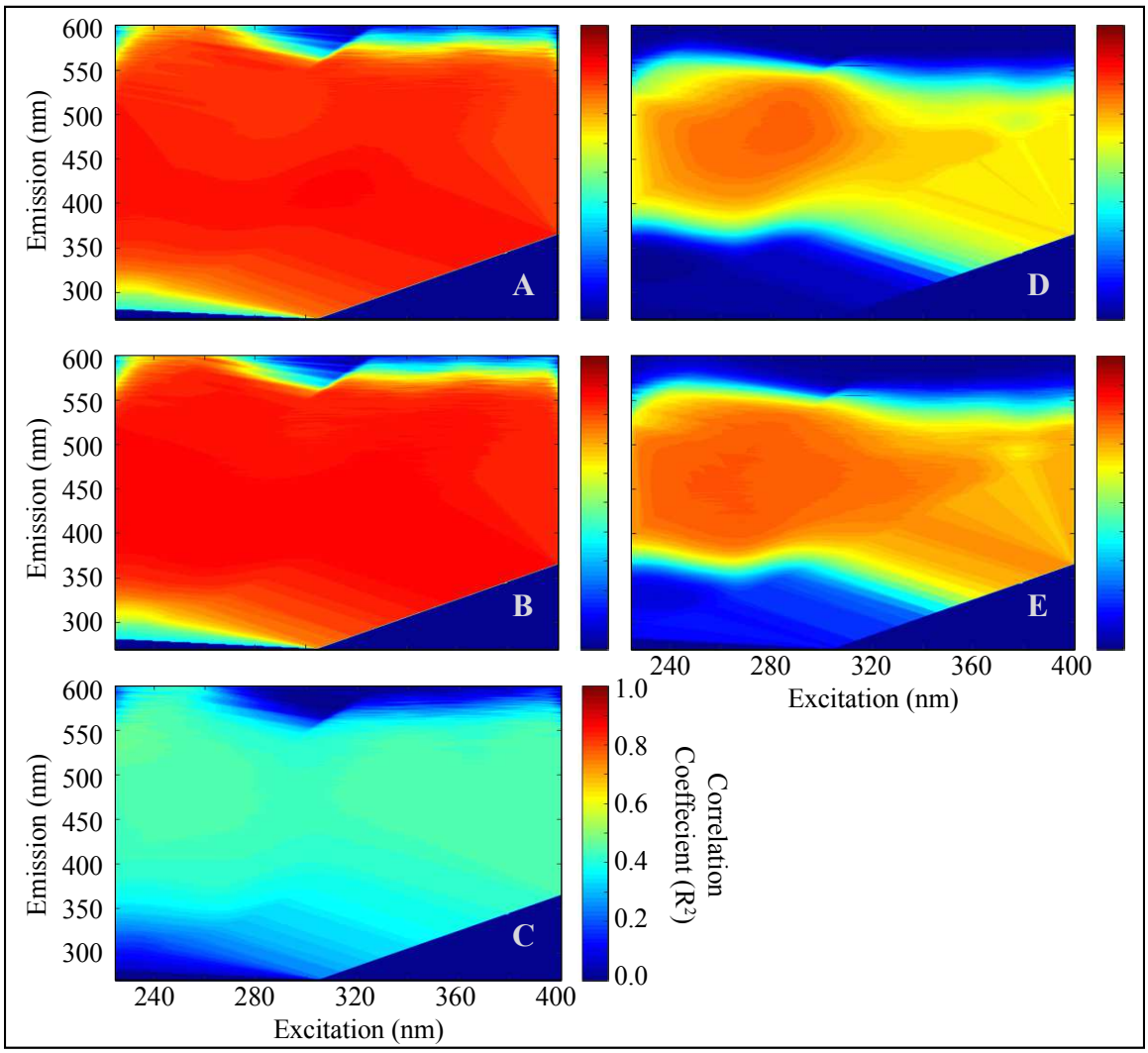

Figure 4. Correlation coefficients for fluorescence intensities of WS-EFF samples in relation to TTHMFP (Figure 4A), DHANFP (Figure 4B) and TONOFP (Figure 4C) and of BL-RAW samples in relation to TTHMFP (Figure 4D) and DHANFP (Figure 4E).

7. References

Adeniran, B. and Mokaya, R., 2015. Low temperature synthesized carbon nanotube superstructures with superior CO2 and hydrogen storage capacity. Journal of Materials Chemistry A 3 (9), 5148-5161.

Ago, H., Kugler, T., Cacialli, F., Salaneck, W. R., Shaffer, M. S. P., Windle, A. H. and Friend, R. H., 1999. Work functions and surface functional groups of multiwall carbon nanotubes. Journal of Physical Chemistry B 103 (38), 8116-8121.

Andersen, C. M. and Bro, R., 2003. Practical aspects of PARAFAC modeling of fluorescence excitation-emission data. Journal of Chemometrics 17 (4), 200-215.

Apul, O. G. and Karanfil, T., 2015. Adsorption of synthetic organic contaminants by carbon nanotubes: A critical review. Water Research 68, 34-55.

Balasubramanian, K. and Burghard, M., 2005. Chemically functionalized carbon nanotubes. Small 1 (2), 180-192.

Birch, M. E., Ruda-Eberenz, T. A., Chai, M., Andrews, R. and Hatfield, R. L., 2013. Properties that influence the specific surface areas of carbon nanotubes and nanofibers. Annals of Occupational Hygiene 57 (9), 1148-1166.

Cho, H.-H., Smith, B. A., Wnuk, J. D., Fairbrother, D. H. and Ball, W. P., 2008. Influence of surface oxides on the adsorption of naphthalene onto multiwalled carbon nanotubes. Environmental Science & Technology 42 (8), 2899-2905.

Cory, R. M., Miller, M. P., McKnight, D. M., Guerard, J. J. and Miller, P. L., 2010. Effect of instrument-specific response on the analysis of fulvic acid fluorescence spectra. Limnology and Oceanography-Methods 8, 67-78.

Dai, N. and Mitch, W. A., 2013. Relative importance of N-nitrosodimethylamine compared to total N-nitrosamines in drinking waters. Environmental Science & Technology 47 (8), 3648-3656.

Dai, N., Shah, A. D., Hu, L. H., Plewa, M. J., McKague, B. and Mitch, W. A., 2012. Measurement of Nitrosamine and Nitramine Formation from NO Reactions with Amines during Amine-Based Carbon Dioxide Capture for Postcombustion Carbon Sequestration. Environmental Science & Technology 46 (17), 9793-9801.

Das, R., Hamid, S. B. A., Ali, M. E., Ismail, A. F., Annuar, M. S. M. and Ramakrishna, S., 2014. Multifunctional carbon nanotubes in water treatment: The present, past and future. Desalination 354, 160-179.

De Volder, M., Park, S., Tawfick, S. and Hart, A. J., 2014. Strain-engineered manufacturing of freeform carbon nanotube microstructures. Nature Communications 5.

Devore, J. L., 2004. Probability and statistics for engineering and the sciences, 6, Brooks/Cole, Thomson Learning, Belmont, CA.

Do, T. D., Chimka, J. R. and Fairey, J. L., 2015. Improved (and singular) disinfectant protocol for indirectly assessing organic precursor concentrations of trihalomethanes and dihaloacetonitriles. Environmental Science & Technology 49 (16), 9858-9865.

Draper, N. R. and Smith, H., 1998. Applied regression analysis, John Wiley & Sons, Inc., New York.

Eaton, A. D., Clesceri, L.S., Rice, E.W., Greenberg, A.E. (Eds.) (2005). Standard methods for the examination of water & wastewater, American Public Health Association, Washington, DC.

Hanigan, D., Zhang, J., Herckes, P., Krasner, S. W., Chen, C. and Westerhoff, P., 2012. Adsorption of N-nitrosodimethylamine precursors by powdered and granular activated carbon. Environmental Science & Technology 46 (22), 12630-12639.

Hanigan, D., Zhang, J., Herckes, P., Zhu, E., Krasner, S. and Westerhoff, P., 2015. Contribution and removal of watershed and cationic polymer N-nitrosodimethylamine precursors. Journal American Water Works Association 107 (3), 90-91.

Hrudey, S. E. and Charrois, J. W. A., Eds. (2012). Disinfection by-products and human health. IWA Publishing and Australian Water Association, London.

Huang, H., Fairbrother, H., Teychene, B., Ajmani, G., Chalew, T. A., Gallagher, M. J., Cho, H., Schwab, K. and Jacangelo, J., 2014. Carbon nanotube composite membranes for small 'designer' water treatment systems. Water Science and Technology-Water Supply 14 (5), 917-923.

Hudson, N., Baker, A. and Reynolds, D., 2007. Fluorescence analysis of dissolved organic matter in natural, waste and polluted waters - A review. River Research and Applications 23 (6), 631-649.

Iriarte-Velasco, U., Alvarez-Uriarte, J. I., Chimeno-Alanis, N. and Gonzalez-Velasco, J. R., 2008. Natural Organic Matter Adsorption onto Granular Activated Carbons: Implications in the Molecular Weight and Disinfection Byproducts Formation. Industrial & Engineering Chemistry Research 47 (20), 7868-7876.

Jafari, A., Mahvi, A. H., Nasseri, S., Rashidi, A., Nabizadeh, R. and Rezaee, R., 2015. Ultrafiltration of natural organic matter from water by vertically aligned carbon nanotube membrane. Journal of Environmental Health Science and Engineering 13, 51.

Karanfil, T., Cheng, W., Dastgheib, S., Guo, Y. and Song, H., 2007. DBP formation control by modified activated carbons, Awwa Research Foundation Denver, CO.

Karanfil, T., Erdogan, I. and Schlautman, M. A., 2003. Selecting filter membranes for measuring DOC and UV_{254}. Journal American Water Works Association 95 (3), 86-100.

Komarova, N. y. S., Krivenko, A. G., Ryabenko, A. G., Naumkin, A. V., Maslakov, K. I. and Savilov, S. V., 2015. Functionalization and defunctionalization of single walled carbon nanotubes: Electrochemical and morphologic consequences. Journal of Electroanalytical Chemistry 738, 27-34.

Kovtyukhova, N. I., Mallouk, T. E., Pan, L. and Dickey, E. C., 2003. Individual single-walled nanotubes and hydrogels made by oxidative exfoliation of carbon nanotube ropes. Journal of the American Chemical Society 125 (32), 9761-9769.

Krasner, S. W., Mitch, W. A., McCurry, D. L., Hanigan, D. and Westerhoff, P., 2013. Formation, precursors, control, and occurrence of nitrosamines in drinking water: A review. Water Research 47 (13), 4433-4450.

Krasner, S. W., Weinberg, H. S., Richardson, S. D., Pastor, S. J., Chinn, R., Sclimenti, M. J., Onstad, G. D. and Thruston, A. D., 2006. Occurrence of a new generation of disinfection byproducts. Environmental Science & Technology 40 (23), 7175-7185.

Kristiana, I., Lethorn, A., Joll, C. and Heitz, A., 2014. To add or not to add: The use of quenching agents for the analysis of disinfection by-products in water samples. Water Research 59, 90-98.

Kulshrestha, P., McKinstry, K. C., Fernandez, B. O., Feelisch, M. and Mitch, W. A., 2010. Application of an optimized total N-nitrosamine (TONO) assay to pools: placing N-nitrosodimethylamine (NDMA) determinations into perspective. Environmental Science & Technology 44 (9), 3369-3375.

Kundu, S., Xia, W., Busser, W., Becker, M., Schmidt, D. A., Havenith, M. and Muhler, M., 2010. The formation of nitrogen-containing functional groups on carbon nanotube surfaces: a quantitative XPS and TPD study. Physical Chemistry Chemical Physics 12 (17), 4351-4359.

Liao, X. B., Wang, C. K., Wang, J., Zhang, X. J., Chen, C., Krasner, S. W. and Suffet, I. H., 2014. Nitrosamine precursor and DOM control in effluent-affected drinking water. Journal American Water Works Association 106 (7), 81-82.

Liu, Y., Zhao, Y., Sun, B. and Chen, C., 2013. Understanding the toxicity of carbon nanotubes. Accounts of Chemical Research 46 (3), 702-713.

Lu, C. Y. and Su, F. S., 2007. Adsorption of natural organic matter by carbon nanotubes. Separation and Purification Technology 58 (1), 113-121.

Mayer, L. M., Schick, L. L. and Loder, T. C., 1999. Dissolved protein fluorescence in two Maine estuaries. Marine Chemistry 64 (3), 171-179.

McKnight, D. M., Boyer, E. W., Westerhoff, P. K., Doran, P. T., Kulbe, T. and Andersen, D. T., 2001. Spectrofluorometric characterization of dissolved organic matter for indication of precursor organic material and aromaticity. Limnology and Oceanography 46 (1), 38-48.

McPhail, M. R., Sells, J. A., He, Z. and Chusuei, C. C., 2009. Charging nanowalls: adjusting the carbon nanotube isoelectric point via surface functionalization. Journal of Physical Chemistry C 113 (32), 14102-14109.

Mitch, W. A. and Dai, N. (2012). Water Research Foundation Report #4209: Development and application of a total nitrosamine assay for disinfected waters, Water Research Foundation.

Najm, I. N., Snoeyink, V. L., Lykins, B. W. and Adams, J. Q., 1991. USING POWDERED ACTIVATED CARBON - A CRITICAL-REVIEW. Journal American Water Works Association 83 (1), 65-76.

Niu, J. J., Wang, J. N., Jiang, Y., Su, L. F. and Ma, J., 2007. An approach to carbon nanotubes with high surface area and large pore volume. Microporous and Mesoporous Materials 100 (1-3), 1-5.

Okpalugo, T. I. T., Papakonstantinou, P., Murphy, H., McLaughlin, J. and Brown, N. M. D., 2005. High resolution XPS characterization of chemical functionalised MWCNTs and SWCNTs. Carbon 43 (1), 153-161.

Pan, B. and Xing, B., 2008. Adsorption mechanisms of organic chemicals on carbon nanotubes. Environmental Science & Technology 42 (24), 9005-9013.

Pehlivanoglu-Mantas, E. and Sedlak, D. L., 2008. Measurement of dissolved organic nitrogen forms in wastewater effluents: Concentrations, size distribution and NDMA formation potential. Water Research 42 (14), 3890-3898.

Pifer, A. D. and Fairey, J. L., 2012. Improving on $SUVA_{254}$ using fluorescence-PARAFAC analysis and asymmetric flow-field flow fractionation for assessing disinfection byproduct formation and control. Water Research 46 (9), 2927-2936.

Pifer, A. D. and Fairey, J. L., 2014. Suitability of organic matter surrogates to predict trihalomethane formation in drinking water sources. Environmental Engineering Science 31 (3), 117-126.

Ramanathan, T., Fisher, F. T., Ruoff, R. S. and Brinson, L. C., 2005. Amino-functionalized carbon nanotubes for binding to polymers and biological systems. Chemistry of Materials 17 (6), 1290-1295.

Ren, X., Chen, C., Nagatsu, M. and Wang, X., 2011. Carbon nanotubes as adsorbents in environmental pollution management: A review. Chemical Engineering Journal 170 (2-3), 395-410.

Rook, J. J., 1976. Haloforms in drinking water. Journal American Water Works Association 68 (3), 168-172.

Russell, C. G., Blute, N. K., Via, S., Wu, X. and Chowdhury, Z., 2012. National assessment of nitrosamine occurrence and trends. Journal American Water Works Association 104 (3), E205-E217.

Sen, S., Haggard, B. E., Chaubey, I., Brye, K. R., Costello, T. A. and Matlock, M. D., 2007. Sediment phosphorus release at Beaver Reservoir, Northwest Arkansas, USA, 2002-2003: A preliminary investigation. Water, Air and Soil Pollution 179 (1-4), 67-77.

Shah, A. D. and Mitch, W. A., 2012. Halonitroalkanes, Halonitriles, Haloamides, and N-Nitrosamines: A Critical Review of Nitrogenous Disinfection Byproduct Formation Pathways. Environmental Science & Technology 46 (1), 119-131.

Shapiro, S. S. and Wilk, M. B., 1965. An analysis of variance test for normality (complete samples). Biometrika 52, 591-611.

Shih, Y.-h. and Li, M.-S., 2008. Adsorption of selected volatile organic vapors on multiwall carbon nanotubes. Journal of Hazardous Materials 154 (1-3), 21-28.

Sing, K. S. W., Everett, D. H., Haul, R. A. W., Moscou, L., Pierotti, R. A., Rouquerol, J. and Siemieniewska, T., 1985. Reporting physisorption data for gas solid systems with special reference to the determination of surface area and porosity (recommendations 1984). Pure and Applied Chemistry 57 (4), 603-619.

Singh, B., Fang, Y., Cowie, B. C. C. and Thomsen, L., 2014. NEXAFS and XPS characterisation of carbon functional groups of fresh and aged biochars. Organic Geochemistry 77, 1-10.

StataCorp (2009). Stata statistical software: release 11. College Station, TX, StataCorp LP.

Stedmon, C. A. and Bro, R., 2008. Characterizing dissolved organic matter fluorescence with parallel factor analysis: a tutorial. Limnology and Oceanography-Methods 6, 572-579.

Tawfick, S., De Volder, M., Copic, D., Park, S. J., Oliver, C. R., Polsen, E. S., Roberts, M. J. and Hart, A. J., 2012. Engineering of micro- and nanostructured surfaces with anisotropic geometries and properties. Advanced Materials 24 (13), 1628-1674.

Upadhyayula, V. K. K., Deng, S., Mitchell, M. C. and Smith, G. B., 2009. Application of carbon nanotube technology for removal of contaminants in drinking water: A review. Science of the Total Environment 408 (1), 1-13.

Wang, C. K., Zhang, X. J., Wang, J., Liu, S. M., Chen, C. and Xie, Y. F., 2013. Effects of organic fractions on the formation and control of N-nitrosamine precursors during conventional drinking water treatment processes. Science of the Total Environment 449, 295-301.

Wang, H., Zhou, A., Peng, F., Yu, H. and Yang, J., 2007. Mechanism study on adsorption of acidified multiwalled carbon nanotubes to Pb(II). Journal of Colloid and Interface Science 316 (2), 277-283.

Wang, X., Tao, S. and Xing, B., 2009. Sorption and competition of aromatic compounds and humic acid on multiwalled carbon nanotubes. Environmental Science & Technology 43 (16), 6214-6219.

Wang, Z. G., Cao, J. and Meng, F. G., 2015. Interactions between protein-like and humic-like components in dissolved organic matter revealed by fluorescence quenching. Water Research 68, 404-413.

Wei, G., Yu, H., Quan, X., Chen, S., Zhao, H. and Fan, X., 2014. Constructing all carbon nanotube hollow fiber membranes with improved performance in separation and antifouling for water treatment. Environmental Science & Technology 48 (14), 8062-8068.

Yan Yan, H. and Terentjev, E. M., 2012. Dispersion of carbon nanotubes: mixing, sonication, stabilization, and composite properties. Polymers 4 (1), 275-95.

Yang, C. M., Kim, D. Y. and Lee, Y. H., 2005. Single-walled carbon nanotube network with bimodal pore structures of uniform microporosity and mesoporosity. Journal of Nanoscience and Nanotechnology 5 (6), 970-974.

Yang, K. and Xing, B., 2009. Adsorption of fulvic acid by carbon nanotubes from water. Environmental Pollution 157 (4), 1095-1100.

Zepp, R. G., Sheldon, W. M. and Moran, M. A., 2004. Dissolved organic fluorophores in southeastern US coastal waters: correction method for eliminating Rayleigh and Raman scattering peaks in excitation-emission matrices. Marine Chemistry 89 (1-4), 15-36.

Zhang, S., Shao, T., Kose, H. S. and Karanfil, T., 2010. Adsorption of aromatic compounds by carbonaceous adsorbents: a comparative study on granular activated carbon, activated carbon fiber, and carbon nanotubes. Environmental Science & Technology 44 (16), 6377-6383.

Zhang, Y., Chen, C., Peng, L., Ma, Z., Zhang, Y., Xia, H., Yang, A., Wang, L., Su, D. S. and Zhang, J., 2015. Carboxyl groups trigger the activity of carbon nanotube catalysts for the oxygen reduction reaction and agar conversion. Nano Research 8 (2), 502-511.

Zhang, Z., Pfefferle, L. and Haller, G. L., 2014. Comparing characterization of functionalized multi-walled carbon nanotubes by potentiometric proton titration, NEXAFS, and XPS. Chinese Journal of Catalysis 35 (6), 856-863.

Zhu, Y. W., Murali, S., Stoller, M. D., Ganesh, K. J., Cai, W. W., Ferreira, P. J., Pirkle, A., Wallace, R. M., Cychosz, K. A., Thommes, M., Su, D., Stach, E. A. and Ruoff, R. S., 2011. Carbon-based supercapacitors produced by activation of graphene. Science 332 (6037), 1537-1541.

Appendix 1

Supplementary Information for

"Trihalomethane, Dihaloacetonitrile, and Total *N*-nitrosamine Precursor Adsorption by Carbon Nanotubes: The Importance of Surface Oxides and Pore Volume"

List of Tables and Figures

Table S1. Raw Water Characteristics

Table S2. Manufacturer-specified properties of the selected carbon nanotubes

Table S3. Preliminary DBPFP Removal Testing

Table S4. Chlorine Residuals following filtration in batch studies

Table S5. Fluorescence maximum (F_{MAX}) values

Table S6. Mean percent removal of each PARAFAC component

Table S7. Linear correlations (R) between components of BL-RAW and WS-EFF PARAFAC Models

Figure S1. Gas adsorption isotherms for CNT Types 1-9

Figure S2. Pore volume distributions for CNT Types 1-9

Figure S3. Deconvolutions of carbon spectra from XPS measurements for CNT Types 1-9

Figure S4. Linear regression of fluorescence at R_{MAX}^2 excitation-emission wavelength pairs

Figure S5. PARAFAC component EEMs for Beaver Lake Raw Water

Figure S6. PARAFAC component EEMs for West Side WWTP Effluent

Figure S7. Linear regressions of DBPFP percent removal against percent removal of F_{MAX} of Components.

Figure S8. Sum of squared errors comparing PARAFAC models

Figure S9. Linear regressions of TTHM- and DHANFP against UV_{254}

Methods

Dissolved organic carbon was measured for each filtered sample using a GE 5310C TOC analyzer. Anion concentrations were measured for both BL-RAW and WS-EFF raw waters using a Metrohm 850 Ion Chromatograph with conductivity and UV detectors. Fluorescence EEMs were collected using a dual monochromator fluorescence detector (Agilent Technologies, Model G1321A). Wavelengths used were 250 to 400 nm for excitation and 270 to 600 nm for emission, both in 1 nm increments. A five-point standard curve of quinine sulfate in 0.1 M sulfuric acid was used due to its distinct response at excitation and emission wavelengths of 350 and 450 nm, respectively, and intensity measurements of all spectra were reported in quinine sulfate equivalents (Cory et al., 2010). Absorbance scans were used to correct for inner-filter effects as suggested by McKnight et al. (2001) and the MATLAB program *Cleanscan* (Zepp et al., 2004) was used to correct EEMs for Raleigh and Raman scattering. Values of fluorescence intensity at excitation and emission wavelengths of 345 nm and 425 nm, respectively, are strongly correlated with TTHM precursors (Do et al., 2015) and are shown in Table S1 for both BL-RAW and WS-EFF. Two models were developed using parallel factor (PARAFAC) analysis on arrays of EEMs for each water type to reveal components with distinct excitation-emission signatures and their maximum intensities, F_{MAX} (Andersen and Bro, 2003).

Disinfection by-product formation potential (DBPFP) of the samples was measured using the procedure detailed in Do et al. (2015) Samples were warmed to room temperature, amended with 20 mM sodium bicarbonate, and adjusted to pH 7.0 using NaOH and/or HCl. Pre-formed 14 $g \cdot L^{-1}$ as Cl_2 stock monochloramine solution was prepared immediately before chloramination as detailed previously. The stock total chlorine and monochloramine concentrations were measured on a representative sample volume, following 4,000-6,000 times dilution with Milli-Q water,

using Hach powder pillows with a UV-Vis 2450 spectrophotometer (Shimadzu) at wavelengths of 655- and 552 nm, respectively. Samples were dosed with pre-formed monochloramine at 300 $mg \cdot L^{-1}$ as Cl_2 and stored headspace-free in 1-L chlorine demand free amber glass bottles for 7 days in the dark at room temperature (25 ºC ± 2 ºC). Following the hold time, the monochloramine and total chlorine residuals were measured and quenched with 20.1 g of a salt mixture (mass ratio of 0.9 g ascorbic acid ($C_6H_8O_6$): 1 g KH_2PO_4: 39 g Na_2HPO_4) added to each 1 L sample to halt DBP formation reactions as recommended by Kristiana et al. (2014). Total trihalomethanes (TTHMs) and dihaloacetonitriles (DHANs) in the West Side wastewater treatment plant effluent (WS-EFF) samples were quantified by GC-ECD using a 9-point standard curve that ranged from 1- to 100 $\mu g \cdot L^{-1}$. Similarly, TTHMs and DHANs in the Beaver Lake raw water (BL-RAW) samples were analyzed using a 12-point standard curve that ranged from 0.1- to 100 $\mu g \cdot L^{-1}$. Blanks and check standards were run after every group of six samples.

The pH point of zero charge of the carbon nanotubes (CNTs) was not measured because a stable suspension could not be achieved without CNT modification. Sonication of CNTs in pure water was attempted despite the high probability of damage to the CNT structure (Yan Yan and Terentjev, 2012), but failed to produce the stable suspension necessary for zeta potential measurements.

PARAFAC Analysis

EEMs were analyzed by PARAFAC to further characterize the dissolved organic matter and help generalize the precursor surrogate findings. Given the differences in the water types, separate PARAFAC models were used for BL-RAW and WS-EFF samples, each originally consisting of 57 EEMs. Two outliers were removed from the BL-RAW data set while no outliers were found in WS-EFF samples. Split-half analyses showed that BL-RAW samples could be adequately described by a two- or four-component model and the WS-EFF samples could be described by a two- or three-component model. Models with the greatest number of components (i.e., four components for BL-RAW and three components for WS-EFF) were chosen to explain the data because they had the smallest sum of squared errors (Figure S8).

XPS Data Analysis

Binding energy scales were charge corrected using a C1s peak position of 284.4 eV (Ago et al., 1999; McPhail et al., 2009). C1s peaks were deconvoluted with a Gaussian-Lorentzian mix function, allowed to range from 70-80% Gaussian distribution, and a Shirley background subtraction (McPhail et al., 2009; Zhang et al., 2014). An asymmetry parameter of 0.19 was applied to the peak representing carbon-carbon bonds (Ago et al., 1999); other bonds assigned were alcohols (C-O), carbonyls (C=O), and carboxyls (COO) with an additional peak fitted to the shake-up features satellite located in the higher binding energy region. Peak locations chosen for the carbon spectra deconvolutions were set as allowable ranges based on ranges found in the literature. Actual peak locations were allowed to vary within the set range in order to achieve the best fit determined by the chi-squared value of the model. The assymetric carbon peak representing all types of carbon-carbon bonding was set to 284.38-285.50 eV (Ago et al., 1999; Kovtyukhova et al., 2003; Okpalugo et al., 2005; Wang et al., 2007; Zhang et al., 2014).

Locations of various types of carbon-oxygen bonds are as follows: alcohol at 286.00-287.53 eV, carbonyl at 286.45-288.03 eV, and carboxyl at 288.39-289.55 eV (Ago et al., 1999; Kovtyukhova et al., 2003; Okpalugo et al., 2005; Ramanathan et al., 2005; Wang et al., 2007; McPhail et al., 2009; Singh et al., 2014). Shake-up features associated with π-π^* transitions were fitted at 289.00-291.60 eV (Okpalugo et al., 2005). Each individual peak was allowed to vary from 70- to 80% Gaussian distribution in order to find the best fit (McPhail et al., 2009; Kundu et al., 2010; Zhang et al., 2014).

Model Verification and Permutations

Results in Table 2 are based on reasonable assumptions with respect to a normal distribution of residuals and constant error variance. The results of the Wilk-Shapiro test (Shapiro and Wilk, 1965) for TTHM ($p = 0.788$), DHAN ($p = 0.066$) and TONO ($p = 0.339$) were all greater than $p = 0.05$; we therefore fail to reject a normal distribution of residuals.

Further investigation of the relationships between physical and chemical characteristics of the nine CNT types through simple linear regressions revealed strong correlations between percent alcohol groups and S_{BET} ($R^2 = 0.95$) and CPV ($R^2 = 0.90$). Multiple linear regression models of surface oxide groups and physical characteristics showed that alcohol groups were significant to S_{BET} and CPV when controlling for carbonyl and carboxyl groups. These findings show that multicollinearity of alcohol groups and physical properties results in variance inflation factors ($VIF = (1 - R^2)^{-1}$, where R^2 is relevant to a multiple linear regression model of one independent variable versus the other independent variables) greater than ten, which could make it impossible to observe otherwise significant independent variables in models of DBP ratio. Of the physical and chemical characteristics, carboxyl groups suffer least from variance inflation ($VIF = 1.27$), and it is possible that this variable serves as a surrogate for significance of physical

characteristics. To further study possible significance of alcohol groups in the face of multicollinearity, the carbonyl groups variable, which was insignificant in all models, was deleted from models of TTHM and DHAN Ratios. This deletion revealed negative significance of alcohol groups to DHAN ratio, indicating that an increase in alcohol groups improved removal of DHAN precursors.

As further evidence of multicollinearity, linear regression between S_{BET} and CPV variables also results in a very strong correlation ($R^2 = 0.97$). However, in the multivariate analysis including both physical variables, only CPV was significant to changes in DBPFP Ratio when controlling for surface area. The same cannot be said of S_{BET} when controlling for CPV. As the multivariate model is capable of providing a more comprehensive assessment of the significance of variables than simple linear regression of variable pairs, it is reasonable to conclude that CPV is a more relevant variable to discuss than S_{BET} in terms of relationships to chemical characteristics and DBPFP Ratio.

Nevertheless, Figure S4 shows the linear regressions for the wavelength pair associated with the maximum R^2 value for TTHM ($I_{369/365}$) and DHAN ($I_{379/356}$). Samples were included regardless of DBP type (TTHM and DHAN only) or source water and an aggregate R^2 value of 0.91 indicates that fluorescence measurements can be used as a reliable surrogate of organic precursor concentrations for TTHM and DHAN. As detailed in the SI, UV_{254} was also assessed as a DBP surrogate, but lacked sensitivity at low absorbance values (less than 0.05 cm^{-1}).

Modeling CNT Wall Type

Of the nine types of CNTs studied, two are single-walled (SWCNTs) and seven are multi-walled (MWCNTs). To explore the effects of these designations, a binary variable was added to the model to distinguish between SWCNTs and MWCNTs in addition to their physical

and chemical characteristics (Table 1). This binary variable was significant in both TTHM and DHAN models and showed that DBP ratios were significantly smaller in SWCNT-treated waters (i.e., SWCNTs adsorbed more TTHM and DHAN precursors). Also, controlling for the new binary variable, CPV had negative, significant effects on DBP ratio for DHAN in general (n = 36) and for TTHM in WS-EFF only (n = 18). However, without more observations of SWCNT types and/or greater chemical and physical detail to distinguish between single- and multi-walled CNTs, this study does not focus on the general difference in CNT wall type and its relationship to other variables.

Removal of PARAFAC Components

The maxima locations of PARAFAC Components 1 and 3 in BL-RAW (Figures S5A and S5C) and WS-EFF (Figures S6A and S6C) corresponded to locations previously characterized as humic- and fulvic-like fluorophores (Pifer and Fairey, 2014). Similarly, the maxima locations of Component 2 corresponded to protein-like fluorophores for BL-RAW (Figure S5B) and WS-EFF (Figure S6B) (Hudson et al., 2007). Component 4 in the BL-RAW model was considered negligible due to its location at maximum emission wavelengths and its low F_{MAX} values, which were insensitive to treatment. To gain further insight into the DBP precursors represented by each PARAFAC component and their removal by the nine types of CNTs, mean percent removals were calculated for each component (Table S6) based on F_{MAX} values for BL-RAW and WS-EFF (Table S5).

Using all nine possible combinations of triplicate samples for both raw and treated waters for a given CNT type, a conservatively large range of percent removal values were determined and used to calculate mean removals and 95% confidence intervals using the t-distribution (Table S5) due to small sample estimates of standard deviation. Removal of Components 1, 2

and 3 in WS-EFF by the CNTs all show similar trends in CNT performance to those observed for the removal of total THM formation potential (TTHMFP) and dihaloacetonitrile formation potential (DHANFP) (Figure S7A and S7B). Additionally, removal of Components 1 and 3 show strong correlations to DBPFP in BL-RAW (Figure S7D and S7E). Weak correlations were observed for total *N*-nitrosamine (TONO) formation potential removal (Figure S7C) and Components 2 and 4 in BL-RAW. For all nine CNT types in WS-EFF, Component 2 (protein-like fluorophores) had the highest mean percent removal (32-80%) of the three components. For six CNT types in BL-RAW, negative mean percent removals were calculated for Component 2, which was attibuted to a combination of low concentrations of protein-like compounds in BL-RAW source water and interferences of humic- and fulvic-like fluorophores skewing the magnitude of the fluorescent response, similar to the findings of others (Mayer et al., 1999). Additionally, the samples with negative mean percent removals also have relatively large 95% confidence intervals (12-339%). These observations illustrated the need for further investigation into the independence of individual PARAFAC components.

PARAFAC Component Correlations

Linear associations between PARAFAC components were tested for data sets incorporating samples treated with both low and high doses of CNTs. Correlations may be considered "weak" if $R < 0.5$, "strong" if $R > 0.8$, and "moderate" otherwise (Devore, 2004). As shown in Table S7 for the BL-RAW samples, the correlation is strong between Components 1 and 3 and moderate between Component 1 and Components 2 and 4. In constrast, correlations among Components 2, 3, and 4 are weak with R values between 0.43-0.49. For the WS-EFF samples, all correlations were strong between the three components, with R values of 0.85, 0.94, and 0.97. As such, even if protein-like fluorophore groups were the predominant precursors of

TONO, the influence of humic- and fulvic-like fluorophores would obscure this finding and produce poor correlations such as those observed in Figure S7C.

UV_{254} as a DBP Precursor Surrogate

Performing selected linear comparisons between single dependent variables and DBPFP revealed an interesting relationship between UV_{254} and TTHMFP (Figure S9A) and DHANFP (Figure S9B). While strong linear correlations existed between UV_{254} for the WS-EFF samples (TTHMFP, $R^2 = 0.74$ and DHANFP, $R^2 = 0.78$), those for BL-RAW samples had R^2 values less than 0.01, indicating the sensitivity of the absorbance scans were insufficient for characterization of TTHM and DHAN precursors. The sensitivity of UV_{254} measurements could possibly be improved by utilizing a 5 cm pathlength cuvette, instead of the 1-cm cuvette used in this study. However, fluorescence measurements utilize a much smaller pathlength of 0.5 mm while still maintaining a comparatively high sensitivity. This in addition to its usefulness across multiple water types (Figure S4) indicates fluorescence is a more robust DBP precursor surrogate than UV_{254}.

Table S1. Raw Water Characteristics

Water Type	**BL-RAW[1]**	**WS-EFF[2]**
pH	7.82	7.93
DOC[3] ($mg \cdot L^{-1}$)	2.33	5.98
UV_{254} (cm^{-1})	0.034	0.096
$I_{345/425}$ (QSE)[4]	5.16	14.25
Specific Conductivity ($\mu S \cdot cm^{-1}$)	155	535
Fluoride ($mg \cdot L^{-1}$)	0.11	0.47
Chloride ($mg \cdot L^{-1}$)	4.1	47.9
Bromide ($mg \cdot L^{-1}$)	0.11	0.16
Nitrate ($mg \cdot L^{-1}$)	1.3	23.9
Phosphate ($mg \cdot L^{-1}$)	ND[5]	0.29
Sulfate ($mg \cdot L^{-1}$)	8.0	47.2
Nitrite ($mg \cdot L^{-1}$)	ND	ND

[1]Raw intake water from Beaver Lake collected on July 7, 2014
[2]Effluent from the West Side Wastewater Treatment Plant collected on June 3, 2014
[3]Dissolved Organic Carbon
[4]Average fluorescence intensity at excitation and emission wavelengths of 325 nm and 425 nm respectively
[5]Not detected

Table S2. Manufacturer-specified properties of the selected carbon nanotubes.

CNT[1] Number	CNT Type	Supplier Description	Diameter (nm)	Length (□m)	S_{BET}[2] ($m^2 \cdot g^{-1}$)	Supplier
1	SW[3]	SWNTs (90%, regular length)	1-2	5-30	300-380	NAM, Inc. [4]
2		SW-DW CNTs 60	0.8-1.6	5-30	407	Cheap Tubes, Inc.
3	MW[5]	C-Grade MWNTs	1-3	80-150	NA[6]	NanoTechLabs, Inc.
4		MW CNTs 8 nm	2-5	10-30	500	Cheap Tubes, Inc.
5		MW CNTs 20-30 nm	5-10	10-30	110	Cheap Tubes, Inc.
6		95%, OD/ID: <10/2-7 nm	2-7	5-15	40-600	NAM, Inc.
7		95%, OD/ID: 30-50/5-15 nm	5-15	10-20	90-120	NAM, Inc.
8		PD30L5-20	15-45	5-20	200-400	NanoLab, Inc.
9		PD30L1-5	15-45	1-5	200-400	NanoLab, Inc.

[1]Carbon nanotube
[2]Supplier provided specific surface area from nitrogen adsorption isotherms using the Brunauer-Emmett-Teller (BET) model
[3]Single-walled
[4]Nanostructured & Amorphous Materials, Inc.
[5]Multi-walled
[6]Not Available

Table S3. Preliminary DBPFP Removal Testing

CNT Dose ($mg \cdot L^{-1}$)[1]	Water Type[2]	Average TTHMFP[3] Removal (%)	Average DHANFP[4] Removal (%)
0	BL-RAW	-	-
5	BL-RAW	14	-
50	BL-RAW	51	-
520	BL-RAW	98	-
0	BL-RAW	-	-
5	BL-RAW	26	37
50	BL-RAW	71	94
0	WS-EFF	-	-
5	WS-EFF	11	20
50	WS-EFF	67	96

[1]Single-walled CNTs were used in all dosed samples
[2]Beaver Lake raw water (BL-RAW) was collected on August 15, 2013 for first set of samples and April 5, 2014 for the second set. West Side WWTP effluent (WS-EFF) was collected on April 9, 2014.
[3]Average total trihalomethane formation potential based on duplicate samples
[4]Average dichloroacetonitrile formation potential based on duplicate samples

Table S4. Chlorine Residuals following filtration in batch studies

CNT Type	CNT Dose ($mg \cdot L^{-1}$)	Average Chlorine Residual ($mg \cdot L^{-1}$)	
		BL-RAW	**WS-EFF**
Blank	0	9.29	9.26
1	25	11.30	10.27
	50	11.47	10.18
2	25	13.83	11.32
	50	14.47	11.23
3	25	14.63	12.77
	50	14.90	12.31
4	25	14.09	12.03
	50	14.85	12.37
5	25	14.35	12.40
	50	14.22	10.72
6	25	15.30	12.65
	50	15.23	13.50
7	25	13.19	12.43
	50	14.00	13.18
8	25	14.76	11.20
	50	15.37	10.49
9	25	11.94	11.48
	50	13.80	10.80

Table S5. Fluorescence maximum (F_{MAX}) values

CNT Type	CNT Dose ($mg \cdot L^{-1}$)	Water Type						
		BL-RAW				WS-EFF		
		C1	C2	C3	C4	C1	C2	C3
Blank	0	9.7	5.1	3.0	1.8	17.1	10.1	9.5
		9.9	4.9	3.1	1.8	18.2	11.0	12.5
		9.9	4.3	3.0	1.8	18.0	10.9	12.1
1	25	4.2	1.9	1.1	1.5	8.1	3.5	4.8
		4.2	1.9	1.2	1.6	8.1	3.4	5.0
		4.3	2.0	1.2	1.4	8.4	3.6	5.8
	50	3.2	1.5	0.9	1.6	5.6	2.2	4.0
		3.2	1.5	0.9	1.3	5.6	2.2	4.4
		3.6	1.9	0.9	1.6	5.4	2.1	5.0
2	25	4.7	2.1	1.6	1.5	7.4	4.0	4.0
		4.9	2.1	1.6	1.5	7.5	4.1	4.2
		4.6	2.2	1.5	1.4	7.5	4.1	4.4
	50	3.2	1.6	1.0	1.3	4.4	2.3	2.6
		1.8	1.4	1.0	1.7	4.4	2.3	2.6
		4.0	3.2	1.6	1.7	4.5	2.4	2.9
3	25	8.0	6.5	2.3	2.4	13.1	6.4	9.4
		8.2	8.1	2.2	1.8	13.0	6.2	9.2
		7.8	4.5	2.2	1.8	13.6	6.5	10.1
	50	7.2	6.6	2.1	2.7	10.1	4.2	7.9
		5.2	2.0	1.6	1.6	9.9	4.0	6.8
		7.2	4.0	1.9	1.8	10.0	4.1	7.6
4	25	5.5	3.9	1.6	1.8	8.9	3.5	6.3
		5.6	6.0	1.6	2.0	7.8	3.1	4.7
		5.5	3.8	1.6	1.9	8.3	3.4	6.1
	50	4.2	3.2	1.2	1.6	5.5	2.1	3.9
		4.0	3.5	1.3	1.8	5.6	2.2	4.3
		4.1	3.3	1.2	1.7	5.7	2.2	4.4
5	25	6.1	6.9	1.9	1.8	10.9	4.8	8.2
		6.6	6.9	2.0	1.7	10.8	4.8	7.7
		6.7	9.9	2.0	1.8	11.1	5.0	9.1
	50	4.7	2.8	1.4	1.6	7.8	3.1	6.3
		5.5	4.9	1.7	1.8	7.9	3.2	6.2
		5.0	3.5	1.4	1.8	7.5	3.0	5.1
6	25	6.8	15.3	1.9	1.9	9.2	3.8	6.7
		6.7	13.3	1.9	1.9	9.2	3.9	6.4
		7.4	7.7	2.1	2.2	9.5	3.9	6.5

Table S5 Cont.

CNT Type	CNT Dose ($mg \cdot L^{-1}$)	Water Type						
		BL-RAW				WS-EFF		
		C1	C2	C3	C4	C1	C2	C3
6	50	4.9	3.0	1.3	1.8	6.7	2.5	5.3
		-	-	-	-	6.2	2.4	4.2
		5.6	14.3	1.5	1.8	6.6	2.5	5.3
7	25	9.5	10.5	2.7	2.0	14.2	7.1	10.7
		10.2	11.1	2.9	2.0	14.1	7.2	10.7
		7.9	5.2	2.3	1.9	14.1	7.3	10.9
	50	7.8	17.6	2.1	2.0	11.6	5.1	10.5
		6.7	9.8	2.0	1.9	11.6	5.2	9.0
		8.9	10.8	2.2	2.3	11.7	5.3	9.2
8	25	-	-	-	-	8.9	3.4	7.1
		6.5	7.3	1.7	2.1	9.2	3.6	7.5
		6.1	10.7	1.7	1.7	10.1	3.9	8.4
	50	4.7	8.0	1.5	1.7	6.7	2.5	5.8
		3.7	3.4	1.2	1.4	6.6	2.3	7.4
		4.5	10.0	1.3	1.6	6.5	2.4	5.3
9	25	5.7	8.6	1.5	1.7	9.7	4.0	7.4
		5.5	6.2	1.6	1.7	9.4	3.9	7.1
		5.6	6.8	1.8	2.3	9.5	3.8	7.8
	50	4.7	8.5	1.4	1.7	6.5	2.4	4.8
		4.1	7.5	1.3	2.1	6.6	2.4	5.0
		4.5	4.1	1.4	1.6	6.6	2.5	5.2

Table S6. Mean percent removal of each PARAFAC component

Water Type	CNT Type	Dose = 25 mg·L^{-1} CNTs			
		C1[1]	C2	C3	C4
BL-RAW	1	57 ± 2.5[2]	59 ± 11	62 ± 2.3	16 ± 16
	2	52 ± 5.0	55 ± 14	48 ± 6.3	19 ± 7.8
	3	19 ± 8.4	-37 ± 123	27 ± 6.1	-11 ± 48
	4	44 ± 2.3	2 ± 89	47 ± 2.6	-7 ± 12
	5	34 ± 10	-70 ± 129	36 ± 7.2	2 ± 5.6
	6	29 ± 12	-160 ± 252	35 ± 13	-11 ± 30
	7	6 ± 33	-92 ± 200	12 ± 27	-9 ± 14
	8	36 ± 7.1	-93 ± 129	44 ± 2.6	-5 ± 28
	9	43 ± 4.0	-53 ± 102	46 ± 10	-5 ± 55
WS-EFF	1	54 ± 6.2	67 ± 5.4	53 ± 30	-[3]
	2	58 ± 4.1	62 ± 5.5	62 ± 18	-
	3	25 ± 10.9	40 ± 11	14 ± 43	-
	4	53 ± 11.3	69 ± 7.5	49 ± 35	-
	5	38 ± 7.6	54 ± 8.1	25 ± 43	-
	6	47 ± 6.6	64 ± 5.5	42 ± 25	-
	7	20 ± 7.5	32 ± 10	4 ± 40	-
	8	47 ± 13	66 ± 10	31 ± 42	-
	9	46 ± 6.5	63 ± 6.1	33 ± 33	-

[1]Components 1-4 represented as C1-C4
[2]95% confidence intervals calculated from maximum range of possible removal values
[3]Model for WS-EFF were only validated with a maximum of three components

Table S6 Cont.

Water Type	CNT Type	Dose = 50 mg·L^{-1} CNTs			
		C1	C2	C3	C4
BL-RAW	1	66 ± 7.5	65 ± 18	70 ± 1.2	15 ± 25
	2	69 ± 30	55 ± 62	60 ± 27	10 ± 32
	3	34 ± 31	8 ± 145	39 ± 21	-12 ± 86
	4	58 ± 3.5	29 ± 21	59 ± 4.9	4 ± 21
	5	49 ± 12	20 ± 76	51 ± 12	2 ± 18
	6	47 ± 11	-89 ± 339	54 ± 9.6	1 ± 3.6
	7	21 ± 31	-175 ± 292	31 ± 14	-16 ± 32
	8	56 ± 15	-54 ± 206	56 ± 14	13 ± 23
	9	55 ± 9.0	-44 ± 145	54 ± 8.0	1 ± 38
WS-EFF	1	69 ± 4.1	80 ± 3.5	60 ± 27	-
	2	75 ± 3.0	78 ± 3.4	75 ± 14	-
	3	44 ± 6.4	61 ± 5.9	33 ± 37	-
	4	68 ± 4.3	80 ± 3.6	62 ± 20	-
	5	56 ± 5.7	71 ± 4.9	47 ± 32	-
	6	63 ± 6.5	77 ± 4.6	56 ± 27	-
	7	34 ± 6.2	51 ± 8.2	14 ± 52	-
	8	63 ± 5.0	77 ± 4.7	44 ± 47	-
	9	63 ± 3.9	77 ± 3.4	55 ± 21	-

Table S7. Linear correlations (R) between components of BL-RAW and WS-EFF PARAFAC Models

Water Type		Components		
		C1	**C2**	**C3**
BL-RAW	**C2**	0.51	-	-
	C3	0.97	0.43	-
	C4	0.54	0.47	0.49
WS-EFF	**C2**	0.97	-	-
	C3	0.94	0.85	-

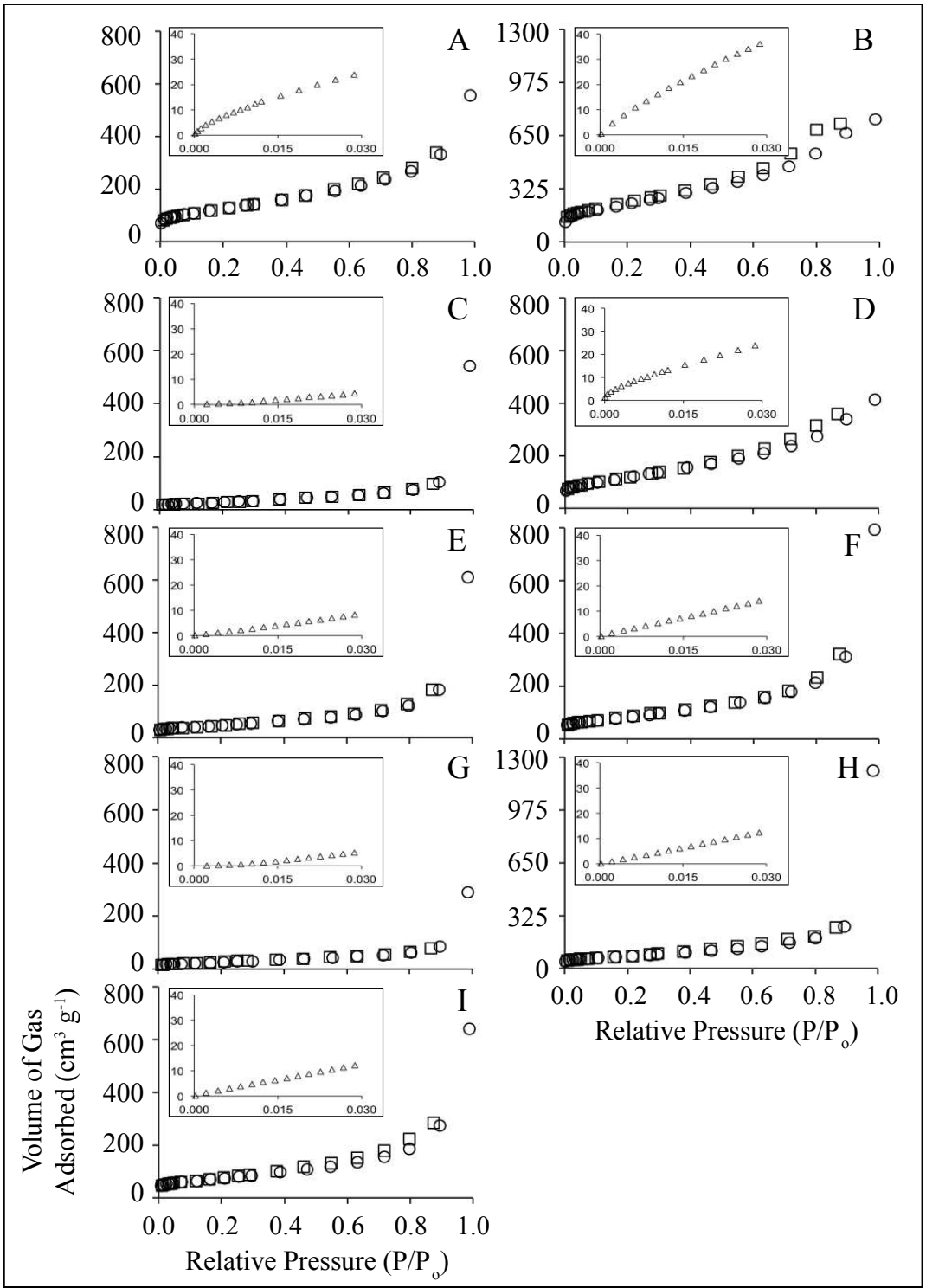

Figure S1. Gas Adsorption Isotherms for CNT Types 1-9 (Figures S1A-S1I). Nitrogen gas adsorption (○) and desorption (□) loops are accompanied by inset carbon dioxide gas adsorption (△) loops. Units are constant for all isotherms.

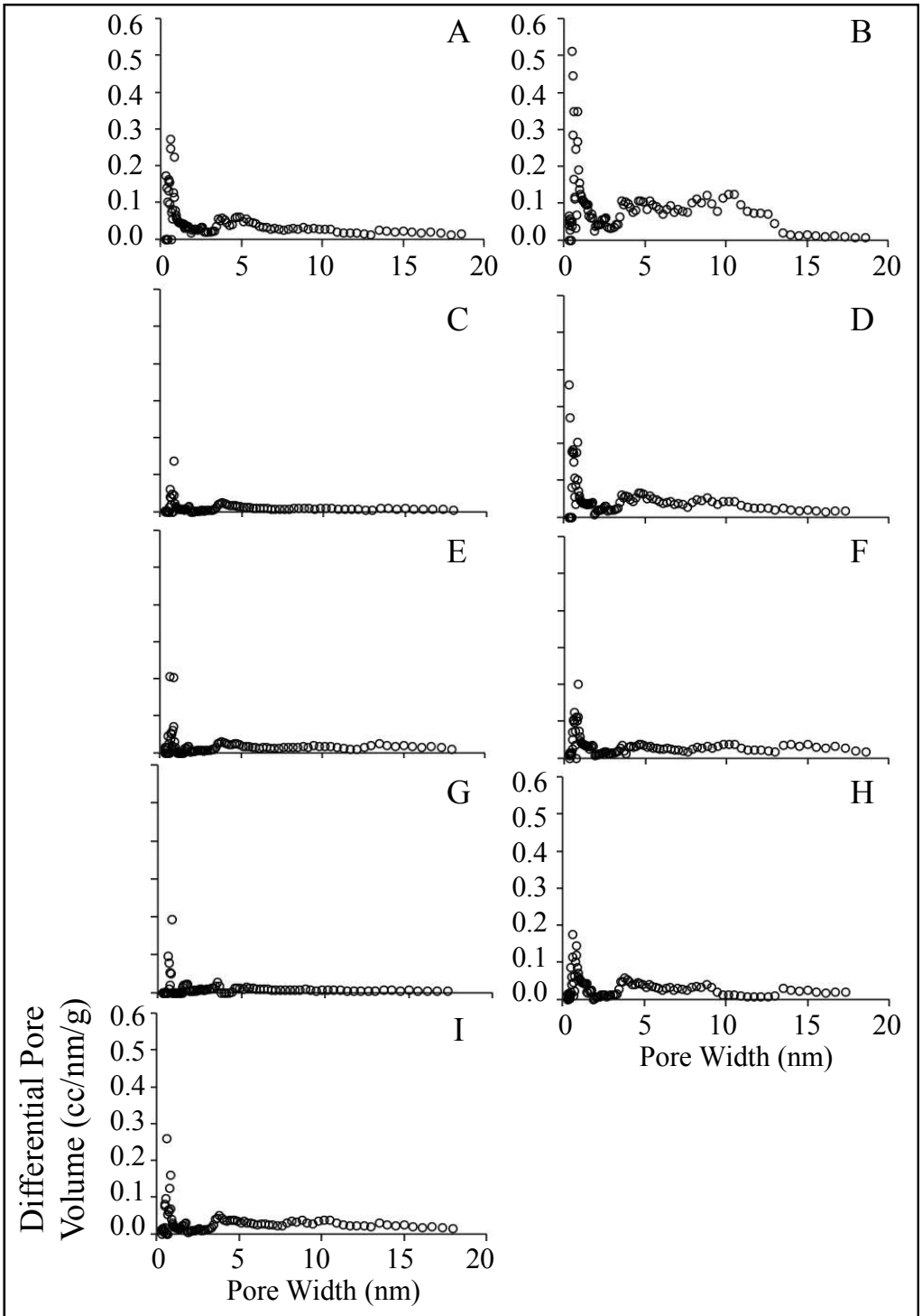

Figure S2. Pore volume distributions for CNT Types 1-9 (Figures S2A-S2I), all with identical scales

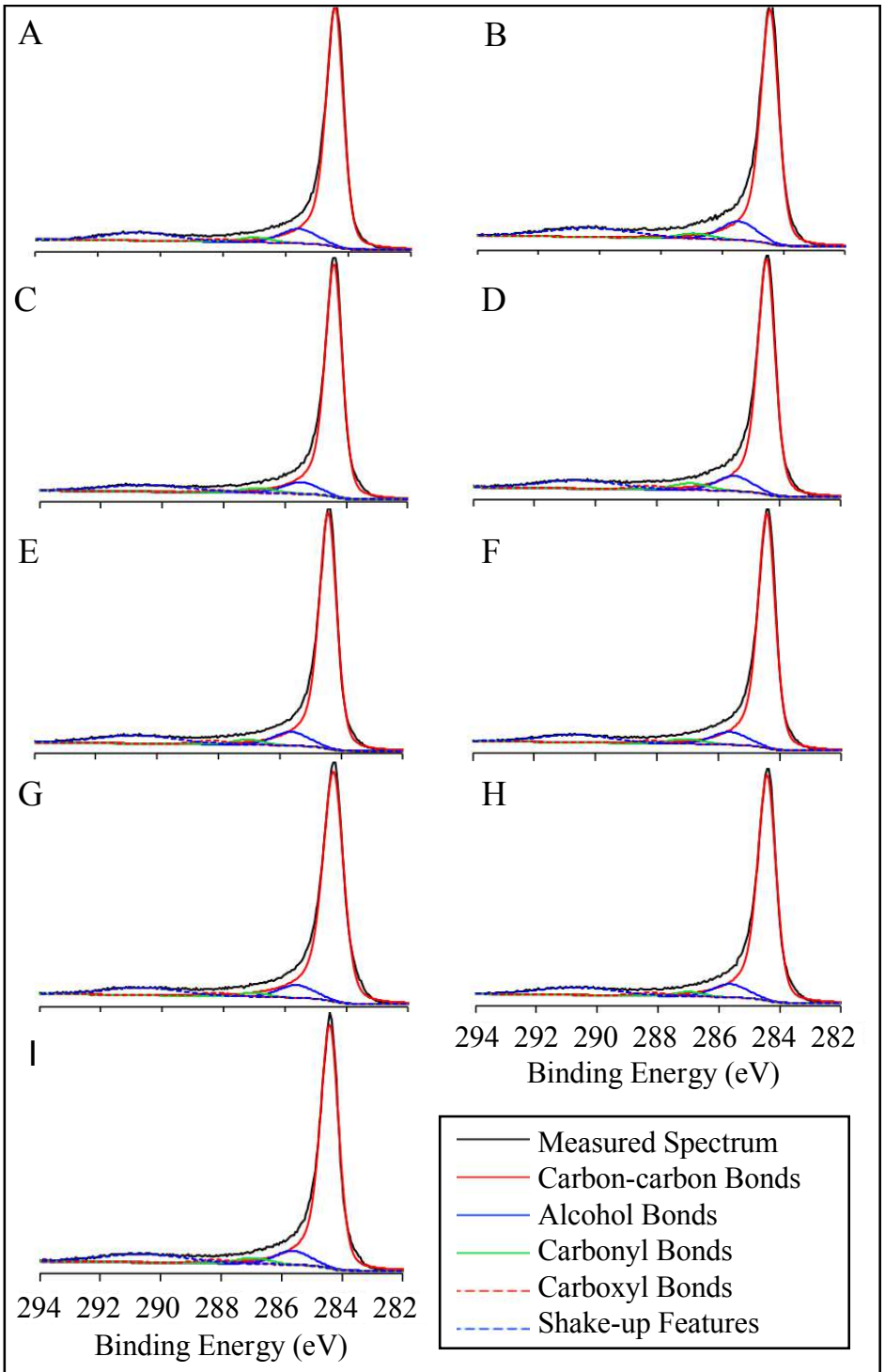

Figure S3. Deconvolutions of Carbon Spectra from XPS Measurements for CNT Types 1-9 (Figures S3A-S3I)

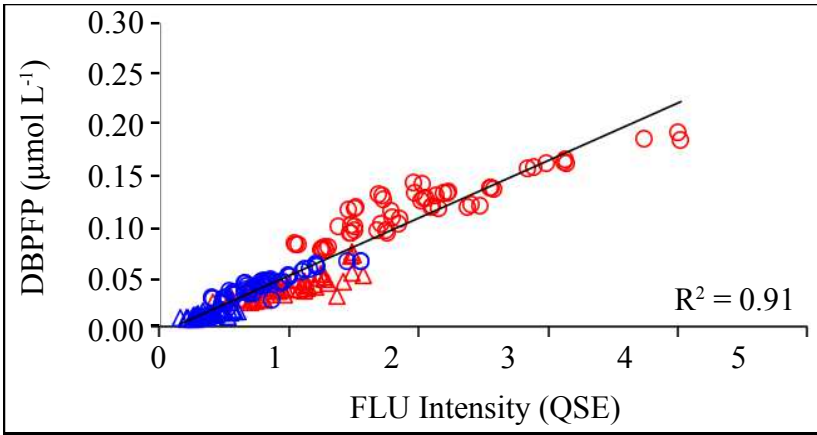

Figure S4. Linear regression of fluorescence at $R_{MAX}{}^{2}$ excitation-emission wavelength pairs against TTHMFP in BL-RAW (△) and WS-EFF (○) and DHANFP in BL-RAW (△) and WS-EFF (○).

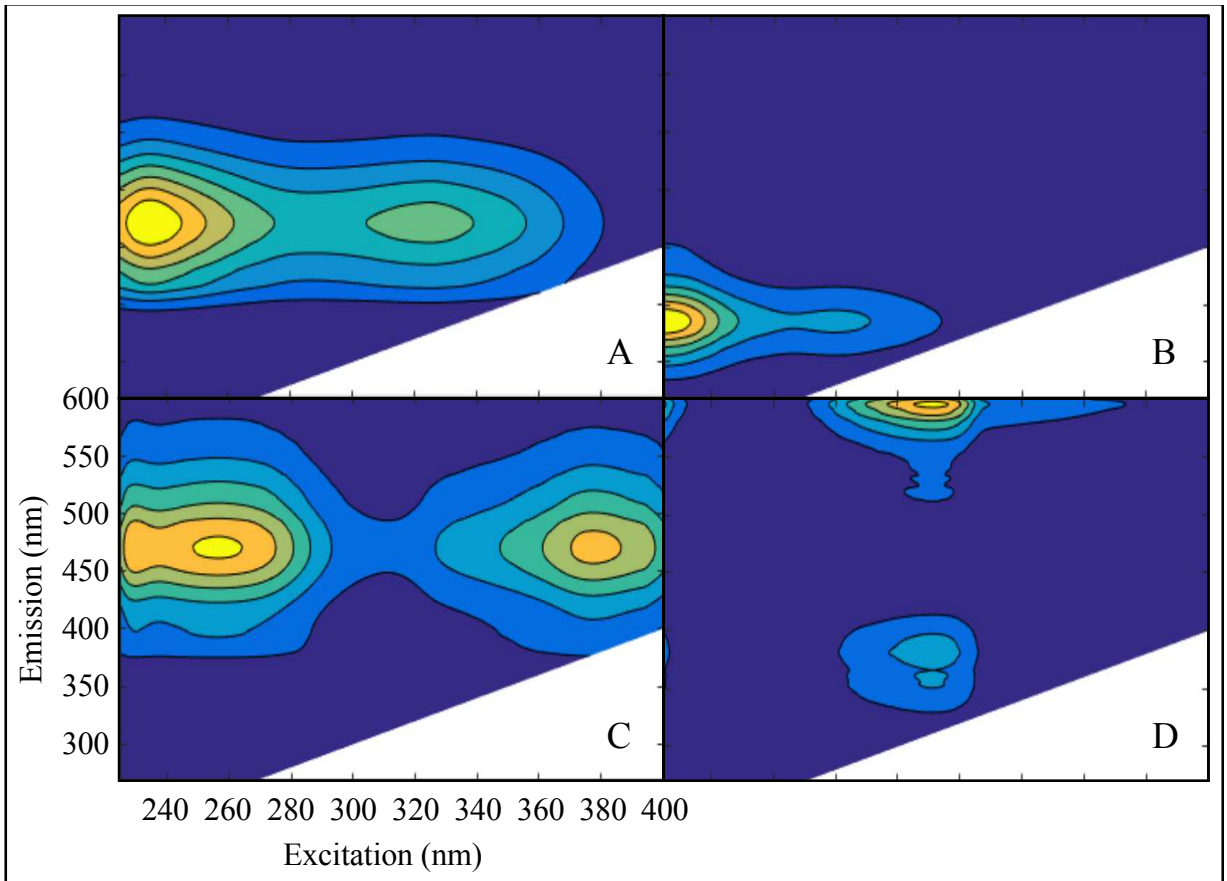

Figure S5. PARAFAC Component EEMs for Beaver Lake Raw Water. A) Component 1, B) Component 2 and D) Component 4 utilize the axes specified in C) Component 3.

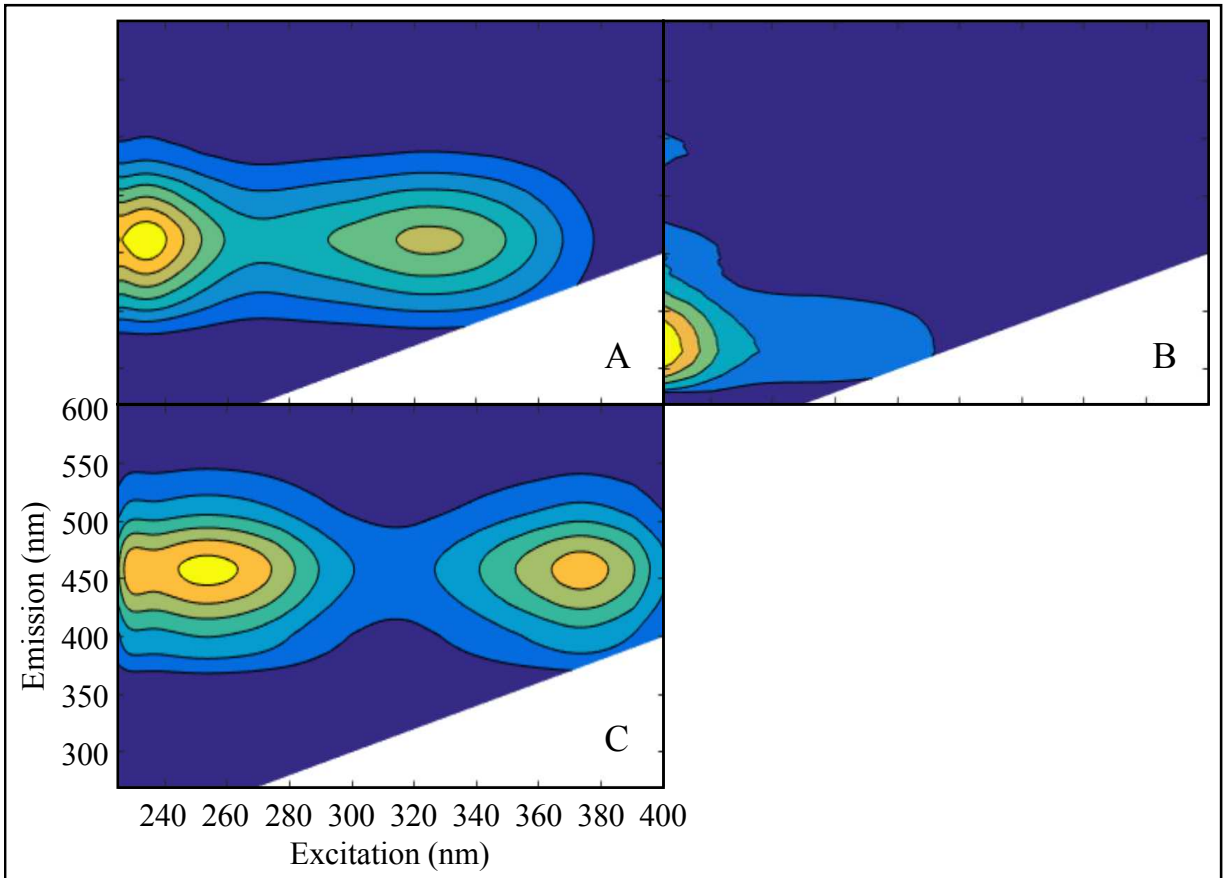

Figure S6. PARAFAC Component EEMs for West Side WWTP Effluent. A) Component 1 and B) Component 2 utilize the axes specified in C) Component 3.

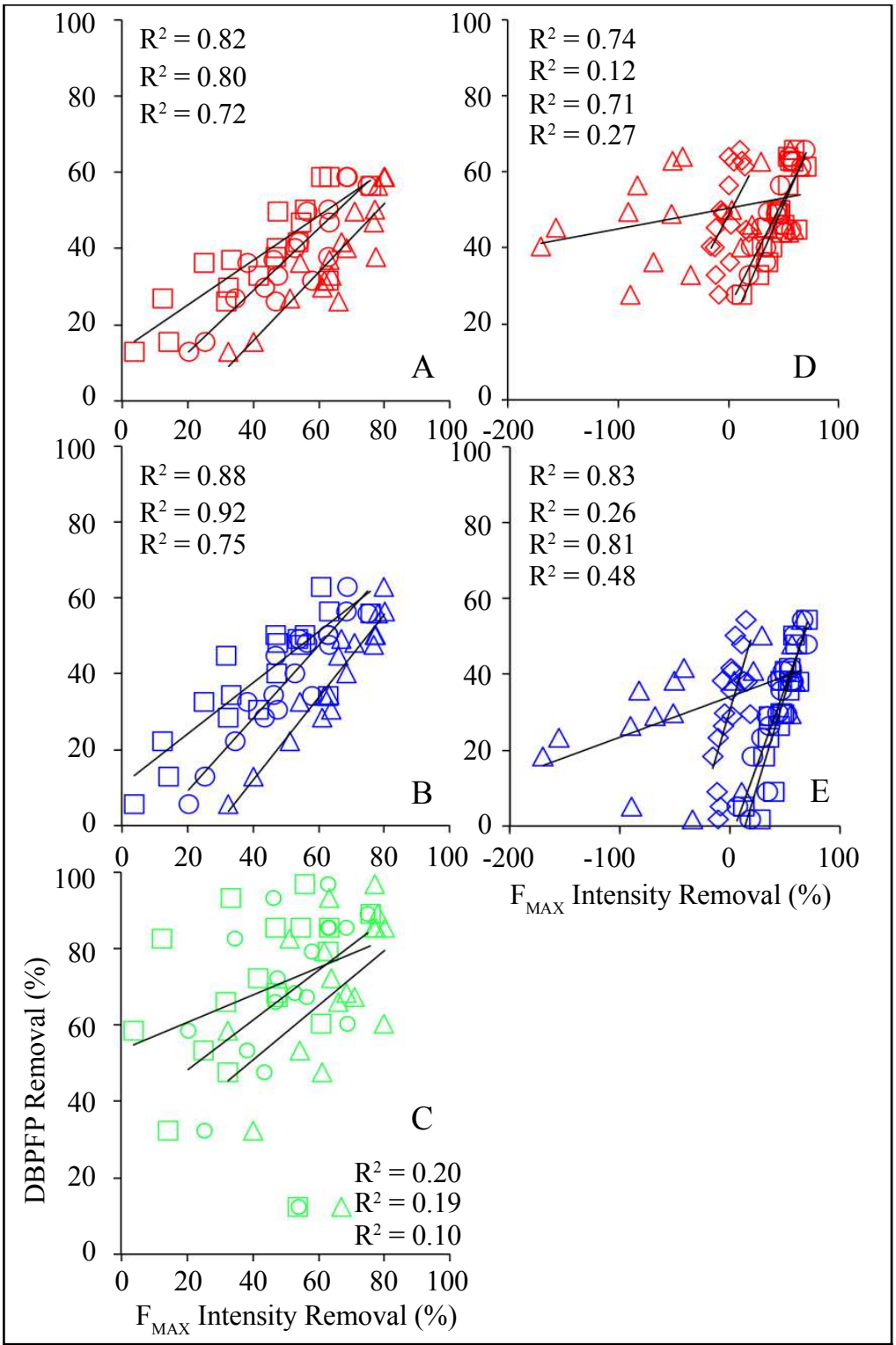

Figure S7. Linear regressions of DBPFP percent removal against percent removal of F_{MAX} of PARAFAC Components 1 (○), 2 (△), 3 (□), and 4 (◇) for TTHMFP, DHANFP, and TONOFP (Figures S8A-S8C) in WS-EFF and TTHMFP and DHANFP (Figures S8D and S8E) in BL-RAW. R^2 values appear according to numerical Component order.

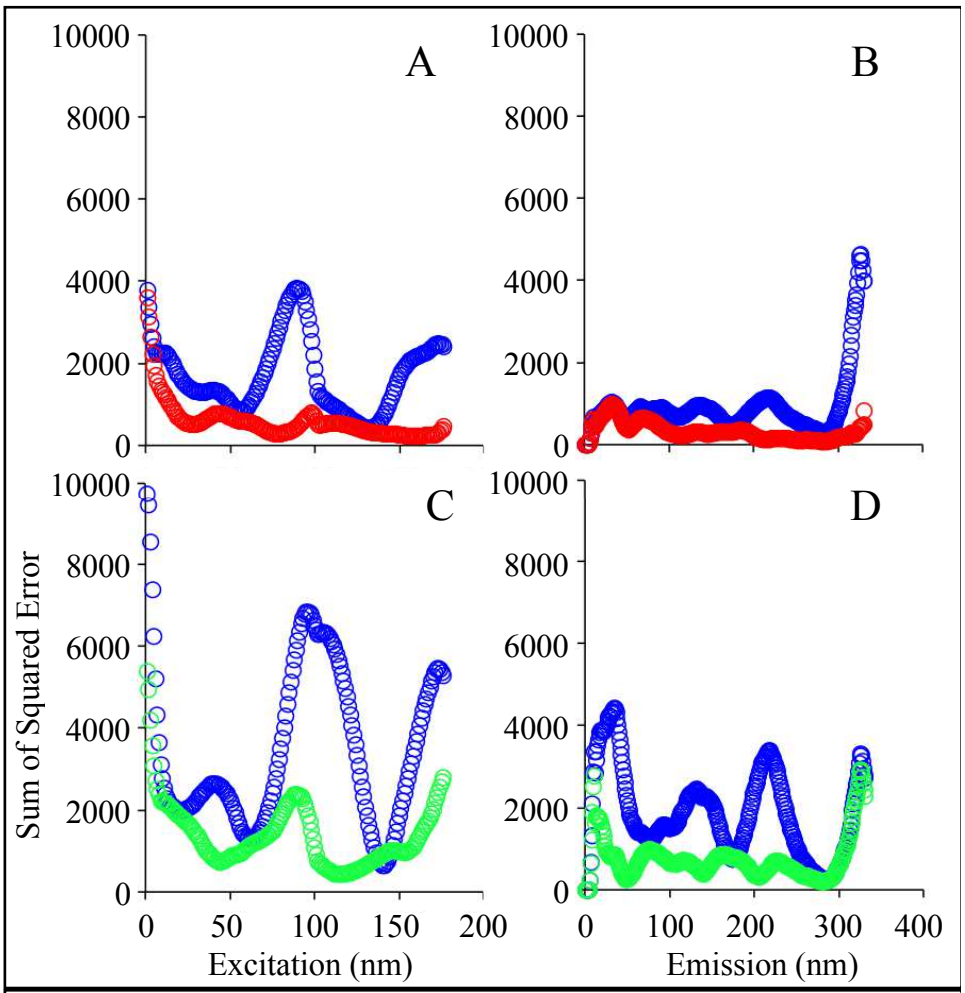

Figure S8. Sum of squared errors for excitation and emission wavelengths based on PARAFAC models with varying quantities of components. Two component (○) and 4 component (○ models were validated for BL-RAW (Figure S9A and S9B). Two component and three component (○) models were validated for WS-EFF (Figure S9C and S9D).

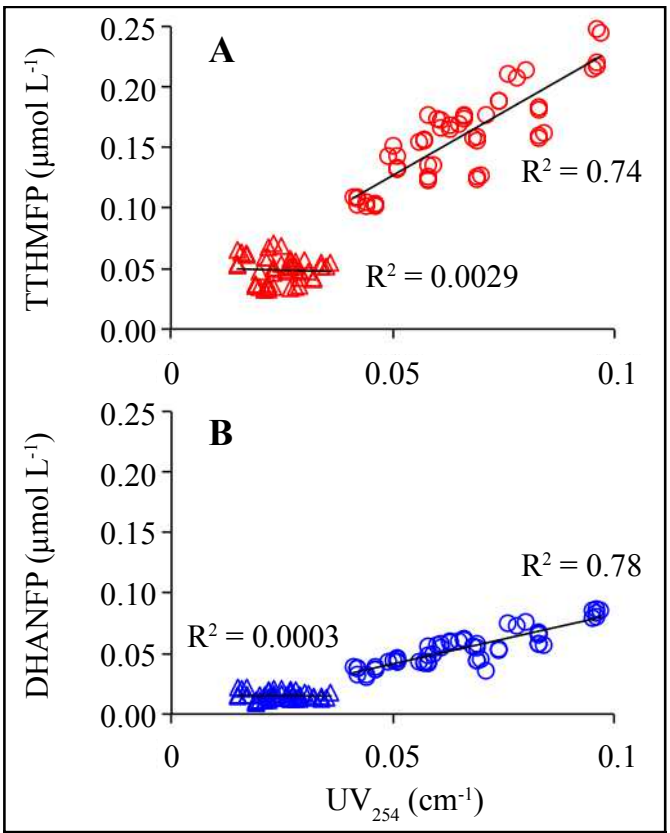

Figure S9. Linear regression of TTHMFP in BL-RAW (○) and WS-EFF (△) (Figure S10A) and DHANFP in BL-RAW (○) and WS-EFF (△) (Figure S10B).

References

Ago, H., Kugler, T., Cacialli, F., Salaneck, W. R., Shaffer, M. S. P., Windle, A. H. and Friend, R. H., 1999. Work functions and surface functional groups of multiwall carbon nanotubes. Journal of Physical Chemistry B 103 (38), 8116-8121.

Andersen, C. M. and Bro, R., 2003. Practical aspects of PARAFAC modeling of fluorescence excitation-emission data. Journal of Chemometrics 17 (4), 200-215.

Cory, R. M., Miller, M. P., McKnight, D. M., Guerard, J. J. and Miller, P. L., 2010. Effect of instrument-specific response on the analysis of fulvic acid fluorescence spectra. Limnology and Oceanography-Methods 8, 67-78.

Devore, J. L., 2004. Probability and statistics for engineering and the sciences, 6, Brooks/Cole, Thomson Learning, Belmont, CA.

Do, T. D., Chimka, J. R. and Fairey, J. L., 2015. Improved (and singular) disinfectant protocol for indirectly assessing organic precursor concentrations of trihalomethanes and dihaloacetonitriles. Environmental Science & Technology 49 (16), 9858-9865.

Hudson, N., Baker, A. and Reynolds, D., 2007. Fluorescence analysis of dissolved organic matter in natural, waste and polluted waters - A review. River Research and Applications 23 (6), 631-649.

Kovtyukhova, N. I., Mallouk, T. E., Pan, L. and Dickey, E. C., 2003. Individual single-walled nanotubes and hydrogels made by oxidative exfoliation of carbon nanotube ropes. Journal of the American Chemical Society 125 (32), 9761-9769.

Kristiana, I., Lethorn, A., Joll, C. and Heitz, A., 2014. To add or not to add: The use of quenching agents for the analysis of disinfection by-products in water samples. Water Research 59, 90-98.

Kundu, S., Xia, W., Busser, W., Becker, M., Schmidt, D. A., Havenith, M. and Muhler, M., 2010. The formation of nitrogen-containing functional groups on carbon nanotube surfaces: a quantitative XPS and TPD study. Physical Chemistry Chemical Physics 12 (17), 4351-4359.

Mayer, L. M., Schick, L. L. and Loder, T. C., 1999. Dissolved protein fluorescence in two Maine estuaries. Marine Chemistry 64 (3), 171-179.

McKnight, D. M., Boyer, E. W., Westerhoff, P. K., Doran, P. T., Kulbe, T. and Andersen, D. T., 2001. Spectrofluorometric characterization of dissolved organic matter for indication of precursor organic material and aromaticity. Limnology and Oceanography 46 (1), 38-48.

McPhail, M. R., Sells, J. A., He, Z. and Chusuei, C. C., 2009. Charging nanowalls: adjusting the carbon nanotube isoelectric point via surface functionalization. Journal of Physical Chemistry C 113 (32), 14102-14109.

Okpalugo, T. I. T., Papakonstantinou, P., Murphy, H., McLaughlin, J. and Brown, N. M. D., 2005. High resolution XPS characterization of chemical functionalised MWCNTs and SWCNTs. Carbon 43 (1), 153-161.

Pifer, A. D. and Fairey, J. L., 2014. Suitability of organic matter surrogates to predict trihalomethane formation in drinking water sources. Environmental Engineering Science 31 (3), 117-126.

Ramanathan, T., Fisher, F. T., Ruoff, R. S. and Brinson, L. C., 2005. Amino-functionalized carbon nanotubes for binding to polymers and biological systems. Chemistry of Materials 17 (6), 1290-1295.

Shapiro, S. S. and Wilk, M. B., 1965. An analysis of variance test for normality (complete samples). Biometrika 52, 591-611.

Singh, B., Fang, Y., Cowie, B. C. C. and Thomsen, L., 2014. NEXAFS and XPS characterisation of carbon functional groups of fresh and aged biochars. Organic Geochemistry 77, 1-10.

Wang, H., Zhou, A., Peng, F., Yu, H. and Yang, J., 2007. Mechanism study on adsorption of acidified multiwalled carbon nanotubes to Pb(II). Journal of Colloid and Interface Science 316 (2), 277-283.

Yan Yan, H. and Terentjev, E. M., 2012. Dispersion of carbon nanotubes: mixing, sonication, stabilization, and composite properties. Polymers 4 (1), 275-95.

Zepp, R. G., Sheldon, W. M. and Moran, M. A., 2004. Dissolved organic fluorophores in southeastern US coastal waters: correction method for eliminating Rayleigh and Raman scattering peaks in excitation-emission matrices. Marine Chemistry 89 (1-4), 15-36.

Zhang, Z., Pfefferle, L. and Haller, G. L., 2014. Comparing characterization of functionalized multi-walled carbon nanotubes by potentiometric proton titration, NEXAFS, and XPS. Chinese Journal of Catalysis 35 (6), 856-863.

Chapter 3

Revealing a Size-Resolved Fluorescence-Based Metric to Track Oxidative Treatment of Total *N*-nitrosamine Precursors in Wastewater-Derived Waters

Abstract

N-nitrosamines are a non-halogenated group of disinfection byproducts that form during chloramination, particularly in drinking waters impacted by wastewater treatment plant (WWTP) effluents. Here, we reveal a size-resolved fluorescence-based precursor surrogate to track total *N*-nitrosamine formation potential (TONOFP) through oxidative treatment. Samples were collected at seven WWTPs, at the finished effluent and prior to final disinfection (i.e., secondary effluent). Asymmetric flow field-flow fractionation (AF4) with inline fluorescence detection at an excitation-emission of 280/340 nm (i.e., $I_{280/340}$) showed protein-rich natural organic matter peaks between 10-445 kDa and 445-1,500 kDa. TONOFP was measured by chemiluminescence on samples dosed with 250 $mg \cdot L^{-1}$-Cl_2 monochloramine at pH 7 for seven days. Metrics from AF4-$I_{280/340}$ (i.e., area under the curve (AUC) and peak height) and $I_{257/277}$ from whole water excitation-emission matrices (EEMs) were leveraged in multivariate models to develop correlations with TONOFP. The TONOFP of the finished effluent divided by that of the secondary effluent (i.e., the *TONOFP Ratio*) was strongly correlated ($R^2 = 0.996$, $p = 0.000$) to a model of AUC for the 10-445 kDa peak, maximum peak height, and $I_{257/277}$. This TONOFP precursor surrogate requires 2 mL of sample and is transformational for assessing the impact of oxidative treatments on *N*-nitrosamine precursor concentrations.

1. Introduction

Drinking water sources impacted by wastewater treatment plant (WWTP) discharges contain natural organic matter (NOM) rich in organic nitrogen.[1] Chloramination, and to a lesser extent ozonation, chlorination, and chlorine dioxide disinfection (Sirivedhin and Gray, 2005), of waters containing WWTP-derived NOM results in formation *N*-nitrosamines, a non-halogenated group of disinfection byproducts (DBPs) (Krasner et al., 2013). Despite forming at low $ng \cdot L^{-1}$ levels, the high toxicity of *N*-nitrosamines has resulted in their consideration for regulation in drinking water (Hrudey and Charrois, 2012). The most commonly occurring *N*-nitrosamine in drinking waters is *N*-nitrosodimethylamine (NDMA), but studies by Mitch and colleagues have shown that NDMA may only comprise ~5% of total *N*-nitrosamines (TONO) in chloramine systems (Dai and Mitch, 2013).

Discovery of a spectroscopic surrogate for TONO precursors could be transformative for developing treatment processes to curb *N*-nitrosamines. Typically, TONO measurement requires 0.5-1.0 L samples (Dai et al., 2012) and takes a week or two to perform, which limits assessment of TONO precursor removal in lab-scale treatment processes. Similar to precursor surrogates for trihalomethanes (TTHMs) (Pifer and Fairey, 2012) and dihaloacetonitriles (DHANs) (Do et al., 2015), a useful surrogate would consist of spectroscopic measurement(s) on waters prior to chloramination that strongly correlate with the TONO formation potential (TONOFP). Preliminary work showed only moderate fluorescence-based correlations with TONOFP ($R^2 <$ 0.50) (Needham et al., 2016), but a recent study points to a possible improvement. Wang et al. (2015) showed that the presence of humics led to underestimation of proteins (35-52%) due to fluorescence quenching. This is notable because protein-like fluorophores are a likely source of TONO precursors (Krasner et al., 2013; Liao et al., 2014; Needham et al., 2016).

To quantify the true (i.e., unquenched) proteins, Wang et al. (2015) recommended separating the humic- and protein-like fractions by exploiting differences in their size distributions. As proteins are larger in molecular weight than humics, size-based separation prior to fluorescence measurement could facilitate more accurate assessments of protein-like fluorophores. Asymmetric flow field-flow fractionation (AF4) is a flow driven separation technology that has been used to measure NOM size distributions and requires no sample pre-concentration and low sample volumes (~0.5 mL) (Pifer et al., 2011). AF4 hyphenated with inline fluorescence detection (FLD) can potentially characterize protein-like fluorophores following separation from interfering humics, but no studies to which the authors are aware have employed this technique for assessing TONO precursors.

The objective of this study is to leverage AF4-based metrics of protein-like fluorophores to develop a TONO precursor surrogate. AF4-FLD fractograms were collected on WWTP effluents before and after oxidative treatments and lake waters with moderately high specific ultraviolet absorbance (SUVA) (Weishaar et al., 2003). Following chloramination of these samples, TONOFP was measured by chemiluminescence and correlations were sought using single and multiple regression. The resultant TONO precursor surrogate can be leveraged to assess the impact of oxidative treatments of *N*-nitrosamine precursor concentrations.

2. Materials and Methods

2.1. Sample Description and Water Quality Measurements

Fourteen sample waters were collected from seven WWTPs, from each plant effluent (called finished effluent) and prior to the final disinfection process (called secondary effluent), which included UV, ozonation, and chlorination. Lake waters were collected during the peak algal growing season from six lakes as algal organic matter is a known TONO precursor (Dai

and Mitch, 2013). Details regarding the sample waters are provided in Table 1. Sample waters were filtered with 0.45-µm polyethersulfone (PES) membranes pre-rinsed with 500 mL of Milli-Q water and stored in low-density polyethylene carboys at 4°C in the dark prior to use. Raw water characteristics were measured upon collection and are summarized in Tables 1, S1, and S2. Fluorescence excitation-emission matrices (EEMs) and water quality parameters were measured following Needham et al. (2016), with the exception of TDN, which is detailed in the SI. Dissolved organic nitrogen (DON) was calculated as the difference in between TDN and inorganic nitrogen (Table 1).

2.2. Experimental Procedures

2.2.1. DBPFP

DBP formation potential (DBPFP) was measured using the protocol developed by Do et al. (2015), which was modified from Standard Methods 5710-B and D (Pifer and Fairey, 2012), with a monochloramine dose of 250 $mg \cdot L^{-1}$ as Cl_2 at pH 7. TTHMFP and DHANFP were measured by gas chromatography with an electron capture detector to test the assumption that the AF4-FLD metrics were most applicable to TONOFP. While formation potential tests at pH 7 may not maximize formation of NDMA (Schreiber and Mitch, 2006), it was selected to achieve quantifiable concentrations of TONO while not incurring base-catalyzed destruction of DHAN (Hua and Reckhow, 2012), which would inhibit assessment of these precursors (Do et al., 2015). TONO analysis is preceded by solid phase extraction (SPE), modified from EPA Method 521, and adapted from Needham et al. (2016) by acidifying samples to pH 2 using sulfamic acid (Dai et al., 2012). An Eco Physics CLD 88sp chemiluminescence NO detector is used to quantify TONO, following the approach detailed by Mitch and Dai (2012). As some TONO can exist in

WWTP samples prior to formation potential tests, TONO measurements were made on secondary and finished effluent samples prior to chloramination.

2.2.2. AF4-FLD Fractograms

AF4-FLD fractograms were collected with a Postnova Analytics AF2000-MT AF4 system hyphenated with a dual monochromator fluorescence detector (Agilent Technologies). A 0.01 mM phosphate buffer at pH 7 was used as the system eluent. The AF4 separation channel was backed with a 10 kDa regenerated cellulose membrane and had a length of 27.4 cm and its width tapered from 2.0 cm near the inlet to 0.7 cm at the outlet. An autosampler was used to inject 0.5 mL of pre-filtered sample water (0.45 μm PES) onto the membrane. The AF4 method developed utilizes a combination of slot flow and high cross flow (Table S4). For the AF4 fractograms, fluorescence was measured at an excitation of 280 nm and a scan of emissions wavelengths between 305-500 nm at 5 nm step sizes to target wavelengths associated with protein-like fluorophores (Hudson et al., 2007). The fluorescence intensity excitation-emission wavelength pair chosen for fractograms was 280 and 340 nm, respectively (i.e., $I_{280/340}$), to maximize the signal to noise ratio. Fractogram x-axes were converted from elution time to molecular weight using a standard curve generated from measurements of polystyrene sulfonate (PSS) standards ranging from 30- to 1,000 kDa (Figure S1). The standard curve was applied to samples through an elution time of 25 minutes when the cross flow transitions to zero, after which the molecular weight is no longer quantifiable. PSS standards with molecular weights of 2,000- and 3,200 kDa were also measured, but did not elute until after the cross flow ceased and were not incorporated into the standard curve. They do, however, illustrate that this non-quantifiable fraction is likely comprised of high molecular weight compounds (i.e., above 1,500 kDa).

2.3. AF4-FLD Processing

AF4-FLD fractograms were analyzed to develop variables to be assessed as TONO precursor surrogates. Fractograms were divided into three sections beginning at an elution time of 8.50 minutes, which corresponds to the end of the void peak. Section 1 covers 8.50 to 14.88 minutes of elution time, with the latter corresponding to a local minimum calculated as the average of the elution times of the local minima of all fractograms. Section 2 covers 14.88 to 25 minutes, and Section 3 is the unquantifiable peak from 25 minutes through the end of the run. The area under the curve (AUC) within the three sections was calculated as the variables *AUC1*, *AUC2*, and *AUC3*. Additionally, the variable *Max* represents the maximum peak height in Sections 1 and 2 taken together. Exploration of the maximum peak height in the individual sections is included in the SI. An additional variable, *Intensity*, was utilized that originated from the EEMs of the unfractionated samples. Specifically, the fluorescence intensity at all wavelengths pairs was correlated to TONOFP to determine the point of maximum R^2, which for TONO was $I_{225/301}$. However, the independent variable *Intensity* was chosen as $I_{225/310}$ for TONO, which was the closest pair to $I_{225/301}$ that fell within previously reported ranges for nitrosamine precursors (Hudson et al., 2007). This *Intensity* value was used to determine which multivariate models showed promise, as detailed in Section 2.4. After significant models were identified, the models were recalculated with each of the 57,750 wavelength pairs measured in the EEMs to determine the best model. The wavelength pair corresponding to the best model is referred to as *Intensity**. Values of *AUC1-3*, *Max*, *Intensity*, and *Intensity** for TONO are provided in Table S5 and discussion of *Intensity* and *Intensity** for TTHM and DHAN are included in the SI.

2.4. Model Development

To assess correlations between TONOFP and AF4-FLD variables, several statistical models were developed. Models were also developed to explore correlations to TTHMFP and DHANFP and are detailed in the SI. Simple linear regression models were developed between TONOFP and each of the AF4-FLD variables and *DON*. Multiple regression models were formulated using combinations of *AUC1-3*, *Max*, *Intensity*, and *DON*. For all models, independent variables were assumed to be nonzero and significant if their coefficients had p-values less than 0.05. All R^2 values presented are adjusted for the number of independent variables to fairly compare models with differing numbers of variables (Montgomery, 2013). Additionally, all model types were explored for their suitability to predict the impact of oxidative treatment (i.e., chlorination, ozonation, and UV treatment) on DBPFP. Using only samples from WWTPs, *DBPFP Ratios* were generated as the formation potential of the finished effluent sample divided by that of the secondary effluent sample for each plant. These ratios indicate the change in DBP precursors from oxidative treatment (n = 7). Similarly, ratios were calculated for the independent variables from AF4-FLD, fluorescence EEMs, and water quality parameters, which included *AUC1-3*, *Max*, *Intensity*, and *DON*. For example, *AUC1 Ratio* is the value of *AUC1* for the finished effluent of a given WWTP divided by the *AUC1* of the secondary effluent sample from the same plant, as shown in Figure S2.

3. Results and Discussion

3.1. AF4-FLD

Figure 1 shows AF4-FLD fractograms (at $I_{280/340}$) for WWTP samples from the secondary effluent and finished effluent. Lake water samples are shown in Figure S3C. The AF4-FLD fractograms had peaks at approximately 11-, 20-, and 31 minutes, although precise peak maxima locations varied amongst the samples. Using Figure S1, the first peak corresponds to 10-445 kDa,

the second peak to 445-1,500 kDa, and the final peak is unquantifiable but likely corresponds to NOM larger than 1,500 kDa. For most of the WWTP samples, the intensity of these peaks decreased following disinfection, indicating partial oxidation or removal of these NOM fractions. However, in a few cases (i.e., Section 1 in Figure 1B, Sections 1-3 in Figure 1C, and Section 2 in Figure 1F), peak heights increased following disinfection, possibly due to physical breakdown of larger NOM (i.e., oxidation of material in Section 3 forming material in Section 1). The impact of the oxidative treatments on TONOFP is explored in subsequent sections.

3.2. Model Development

Models were first generated for the entire data set of TONOFP values (Table 1, n = 20). Neither simple linear or multivariate models produced strong correlations between TONOFP and AF4-FLD metrics or DON, with the strongest linear correlation being to *AUC1* (adjusted R^2 = 0.22). A maximum adjusted R^2 of 0.36 was obtained between TONOFP and *Intensity* ($I_{225/310}$), which was not an improvement over similar models in Needham et al. (2016).

Cursory comparison of TONOFP (Table 1) and *AUC1* (Table S5) indicated three of the four WWTPs utilizing UV disinfection had *higher* TONOFP in finished effluent samples compared to the secondary effluent samples, two of which were mirrored by similar responses in *AUC1*. This indicates that UV disinfection can generate TONO precursors, similar to the findings of Dai et al. (2015), particularly with the presence of coagulant aid polymers (McCurry et al., 2015). *DON Ratio* was not found to be significant in any multivariate models. While poor correlations were observed between *TONOFP* and *AUC1* in models comparing these values directly, notable correlations emerge in models between *TONOFP Ratio* (i.e., TONOFP of the finished effluent sample divided by that of the secondary effluent sample) and ratios of AF4-FLD metrics and *Intensity* (Figure 2). *Intensity* in the *TONOFP Ratio* models corresponds to

$I_{225/310}$, which falls in the region associated with protein-like fluorophores (Hudson et al., 2007). Simple linear regression between *TONOFP Ratio* and *AUC1 Ratio* yields an adjusted R^2 of 0.565 (Figure 2A). A multivariate model for *AUC1 Ratio* and *Max Ratio* (Figure 2B) has an adjusted R^2 of 0.847 and for *AUC1*-, *Max*-, and *Intensity Ratio* (Figure 2C) the adjusted R^2 is 0.983. The p-value of this model is 0.0008 indicating that the model is significant. A model of *AUC1*-, *Max*-, and *Intensity Ratio* was further refined using each of the available 57,750 wavelength pairs in each EEM for *Intensity Ratio*. The best-fitting correlation coefficient corresponded to $I_{257/277}$, with an adjusted R^2 value of 0.996 (Figure 2D). While this pair is outside the range typically reported for protein-like fluorophores, it is most closely adjacent to a subset of proteins, specifically tryptophan-like fluorophores.(Coble, 1996) The distribution of data indicates the model can predict *TONOFP Ratios* spanning from 0.136 to 1.701, encompassing both destruction and formation of TONO precursors from oxidative treatment. Another test of the model's robustness was an inquiry into the influence of individual observations, which indicated no single observation held undue influence on the model as a whole and is discussed further in the SI. Further, as strong correlations were only found for models of *TONOFP Ratio* rather than discrete values of *TONOFP*, the model cannot be utilized to predict individual values of TONOFP, but rather can be leveraged to predict the effect of oxidative treatment on TONO precursor concentrations.

To give further insight into the nature of the precursor surrogate, TONO was measured on the WWTP samples prior to chloramination (Table S3). These data indicate background TONO was present at concentrations ranging from 89-192 ng•L as NDMA, which comprised 7-54% of the TONO measured following the DBPFP tests. However, no significant models were generated excluding the background TONO (see details in the SI). This, coupled with the

strength of the models in which *TONOFP Ratios* were calculated including the background TONO (Figure 2), suggests that the independent variables in the model likely characterize the background TONO in addition to the protein-like TONO precursors that subsequently reacted with chloramines in the DBPFP tests. As such, it is likely that the background TONO affected the fluorescence-based metrics, a topic that should be studied systematically in future work.

The AF4-FLD method developed here is suitable for the separation and characterization of protein-like fluorophores in samples from WWTPs and lake waters with moderately high SUVA values. Following transformation of the data to indicate changes produced by oxidative treatment, multivariate analysis revealed a strong size-resolved fluorescence-based TONO precursor surrogate. With an adjusted R^2 of 0.996, a combination of AF4-FLD metrics (*AUC1* and *Max*) and fluorescence EEMs ($I_{257/277}$) can predict TONOFP ratios across a wide range in which TONO precursors were both created and destroyed.

3.3. Implications

As the fluorescence metrics require just 2 mL of sample, this TONO precursor surrogate could be leveraged to develop treatment processes to assess *N*-nitrosamine precursor concentrations. Upcoming studies include evaluation of this surrogate to assess other TONO precursor removal processes (i.e. sorption) and characterization of the chemical moieties within the 10-445 kDa and 445-1,500 kDa peaks. The novel AF4-FLD method could provide insights into the nature of protein-rich NOM relevant to other areas of environmental science, including membrane fouling and biofilm soluble microbial products.

4. Associated Content

Notes

The authors declare no competing financial interest.

Acknowledgements

Financial support from the National Science Foundation (CBET #1254350 to JLF) and the University of Arkansas Doctoral Academy Fellowship (to EMN) is gratefully acknowledged. The authors acknowledge Erik Pollock of the University of Arkansas Stable Isotopes Lab for running the total nitrogen samples.

5. Figures and Tables

Table 1. Sample Water Characteristics and Collection Details

Sample Name	Date Collected	Disinfection Method	pH	DOC (mg·L^{-1})	SUVA (L·mg^{-1}·□$^{-1}$)	DON[o] (mg·L^{-1})	TONOFP[p] (ng·L^{-1})	TTHMFP[q] (µg·L^{-1})	DHANFP[r] (µg·L^{-1})
BRV_SEC[a]	4/13/16	UV	7.81	10.1	1.79	13.78	2,640	73.2	20.6
BRV_FIN[b]	4/13/16	UV	7.69	12.3	1.54	16.59	359	87.3	20.2
BTN_SEC[c]	3/25/16	UV	7.53	5.4	1.86	3.07	973	37.3	10.4
BTN_FIN[c]	3/25/16	UV	7.85	5.5	1.79	2.82	1,655	38.1	10.2
NACA_SEC[d]	3/31/16	UV	7.65	7.9	1.64	4.64	1,603	58.1	15.7
NACA_FIN[d]	3/31/16	UV	7.69	7.8	1.60	6.28	2,398	50.8	12.1
NLD_SEC[e]	3/18/16	Ozone	7.82	9.6	1.30	2.85	1,576	52.0	14.2
NLD_FIN[e]	3/18/16	Ozone	7.73	8.1	0.78	2.87	241	33.1	3.4
RGS_SEC[f]	3/25/16	Chlorine	7.44	6.6	1.70	3.45	1,433	41.9	12.6
RGS_FIN[f]	3/25/16	Chlorine	7.69	6.7	1.54	3.67	462	38.1	10.9
SPD_SEC[g]	3/25/16	Chlorine	7.70	7.7	1.70	2.60	2,414	49.8	14.8
SPD_FIN[g]	3/25/16	Chlorine	7.64	7.5	1.57	2.47	1,724	47.1	13.7
WS_SEC[h]	3/17/16	UV	7.40	5.2	1.63	3.41	963	30.3	8.2
WS_FIN[h]	3/17/16	UV	7.78	5.3	1.55	3.41	1,016	29.3	8.0
CAL[i]	7/12/16	-	7.35	8.56	2.94	0.19	366	119.9	28.6
FAY[j]	7/1/16	-	8.10	4.48	1.44	ND	281	21.7	5.5
GRN[k]	7/12/16	-	8.11	6.71	1.59	ND	773	82.6	6.7
PTN[l]	7/1/16	-	7.42	2.91	1.92	ND	384	20.4	7.7
TUL[m]	7/1/16	-	8.12	4.41	2.64	ND	383	45.3	12.2
WIL[n]	6/21/16	-	8.03	6.89	2.54	ND	264	70.9	22.0

[a]*Berryville* Waste Water Plant, Berryville, AR; Secondary Effluent (SEC); [b]Finished *Effluent* (FIN) [c]*Bentonville* Wastewater Treatment Plant, Bentonville, AR; [d]*Northwest* Arkansas Conservation Authority Regional Treatment Facility, Bentonville, AR; [e]*Noland* Wastewater Treatment Facility, Fayetteville, AR; [f]*Rogers* Pollution Control, Rogers, AR; [g]*Springdale* Wastewater Treatment Plant, Springdale, AR; [h]*West* Side Wastewater Treatment Facility, Fayetteville, AR; [i]*Franklin* Township, AR; [j]*Fayetteville*, AR; [k]*Brinkley*, AR; [l]*Cabot*, AR; [m]*Influent* of A.B. Jewel Water Treatment Plant from Lake Oolagah, Tulsa, AR; [n]*Greenland* Township, AR; [o]*Dissolved* Organic Nitrogen; [p]*Total N*-Nitrosamine Formation Potential; [q]*Total* Trihalomethane Formation Potential; [r]*Dihaloacetonitrile* Formation Potential

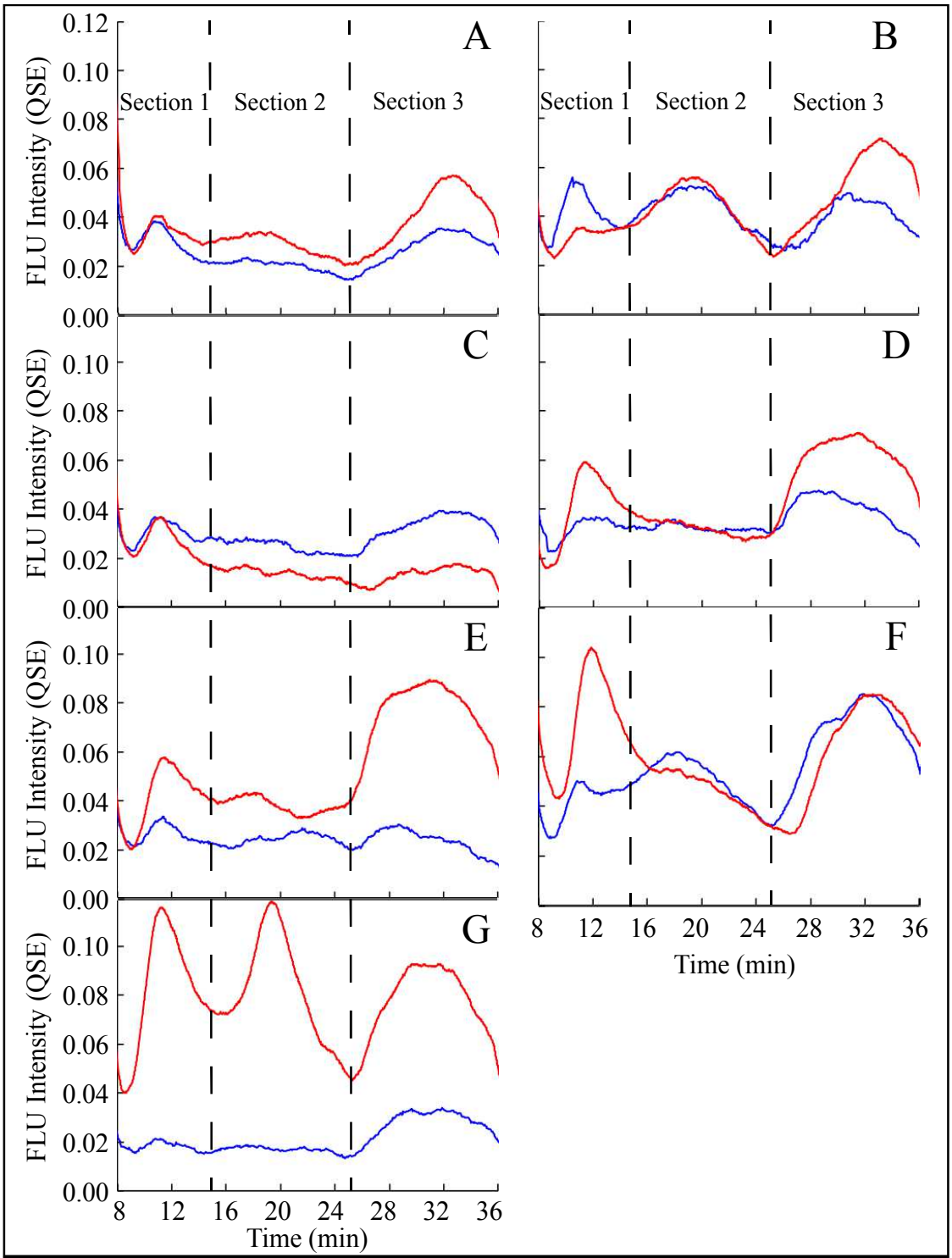

Figure 1. AF4-FLD fractograms ($I_{280/340}$) for WWTP samples taken prior to the final disinfection stage, referred to as secondary effluent (—), and finished effluent samples (—). BRV (Panel A), BTN (Panel B), NACA (Panel C), and WS (Panel D) WWTPs utilize UV disinfection; RGS (Panel E) and SPD (Panel F) use chlorine disinfection and NLD (Panel G) uses ozone disinfection. Dashed vertical lines indicate the times used to distinguish Sections 1-3 and the variables *AUC1-3*.

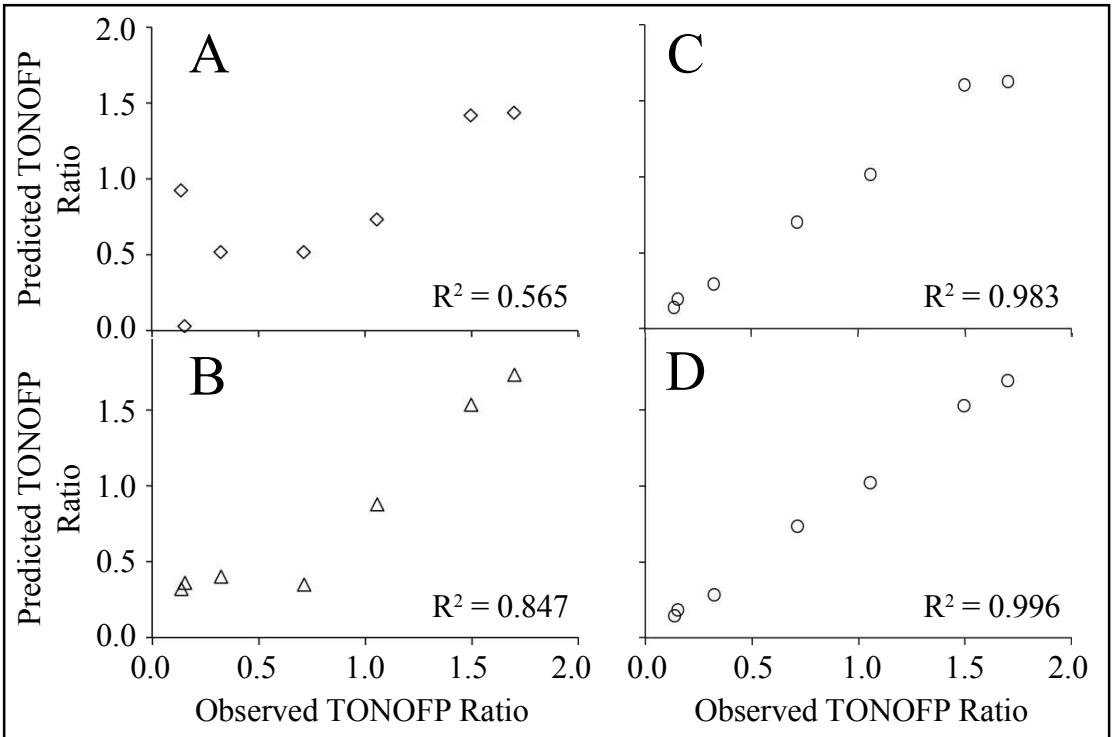

Figure 2. Multivariate models of *TONOFP Ratio* with *AUC1 Ratio* (Panel A), *AUC1*- and *Max Ratio* (Panel B), and *AUC1*-, *Max*-, and *Intensity Ratio* ($I_{225/310}$) (Panel C), and *AUC1*-, *Max*-, and *Intensity* Ratio* ($I_{257/277}$) (Panel D). Observed *TONOFP Ratios* were calculated for each WWTP as the TONOFP of the secondary effluent sample divided by the finished effluent sample. The model in Panel A is: *TONOFP Ratio* = 1.38 *AUC1 Ratio* - 0.23. The model in Panel B is: *TONOFP Ratio* = 3.97 *AUC1 Ratio* - 3.44 *Max Ratio* + 0.23. The model in Panel C is: *TONOFP Ratio* = 4.56 *AUC1 Ratio* - 5.04 *Max Ratio* + 0.75 *Intensity Ratio* - 0.01. The model in Panel D is: *TONOFP Ratio* = 4.12 *AUC1 Ratio* - 4.36 *Max Ratio* + 0.63 *Intensity* Ratio* - 0.09. All R^2 values are adjusted for the number of independent variables.

6. References

Coble, P. G., 1996. Characterization of marine and terrestrial DOM in seawater using excitation emission matrix spectroscopy. Marine Chemistry 51 (4), 325-346.

Dai, N. and Mitch, W. A., 2013. Relative importance of N-nitrosodimethylamine compared to total N-nitrosamines in drinking waters. Environmental Science & Technology 47 (8), 3648-3656.

Dai, N., Shah, A. D., Hu, L. H., Plewa, M. J., McKague, B. and Mitch, W. A., 2012. Measurement of Nitrosamine and Nitramine Formation from NO Reactions with Amines during Amine-Based Carbon Dioxide Capture for Postcombustion Carbon Sequestration. Environmental Science & Technology 46 (17), 9793-9801.

Dai, N., Zeng, T. and Mitch, W. A., 2015. Predicting N-Nitrosamines: N-Nitrosodiethanolamine as a Significant Component of Total N-Nitrosamines in Recycled Wastewater. Environmental Science & Technology Letters 2 (3), 54-58.

Do, T. D., Chimka, J. R. and Fairey, J. L., 2015. Improved (and singular) disinfectant protocol for indirectly assessing organic precursor concentrations of trihalomethanes and dihaloacetonitriles. Environmental Science & Technology 49 (16), 9858-9865.

Hrudey, S. E. and Charrois, J. W. A., Eds. (2012). Disinfection by-products and human health. IWA Publishing and Australian Water Association, London.

Hua, G. H. and Reckhow, D. A., 2012. Evaluation of bromine substitution factors of DBPs during chlorination and chloramination. Water Research 46 (13), 4208-4216.

Hudson, N., Baker, A. and Reynolds, D., 2007. Fluorescence analysis of dissolved organic matter in natural, waste and polluted waters - A review. River Research and Applications 23 (6), 631-649.

Krasner, S. W., Mitch, W. A., McCurry, D. L., Hanigan, D. and Westerhoff, P., 2013. Formation, precursors, control, and occurrence of nitrosamines in drinking water: A review. Water Research 47 (13), 4433-4450.

Liao, X. B., Wang, C. K., Wang, J., Zhang, X. J., Chen, C., Krasner, S. W. and Suffet, I. H., 2014. Nitrosamine precursor and DOM control in effluent-affected drinking water. Journal American Water Works Association 106 (7), 81-82.

McCurry, D. L., Krasner, S. W., von Gunten, U. and Mitch, W. A., 2015. Determinants of disinfectant pretreatment efficacy for nitrosamine control in chloraminated drinking water. Water Research 84, 161-170.

Mitch, W. A. and Dai, N. (2012). Water Research Foundation Report #4209: Development and application of a total nitrosamine assay for disinfected waters, Water Research Foundation.

Montgomery, D. C., 2013. Applied Statistics and Probability for Engineers, 6th Edition, John Wiley & Sons.

Needham, E. M., Sidney, S. M., Chimka, J. R. and Fairey, J. L., 2016. Trihalomethane, dihaloacetonitrile, and total N-nitrosamine precursor adsorption by carbon nanotubes: the importance of surface oxides and pore volume. Environmental Science-Water Research & Technology 2 (6), 1004-1013.

Pifer, A. D. and Fairey, J. L., 2012. Improving on $SUVA_{254}$ using fluorescence-PARAFAC analysis and asymmetric flow-field flow fractionation for assessing disinfection byproduct formation and control. Water Research 46 (9), 2927-2936.

Pifer, A. D., Miskin, D. R., Cousins, S. L. and Fairey, J. L., 2011. Coupling asymmetric flow-field flow fractionation and fluorescence parallel factor analysis reveals stratification of dissolved organic matter in a drinking water reservoir. Journal of Chromatography A 1218 (27), 4167-4178.

Schreiber, I. M. and Mitch, W. A., 2006. Nitrosamine formation pathway revisited: The importance of chloramine speciation and dissolved oxygen. Environmental Science & Technology 40 (19), 6007-6014.

Sirivedhin, T. and Gray, K. A., 2005. 2. Comparison of the disinfection by-product formation potentials between a wastewater effluent and surface waters. Water Research 39 (6), 1025-1036.

Wang, Z. G., Cao, J. and Meng, F. G., 2015. Interactions between protein-like and humic-like components in dissolved organic matter revealed by fluorescence quenching. Water Research 68, 404-413.

Weishaar, J. L., Aiken, G. R., Bergamaschi, B. A., Fram, M. S., Fujii, R. and Mopper, K., 2003. Evaluation of specific ultraviolet absorbance as an indicator of the chemical composition

and reactivity of dissolved organic carbon. Environmental Science & Technology 37 (20), 4702-4708

Appendix 2

Supplementary Information for

"Revealing a Size-Resolved Fluorescence-Based Metric to Track Oxidative Treatment of Total *N*-nitrosamine Precursors in Wastewater-Derived Waters"

List of Supporting Information

Dissolved Organic Nitrogen Method and Calculations

Fractogram Peak Maxima

Models of TTHMFP and DHANFP

Background TONO

Influence of Individual Observations

TONOFP Method Development

Table S1. Raw Water Anion and Cation Concentrations

Table S2. Total Dissolved Nitrogen

Table S3. TONO in WWTP Samples Prior to Formation Potential Tests

Table S4. AF4 Method Details

Figure S1. AF4-FLD Standard Curve

Table S5. Raw Data for Variables in Model of TONOFP Ratio

Figure S2. Derivation of Variables from AF4-FLD Fractograms and Fluorescence EEMs

Figure S2. AF4-FLD Fractograms for All Samples

Table S6. Multivariate Models of TONOFP-, TTHMFP-, and DHANFP Ratio

Table S7. Influence of Observations

Figure S3. SPE Standard Curves

Figure S4. TONO Reaction Chamber Degradation

Dissolved Organic Nitrogen Method and Calculations

Total dissolved nitrogen (TDN) was measured using a Shimadzu TOC/TN analyzer with a 6-point standard curve and is given in Table S2. Dissolved organic nitrogen was calculated as the difference between the measured TDN and the sum of nitrate, nitrite, and ammonium expressed as $mg \bullet L^{-1}$ as N (Table S1) and is reported in Table 1.

Fractogram Peak Maxima

The variable *Max* utilized in the significant model of *TONOFP Ratio* against *AUC1-*, *Max-*, and *Intensity Ratio* is derived from the maximum peak height of Sections 1 and 2 of the AF4-FLD fractograms. The variables *AUC1-3* are specific to Sections 1-3, but *Max* is calculated from the range of Sections 1 and 2 together. The variables *Max1 Ratio* and *Max2 Ratio* were also calculated as the maximum peak height in Sections 1 and 2, respectively. These variables were used in place of *Max Ratio* in the same model with three independent variables that was previously significant. However, the inclusion of either *Max1 Ratio* or *Max2 Ratio* made all of the variables in the model insignificant and the adjusted R^2 values drop from 0.988 to 0.339 and 0.352, respectively.

Models of TTHMFP and DHANFP

Similarly to the determination of *Intensity* for TONOFP, initial wavelength pairs were determined based on simple linear correlations between TTHMFP or DHANFP and fluorescence EEMs. For TTHMFP, the best linear correlations existed at $I_{226/421}$ and the best correlations for DHANFP were at $I_{227/592}$, both of which are similar to values found in the literature (Hudson et al., 2007). Using these *Intensity* values for TTHMFP and DHANFP, no multivariate models could be developed in which all independent variables were significant (Table S6). Maximum linear correlations to AF4-FLD metrics for TTHMFP (adjusted R^2 = -0.05) and DHANFP

(adjusted R^2 = -0.03) were also weak. This is an expected result given that protein-like fluorophores (i.e., those characterized by the AF4-FLD technique employed in this study) are not likely precursors of TTHMs and DHANs. Rather, humic substances are widely considered to be precursors of these groups of DBPs, which have been shown to be approximately 0.1-8 kDa in size (Her et al., 2002). This range is smaller than the pore size of the 10 kDa regenerated cellulose membrane used for AF4 separation and the size range for *AUC1* (10-445 kDa), one of the significant variables in the *TONOFP Ratio* model. As such, it is likely that the weak correlation coefficients with TTHMFP and DHANFP indicate that the AF4 method is not measuring the humic-like precursors of these DBP types, but only the larger protein-like precursors of TONO. The data analysis method described in Section 2.3, in which models including EEM intensity are generated for each of the 57,750 wavelength pairs, was also applied to models of *TTHMFP Ratio* and *DHANFP Ratio*. In single variable models of *DBPFP Ratio* against all Intensity values, the best correlation was $I_{226/596}$ for *TTHMFP Ratio* and $I_{225/531}$ for *DHANFP Ratio*. These models had adjusted R^2 values of 0.899 and 0.990, respectively. If variables such as *AUC1 Ratio* and *Max Ratio* (as are used in the best multivariate model of *TONOFP Ratio*) are applied to models of *TTHMFP*- and *DHANFP Ratio*, the adjusted R^2 values can be improved to 0.990 and 0.998, respectively. However, the modest improvement on already strong models confirms the previous assumption that the AF4-FLD method is not likely relevant to precursors of TTHMs and DHANs.

Background TONO

TONO in WWTP samples was measured prior to the formation potential tests (referred to as background TONO) and following chloramination (referred to as TONOFP in Table 1, but these values include the background TONO) by solid phase extraction (SPE) and

chemiluminescence detection (Table S3). The background TONO was subtracted out to determine the amount of TONO that formed from chloramination in the formation potential tests (referred to as the adjusted TONOFP). Additional models were generated with these adjusted TONOFP values; the models used the same values of *A1 Ratio*, *Max Ratio*, and *Intensity Ratio*. A model of *Adjusted TONOFP Ratio* against only *A1 Ratio* had an adjusted R^2 value of -0.058. When *Adjusted TONOFP Ratio* was modeled against *A1 Ratio* and *Max Ratio*, the adjusted R^2 value was -0.222. Finally, a model of *A1*-, *Max*-, and *Intensity Ratio* against *Adjusted TONOFP Ratio* yielded an adjusted R^2 value of -0.291. The correlation coefficients of the same variables modeled against *TONOFP Ratio* (rather than *Adjusted TONOFP Ratio*) yielded adjusted R^2 values of 0.565, 0.847, and 0.983, respectively. Ultimately, there is no correlation between the AF4-FLD and fluorescence EEM metrics and the TONOFP when the background TONO in the samples is corrected for and excellent correlations exist when values of TONOFP include background TONO and TONO formed during formation potential tests. This indicates that it is likely that the independent variables in the model incorporate information about both the TONO precursors and the background *N*-nitrosamines in the untreated water.

Influence of Individual Observations

To test the robustness of the model of *TONOFP Ratio* against *AUC1*-, *Max*-, and *Intensity Ratio*, the data set was manipulated by removing the observations from each WWTP one at a time and observing the effect on the correlation coefficient and significance of the model. This process was conducted for models of TONO, TTHM, and DHAN and the results are given in Table S8. The intent of the test is to observe changes in the model resulting from the removal of a given observation and determine if that observation has comparatively more influence than the other six observations. For the model of TONO, the adjusted R^2 is 0.983 when using all

seven observations and ranges from 0.983-0.996 when each of the points is removed from the data set. Similarly, the p-value is initially 0.0008 and ranges from 0.0027-0.0102 during the test. For comparison, the model of TTHM has an initial adjusted R^2 value of 0.680, but ranges from 0.007 to 0.950 if select points are removed. Similarly, the model of DHAN varies from its initial adjusted R^2 of 0.810 to a range of -0.254 to 0.994. In essence, the models of TTHM and DHAN show large variation when only one observation is removed, in contrast to the small variations observed in the model for TONO.

TONOFP Method Development

Published studies involving TONO measurements do not fully address the issues of sample injection volume and reaction chamber degradation. In cases where the maximum injection volumes are provided (Mitch and Dai, 2012), they are not accompanied by a fulsome explanation as to why certain volumes were selected. Similarly, degradation of the reaction chamber sensitivity over time and due to sample injection volume is also not discussed in detail. Additionally, TONO standard curves are not prepared in the same manner as samples, but instead injected directly into the reaction chamber without first being subjected to the SPE process.

The first step to address these issues was to develop a method for running NDMA standards through the same SPE process as unknown samples. Standards consisting of NDMA were diluted in 500 mL volumes of water (i.e., the same used for unknown samples) and analyzed using the process described in Needham et al. (2016). Figure S4 shows six standard curves generated from the SPE-TONO procedure, which were used in six different TONO runs. The differences between each standard curve in Figure S4 were attributed to differing reaction chamber compositions, but all had strong linear relationships as indicated by the high R^2 values

($R^2 > 0.98$). Subjecting standards to the SPE process is preferred for future TONO analyses due to the variation amongst these standard curves.

Experience with the TONO reaction chamber shows that the detector response decreases with increasing cumulative injection volume. Additionally, the resultant concentrations can vary with changes in the injection volumes, which is undesirable for unknown samples. Based on injections of identical masses of NDMA using varying injection volumes, an ideal range of injection volumes was identified (50-200 μL), which balances the needs to achieve adequate NDMA recovery while minimizing disturbances to the detector baseline or changes in peak width. To account for degradation of the reaction chamber, standards that have undergone the SPE process are impractical given the time and resource requirements needed. Instead, direct inject (D-Inj) standards were used, in which NDMA standards prepared in methanol were pretreated with 20 $g \cdot L^{-1}$ mercuric chloride in Milli-Q water and 50 $g \cdot L^{-1}$ sulfanilamide in 1 N HCl and injected directly into the TONO reaction chamber without going through the SPE process. A TONO run was conducted with alternating 100 μL injections of standards subjected to SPE and D-Inj standards of similar mass (Figure S5). Detector response appears roughly constant for both D-Inj and SPE standards until a cumulative injection volume of approximately 900 μL. Thereafter, the response of both standards decreases linearly through the end of the run. Based on preliminary data, recent TONO measurements included D-Inj standard injections at the beginning of each run, after the standard curve, and at the end of each run. These data indicate a similar phenomenon that is reminiscent of a piecewise mathematical function. While the slopes of the decreasing portions of each data set in Figure S5 are not equal, their similarity allows for some correction for detector response degradation using periodic D-Inj standards throughout TONO runs. This method is preferable to the use of SPE standards due to the time and labor

required to obtain them. While imperfect, this method was deemed an appropriate signal adjustment technique, in contrast to an assumption that chamber degradation does not occur, and was adopted for use before and after the standard curve and after the unknown samples in the run, to allow the sample concentrations to be corrected for the degradation of the TONO reaction chamber.

Table S1. Raw Water Anion and Cation Concentrations

Sample Name[a]	Anion Concentration (mg•L^{-1})[b]							Cation Concentration (mg•L^{-1})				
	F^-	Cl^-	NO_2^-	Br^-	NO_3^-	PO_4^{2-}	SO_4^{2-}	Na^+	K^+	NH_4^+	Ca^{2+}	Mg^{2+}
BRV_SEC	0.9	210.5	ND[c]	0.2	12.6	2.1	148.1	244.4	25.2	ND	7.9	22.3
BRV_FIN	ND	2.5	ND	ND	ND	6.6	217.4	24.3	2.5	ND	0.8	5.2
BTN_SEC	0.8	13.5	0.2	0.5	1.9	0.4	22.3	27.3	9.8	ND	3.2	41.5
BTN_FIN	0.8	13.5	0.2	0.6	1.9	0.4	22.1	27.4	9.9	ND	3.1	40.6
NACA_SEC	0.8	25.3	ND	0.6	2.9	0.4	21.5	4.9	1.4	ND	0.5	4.5
NACA_FIN	0.8	24.5	ND	0.6	2.8	ND	20.9	4.8	1.4	ND	0.4	4.4
NLD_SEC	ND	2.6	ND	ND	ND	82.7	40.9	5.4	1.5	ND	0.6	5.2
NLD_FIN	ND	2.6	ND	ND	ND	ND	37.8	5.4	1.5	ND	0.6	5.2
RGS_SEC	0.8	31.4	ND	0.5	2.3	0.5	36.2	63.2	11.8	ND	2.8	48.0
RGS_FIN	0.8	33.3	0.2	ND	2.4	ND	37.9	63.9	12.1	ND	2.8	48.8
SPD_SEC	0.9	44.5	ND	ND	1.5	0.4	58.3	100.6	24.0	ND	2.8	30.8
SPD_FIN	0.9	45.5	ND	ND	1.5	ND	59.4	100.2	24.1	ND	2.8	31.0
WS_SEC	ND	2.5	ND	0.4	ND	ND	53.6	28.8	7.2	ND	4.8	47.7
WS_FIN	ND	2.5	ND	ND	ND	ND	55.8	30.0	7.3	ND	4.7	48.4
CAL	0.1	12.7	ND	0.4	0.1	0.4	1.53	6.9	1.3	ND	1.5	5.0
FAY	0.1	4.72	ND	0.3	0.2	ND	7.00	4.1	2.1	0.5	1.9	38.1
GRN	0.2	51.7	ND	0.5	ND	0.5	36.9	31.7	1.4	1.5	17.4	25.4
PTN	0.1	1.68	ND	0.3	0.1	ND	3.45	3.3	0.7	ND	0.8	2.0
TUL	0.2	11.6	ND	0.3	0.2	ND	60.3	10.3	3.1	ND	10.1	46.3
WIL	0.1	1.74	ND	0.3	0.1	0.4	4.13	1.9	1.2	0.2	1.9	24.9

[a] *See* Table 1 for details regarding the Sample Names

[b] *Nitrite* and nitrate reported as mg•L^{-1} as N

[c] *Not* detected

Table S2. Total Dissolved Nitrogen and conductivity

Sample Name[a]	Total Dissolved Nitrogen ($mg \bullet L^{-1}$)	Conductivity ($\mu S \bullet cm^{-1}$)
BRV_SEC	16.63	1,520
BRV_FIN	16.59	1,559
BTN_SEC	5.14	453
BTN_FIN	4.85	453
NACA_SEC	7.51	598
NACA_FIN	9.07	591
NLD_SEC	2.85	653
NLD_FIN	2.87	661
RGS_SEC	5.71	668
RGS_FIN	6.24	685
SPD_SEC	4.12	835
SPD_FIN	4.02	845
WS_SEC	3.41	490
WS_FIN	3.41	492
CAL	0.25	87
FAY	0.18	252
GRN	0.90	463
PTN	0.00	39
TUL	0.00	333
WIL	0.00	164

[a] See Table 1 for details regarding the Sample Names

Table S3. TONO in WWTP Samples Prior to Formation Potential Tests

Sample Name[a]	TONO[b] Prior to FP[c] Tests (ng•L^{-1} as NDMA)	Percentage of TONOFP[d] (%)
BRV_SEC	182	7
BRV_FIN	192	53
BTN_SEC	130	13
BTN_FIN	123	7
NACA_SEC	165	10
NACA_FIN	93	4
NLD_SEC	143	9
NLD_FIN	130	54
RGS_SEC	93	6
RGS_FIN	97	21
SPD_SEC	149	6
SPD_FIN	119	7
WS_SEC	89	9
WS_FIN	94	9

[a] *See* Table 1 for details regarding the Sample Names. [b] Total *N*-nitrosamines. [c] Formation potential. [d] TONO formation potential

Table S4. AF4 Method Details

Stage	Time (min)	Tip Flow ($mL \bullet min^{-1}$)	Focus Flow ($mL \bullet min^{-1}$)	Cross Flow ($mL \bullet min^{-1}$)	Slot Flow ($mL \bullet min^{-1}$)	Profile
Focusing	0	0.2	1.8	1.0	0.5	Constant
Transition	5	0.2	1.8	1.0	0.5	Linear
Elution	6	2.0	0	1.0	0.5	Constant
	8	2.0	0	1.0	0.5	Linear
	10	1.1	0	0.1	0.5	Constant
	25	1.1	0	0.1	0.5	Linear
	26	1.0	0	0	0.5	Constant
	36	1.0	0	0	0.5	-

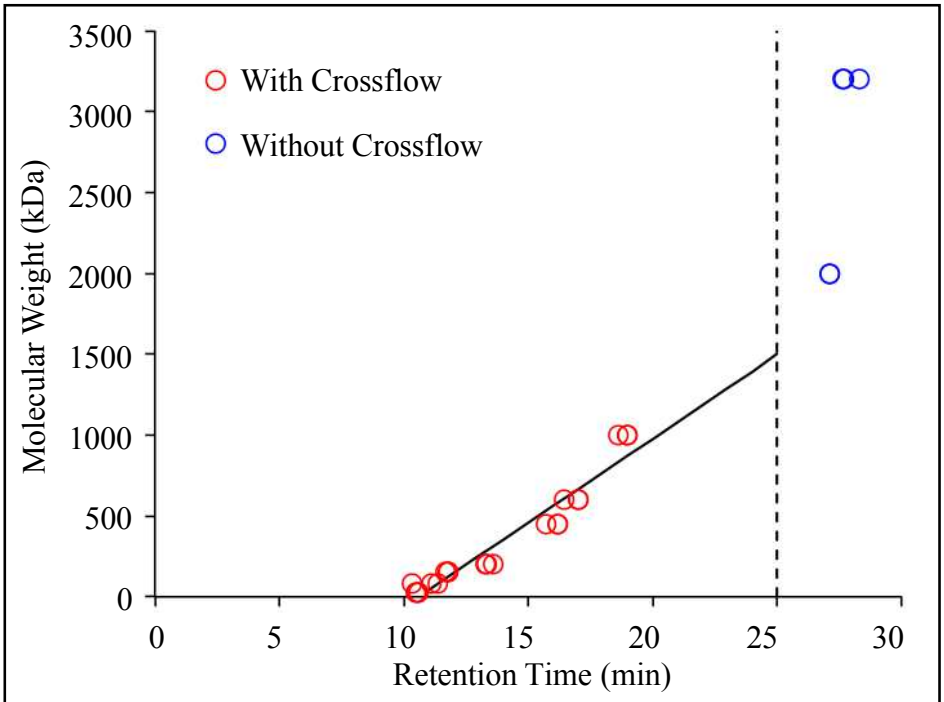

Figure S1. AF4-FLD standard curve generated from the elution time peak maxima of various sizes of polystyrene sulfonate (PSS) standards and with a linear fit of y = 104.1x - 1 104.2 (R^2 = 0.929). Only PSS standards that eluted during crossflow were used in the standard curve.

Table S5. Raw Data for Variables in Model of TONOFP Ratio

Sample Name[a]	*AUC1*[b]	*AUC2*	*AUC3*	*Max*	*Intensity*[c]			*Intensity**[g]		
					TONO[d]	**TTHM**[e]	**DHAN**[f]	**TONO**[h]	**TTHM**[i]	**DHAN**[j]
BRV_SEC	15.18	30.28	48.35	0.041	16.19	70.67	1.87	1.69	1.45	10.20
BRV_FIN	12.76	21.08	33.16	0.038	20.41	77.99	2.35	2.35	2.17	11.57
BTN_SEC	15.51	46.50	61.59	0.056	10.57	30.48	1.18	1.29	1.25	5.88
BTN_FIN	18.83	46.19	46.41	0.054	15.00	33.41	1.48	1.97	1.51	6.27
NACA_SEC	11.82	14.55	15.26	0.037	14.78	48.48	1.92	1.63	1.86	8.40
NACA_FIN	14.21	26.19	39.65	0.037	23.59	53.55	1.96	2.72	1.67	7.87
NLD_SEC	42.85	85.64	90.87	0.118	27.53	45.49	1.73	2.75	1.75	8.28
NLD_FIN	8.20	17.78	33.00	0.022	8.60	16.62	0.98	1.21	1.12	3.45
RGS_SEC	22.30	40.13	89.63	0.058	16.60	33.56	1.39	1.80	1.49	5.98
RGS_FIN	12.17	25.52	27.98	0.034	15.94	32.45	1.68	1.85	1.65	6.07
SPD_SEC	38.61	50.85	76.74	0.104	16.19	42.63	1.57	1.50	1.64	7.21
SPD_FIN	21.10	53.48	80.78	0.062	26.15	46.15	1.57	2.76	2.02	7.66
WS_SEC	22.27	33.83	71.03	0.059	13.53	26.88	1.17	1.66	1.14	4.72
WS_FIN	15.59	33.97	47.03	0.037	16.88	29.81	1.50	2.41	1.46	5.30
CAL	11.60	28.01	83.35	0.033	16.69	116.84	3.27	1.03	3.00	31.76
FAY	17.08	39.22	37.79	0.056	5.15	19.36	0.68	0.56	0.76	4.02
GRN	3.48	22.01	14.24	0.035	9.16	54.99	1.58	0.61	1.30	12.60
PTN	2.50	5.22	11.19	0.008	10.42	41.35	1.48	0.88	1.35	9.67
TUL	3.39	10.05	16.16	0.012	6.06	46.02	1.58	0.54	1.34	12.28
WIL	17.76	23.97	88.69	0.050	8.20	58.32	2.25	0.65	1.77	18.69

[a] For details on sample names, see Table 1. [b] AF4-FLD derived variables are defined in Section 2.3. [c] Fluorescence EEM intensity (QSE) at the point of maximum R^2 with given type of DBPFP. [d] Point of maximum R^2 ($I_{Ex/Em}$) at excitation and emission wavelengths of 225 and 310 nm, respectively ($I_{225/310}$). [e] $I_{226/421}$. [f] $I_{227/592}$. [g] Intensity of the best-fitting wavelength pair. [h] $I_{257/277}$. [i] $I_{226/596}$. [j] $I_{225/531}$.

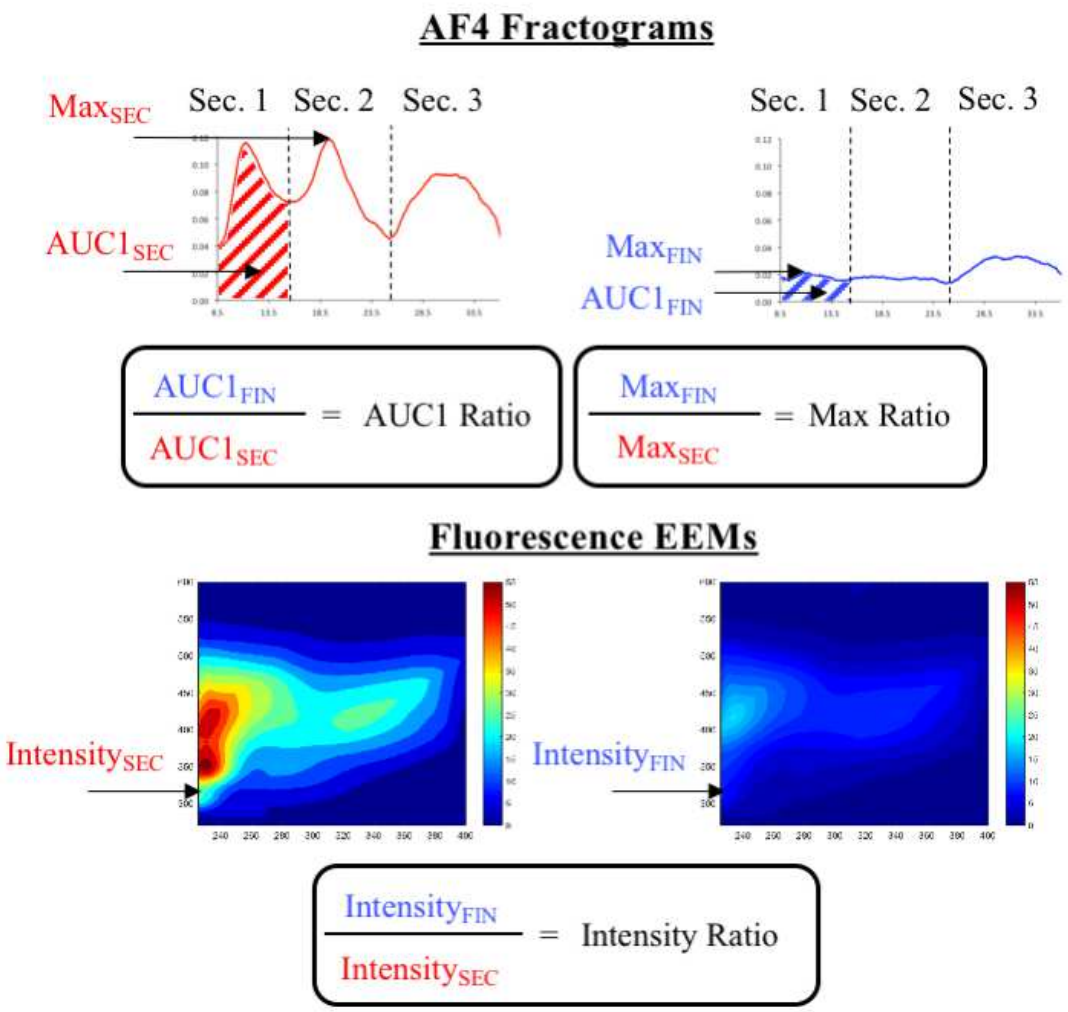

Figure S2. Origin of variables derived from AF4-FLD fractograms and fluorescence EEMs and sample calculations of AUC1 Ratio, Max Ratio, and Intensity Ratio.

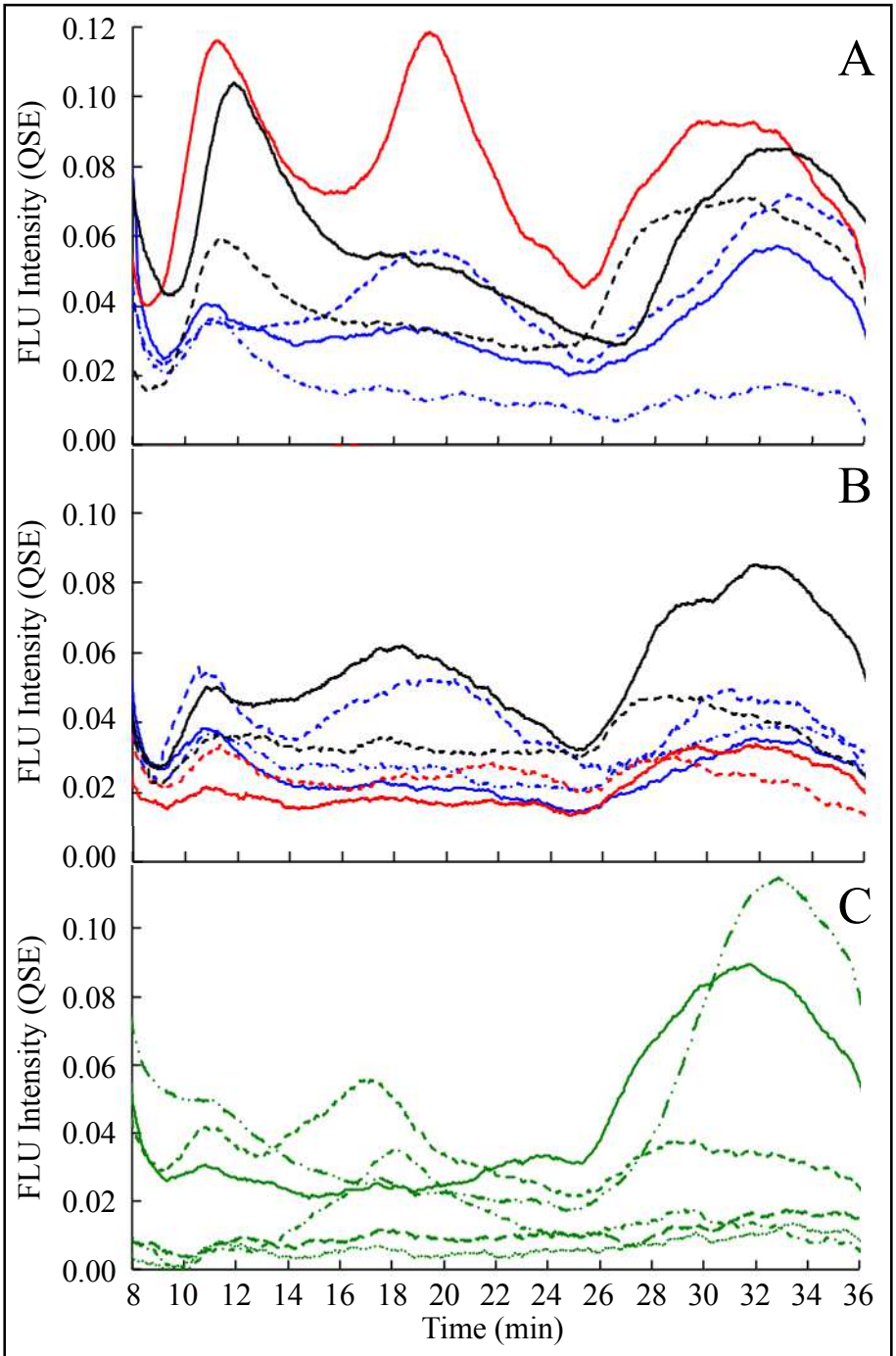

Figure S3. AF4-fluorescence fractograms at excitation and emission wavelenghts of 280 nm and 340 nm, respectively , beginning after the elution of the void peak. WWTPs include BRV (—), BTN (- - -), NACA (·····), NLD (—), RGS (- - -), SPD (—), and WS (- - -) with secondary effluent samples in Panel A and finished effluent samples in Panel B. Natural waters CAL (—), FAY (- - -), GRN (·····), PTN (·····), TUL (—), and WIL (- - -) are shown in Panel C.

Table S7. Multivariate Models of TONOFP-, TTHMFP-, and DHANFP Ratio

DBP Type	p-values[a]				Adjusted
	AUC1	***Max***	***Intensity***	**Model**	**R^2**
TONO	(0.031)	-	-	(0.031)	0.565
	(0.010)	(0.033)	-	(0.010)	0.847
	(0.001)	(0.001)	(0.006)	(0.001)	0.988
TTHM	0.204	-	-	0.204	0.159
	0.101	(0.038)	-	(0.044)	0.684
	0.146	(0.035)	(0.002)	(0.001)	0.990
DHAN	0.158	-	-	0.158	0.227
	0.466	0.213	-	0.174	0.375
	(0.000)	(0.000)	(0.000)	(0.000)	0.998

[a]Only p-values < 0.05 considered significant, shown in parentheses

Table S8. Influence of Observations

Sample Removed[a]	Adjusted R^2			p-value[b]		
	TONO	**TTHM**	**DHAN**	**TONO**	**TTHM**	**DHAN**
None	0.988	0.680	0.810	0.0008	0.1031	0.0483
BRV	0.985	0.757	0.838	0.0092	0.1420	0.0956
BTN	0.983	0.814	0.746	0.0102	0.1094	0.1486
NACA	0.996	0.950	0.764	0.0027	0.0299	0.1380
NLD	0.985	0.007	-0.254	0.0089	0.5318	0.6479
RGS	0.984	0.619	0.796	0.0096	0.2199	0.1197
SPD	0.985	0.637	0.994	0.0089	0.2095	0.0037
WS	0.991	0.660	0.748	0.0053	0.1971	0.1473

[a] *For* details on sample names, see Table 1
[b] *Values* of $p < 0.05$ assumed to be significant

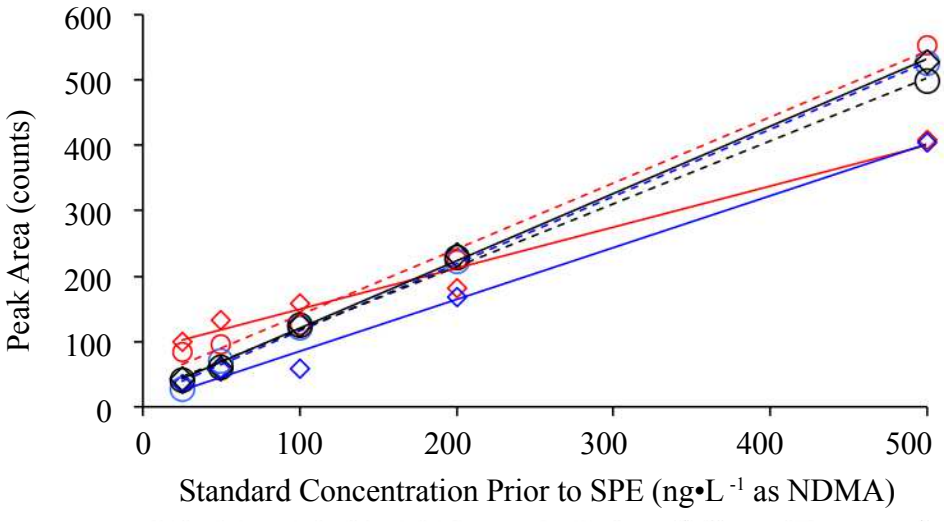

Figure S4. TONO response presented as Peak Area for 5-point standard curves of NDMA followed by solid phase extraction (SPE). Each standard curve was measured on a different reaction chamber: Jan. 20, 2016 (~~◇~~), Jan. 22, 2016 (~~○~~), Jan. 25, 2016 (~~◇~~), June 6, 2016, morning (~~○~~), June 6, 2016, evening (~~◇~~), and June 7, 2016 (~~○~~).

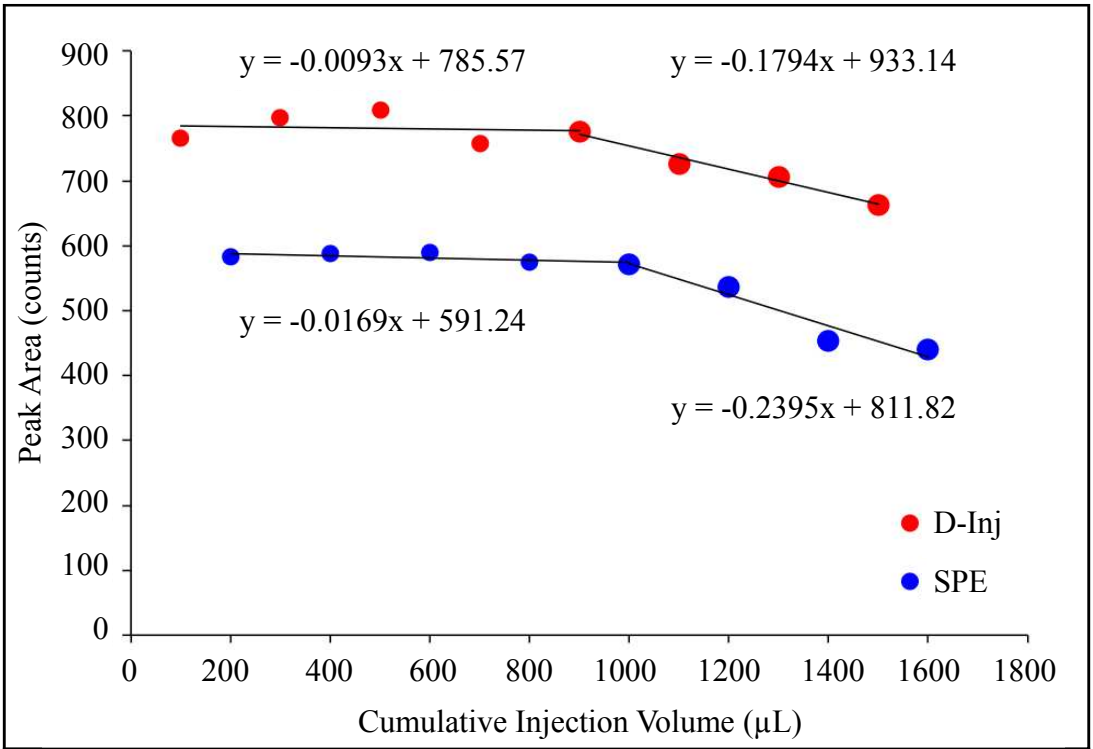

Figure S5. TONO response presented as Peak Area for alternating 100 µL injections of a 0.15 ng·µL^{-1} NDMA standard injected directly (D-Inj) and a 600 ng·L^{-1} NDMA standard injected following solid phase extraction (SPE). Linear fits provided for two piecewise sections of each data set.

References

Her, N., Amy, G., Foss, D. and Cho, J. W., 2002. Variations of molecular weight estimation by HP-size exclusion chromatography with UVA versus online DOC detection. Environmental Science & Technology 36 (15), 3393-3399.

Hudson, N., Baker, A. and Reynolds, D., 2007. Fluorescence analysis of dissolved organic matter in natural, waste and polluted waters - A review. River Research and Applications 23 (6), 631-649.

Mitch, W. A. and Dai, N. (2012). Water Research Foundation Report #4209: Development and application of a total nitrosamine assay for disinfected waters, Water Research Foundation.

Needham, E. M., Sidney, S. M., Chimka, J. R. and Fairey, J. L., 2016. Trihalomethane, dihaloacetonitrile, and total N-nitrosamine precursor adsorption by carbon nanotubes: the importance of surface oxides and pore volume. Environmental Science-Water Research & Technology 2 (6), 1004-1013

Chapter 4

Trihalomethane, Dihaloacetonitrile, and Total *N*-nitrosamine Precursor Adsorption by Modified Carbon Nanotubes (CNTs) and Freeform CNT Microstructures

Abstract

N-nitrosamines are a non-halogenated group of disinfection byproducts that form during chloramination, particularly in drinking waters impacted by wastewater treatment plant (WWTP) effluents. Here, we reveal a size-resolved fluorescence-based precursor surrogate to track total *N*-nitrosamine formation potential (TONOFP) through oxidative treatment. Samples were collected at seven WWTPs, at the finished effluent and prior to final disinfection (i.e., secondary effluent). Asymmetric flow field-flow fractionation (AF4) with inline fluorescence detection at an excitation-emission of 280/340 nm (i.e., $I_{280/340}$) showed protein-rich natural organic matter peaks between 10-445 kDa and 445-1,500 kDa. TONOFP was measured by chemiluminescence on samples dosed with 250 mg□L^{-1}-Cl_2 monochloramine at pH 7 for seven days. Metrics from AF4-$I_{280/340}$ (i.e., area under the curve (AUC) and peak height) and $I_{257/277}$ from whole water excitation-emission matrices (EEMs) were leveraged in multivariate models to develop correlations with TONOFP. The TONOFP of the finished effluent divided by that of the secondary effluent (i.e., the *TONOFP Ratio*) was strongly correlated ($R^2 = 0.996$, $p = 0.000$) to a model of AUC for the 10-445 kDa peak, maximum peak height, and $I_{257/277}$. This TONOFP precursor surrogate requires 2 mL of sample and is transformational for assessing the impact of oxidative treatments on *N*-nitrosamine precursor concentrations.

1. Introduction

In drinking water treatment plants (DWTPs) and distribution systems, free chlorine or chloramines react with natural organic matter (NOM) in source water to form disinfection byproducts (DBPs), such as trihalomethanes (THMs) (Rook, 1976) and dihaloacetonitriles (DHANs) (Krasner et al., 2006). *N*-nitrosamines, a non-halogenated group of DBPs, can also form, particularly in waters impacted by wastewater treatment plant (WWTP) effluents (Krasner et al., 2013) that are disinfected with chloramines (Mitch et al., 2003). As such, formation of *N*-nitrosamines is a particular concern in direct potable reuse (Zeng et al., 2016) and DWTPs using less pristine source waters (Dai and Mitch, 2013). *N*-nitrosamines exert high toxicity relative to regulated DBPs and, as such, are under consideration for regulation in drinking water (Hrudey and Charrois, 2012). Most *N*-nitrosamine research has focused on *N*-nitrosodimethylamine (NDMA) as it is the most commonly occurring *N*-nitrosamine present in drinking water systems (Russell et al., 2012). However, NDMA has been shown to comprise just ~5% of total *N*-nitrosamines (TONO) in chloramine systems (Dai and Mitch, 2013) but little information exists regarding removal/transformation of TONO precursors. To address this important research gap, this study focuses on the removal of TONO precursors by engineered sorbents, with an emphasis on carbon nanotubes (CNTs) and presents a novel application scheme for CNTs to curb TONO formation in finished drinking waters.

CNTs have been shown to adsorb THM, DHAN, and TONO precursors in batch applications (Needham et al., 2016) and can be manufactured with varying size (Balasubramanian and Burghard, 2005), shape (De Volder et al., 2014), texture (Birch et al., 2013), and functionalities (Cho et al., 2008) to suit a particular application. The versatility of available CNT properties makes them a potentially valuable sorbent for use in DBP control. A

recent study by this research group showed that CNTs can have high affinity for total *N*-nitrosamine (TONO) precursors, which was in part attributed to electrostatic attractive forces between negatively charged CNT surface oxides and positively charged amine groups within the TONO precursors (Needham et al., 2016). Further, enhanced adsorption of DBP (i.e., TTHM, DHAN, and TONO) precursors was attributed to increased CNT cumulative pore volume, which was created by electrostatic repulsive forces between negatively charged CNT surface oxides. This finding contrasts studies with activated carbon that have shown negatively charged surface oxides decrease DOM adsorption (and concomitantly DBP precursors, presumably) because of electrostatic repulsion (Dastgheib et al., 2004). As such, the association of increased CPV and negatively charged surface oxides was explored further in this present study.

Due to the high cost of CNTs relative to sorbents such as activated carbon, the application mode and utility of CNTs as a DBP precursor adsorbent needs significant development before use in DWTPs could be considered. Packed-bed reactors are impractical due to high headloss in filters produced by small CNT particle sizes; batch treatments would be compromised by fate and toxicity concerns associated with unrecovered CNTs (Liu et al., 2013; Das et al., 2014) and low precursor loadings (i.e., equilibrium with effluent precursor concentrations). On the other hand, freeform CNT microstructures can be grown on and affixed to substrates with precise control of size, shape, surface chemistry, and porosity (De Volder et al., 2014). These structures are typically referred to as patterned CNT forests and could potentially be manufactured in large sheets, several meters in length and width. We envision these sheets (referred to herein as "CNT mats") in stacked arrays through which water flows between the CNT mat layers. As part of a proof-of-concept for this application, six unique CNT mats were acquired, each between 0.2-0.4 cm^2 in area, and tested in bench scale studies. As this area is too

small to practically generate sufficient samples volume for DBPFP tests (~550 mL), DBP precursor surrogates are needed to assess performance. Metrics from fluorescence excitation-emission matrices (EEMs) are known surrogates of TTHM and DHAN precursors (Do et al., 2015). For TONO, metrics from EEMs coupled with asymmetric flow field-flow fractionation hyphenated with inline fluorescence detection (AF4-FLD) have been shown to be a strong surrogate ($R^2 = 0.996$) for tracking changes in TONO precursors due to oxidative treatment (Needham et al., 2017). Importantly, the TONO precursor surrogate requires only 2 mL of sample volume, instead of the 500 mL required to measure TONO directly. However, this TONO precursor surrogate has not been tested with adsorption processes, which was done as part of the present study.

The objective of this study is to identify physicochemical properties of surface-modified CNTs for enhanced TTHM-, DHAN, and TONO-precursor adsorption. Twelve commercially available CNTs were selected and screened based on their physical and chemical characteristics. Specific surface area and pore volume distributions were determined by gas adsorption isotherms and the distribution of surface functional groups was acquired using x-ray photoelectron spectroscopy (XPS). Three CNT types – selected to include a suite of characteristics – and an activated carbon used widely at DWTPs – were tested in batch studies over a range of sorbent doses and pH conditions to reveal mechanistic insights into the sorption process. Removal of TTHM-, DHAN-, and TONO-precursors was indirectly measured using a modified DBP formation potential (DBPFP) test (Do et al., 2015). Numerical models were developed to assess the importance of physicochemical properties relevant to the adsorption of TTHM-, DHAN-, and TONO-precursors. Additionally, continuous flow studies with CNT mats were completed as part

of a proof-of-concept of this novel application and assessed by leveraging DBP precursor surrogates from fluorescence EEMs and AF4-FLD fractograms.

2. Materials and Methods

2.1. Site Description and Sample Collection

WWTP effluent enriched with TONO precursors (Needham et al., 2016) was chosen for use in batch sorption experiments with bulk CNTs and continuous flow-through tests with CNT mats. Source water was collected from the West Side WWTP (Fayetteville, AR) on October 11, 2016 for batch samples and January 5, 2017 for continuous flow tests. The plant practices biological nutrient removal and depth filtration followed by ultraviolet disinfection, which has been shown previously to produce TONO precursor concentrations (Needham et al., 2017). and effluent aeration. Raw water characteristics of the West Side WWTP effluent (WS-EFF) including pH, conductivity, dissolved organic carbon (DOC), major anions and cations, and UV_{254} were measured upon collection and are detailed in Table S1. Waters were stored in low-density polyethylene carboys at 4° C in the dark prior to use.

2.2. Batch Adsorbent Selection

Twelve types of commercially available modified CNTs were purchased from four manufacturers and are detailed in Table 1. To build upon previous work (Needham et al., 2016), CNTs selected for screening for the batch experiments span wide ranges in oxygen-containing functional groups, total surface oxygen content (0.4-15%), and CPV (1.2-8.3 $cm^3 \bullet g^{-1}$), which were determined as follows. The Brunauer-Emmett-Teller surface area (S_{BET}) and the pore volume distributions of the CNTs were measured with a Quantachrome Nova 2200e Surface Area and Pore Size Analyzer using combined N_2 and CO_2 gas adsorption isotherms at 77 K and 273 K, respectively. Adsorption isotherms spanned partial pressures of 0.005-0.99 with 0.011-

0.095 step sizes. Density functional theory models assuming cylindrical pore geometries were utilized to develop pore volume distributions and calculate CPV. Surface chemistry was quantified via XPS measurements on a PHI 5000 VersaProbe spectrometer with an AlKα source. A comparison of the relative areas of the carbon and oxygen peaks yielded the oxygen content (%) on the surface. Methods for carbon spectra deconvolution were based on previous work (Needham et al., 2016) and are detailed in the SI. From the carbon peak, relative percentages of alcohol, carbonyl, and carboxyl groups were determined.

Three CNT types were selected for batch tests based on their physical and chemical CNT characteristics. Specifically, CNT types with dissimilar CPV, oxygen content, and percentage of carboxyl groups were selected, as these characteristics have been associated with increased adsorption of TONO precursors (Needham et al., 2016). Of the three CNT types chosen, one was from Carbon Solutions, Inc. – a single-walled P3 (CNT-1); the other two types chosen were from Nanostructured and Amorphous Materials, Inc – a multi-walled, carboxyl group functionalized CNT (CNT-2) and a single-walled, alcohol-group functionalized CNT (CNT-3). Calgon Filtrasorb 400 powdered activated carbon (PAC, 60×140 U.S. Mesh fraction) was also used in batch experiments to compare the performance of CNTs to a commonly used adsorbent in water treatment. Table 1 summarizes the physical and chemical characteristics of each sorbent that was screened, including the four chosen for batch application.

2.3. Characterizations of Patterned CNT Forests

Freeform CNT microstructures grown on a catalyst underlayer (previously introduced as CNT mats) were obtained from Michael De Volder of the Institute for Manufacturing at the University of Cambridge. The patterned CNT forests are manufactured through strain-engineered growth of vertically aligned CNTs on a silicon wafer (De Volder et al., 2014). As the CNTs are

affixed to a substrate, physical characterization via gas adsorption isotherms was not possible. However, some physical attributes including the size and shape of the microstructures were observed via scanning electron microscopy (SEM) using a Philips XL30 ESEM (Figure 1A-D). Chemical characteristics were quantified via XPS using the methods described in Section 2.2 and results shown in Table 1; individual CNT mat dimensions are given in Table S2.

2.4. Experimental Procedures

2.4.1. Bottle-point Isotherms

Two groups of batch experiments were conducted, one with varying sorbent dose and the other with varying pH at a set sorbent dose. For the dose-varying experiments, sorbent doses of 5-, 10-, 20-, 35-, and 50 $mg \bullet L^{-1}$ were tested and the pH was not adjusted (pH = 8.0). For the pH-varying experiments, the sorbent dose was set at 20 $mg \bullet L^{-1}$ and the initial pH was adjusted to 4.0, 6.0, 8.0, and 10.0. To achieve these pH set points, sample waters were buffered with 1 mM with glacial acetic acid for pH 4.0, 5 mM phosphate for pH 6.0, and 1 mM borate for both pH 8.0 and 10.0. CNTs were added to the WS-EFF (after pH adjustment in the case of pH-varying samples) and tumbled for 3 days to allow samples to reach equilibrium (Needham et al., 2016). Following the 3-day equilibration period, the pH drift was less than 0.2 pH units all pH-adjusted samples. Next, the samples were filtered through a pre-rinsed 0.45-micron polyethersulfone (PES) membrane (Karanfil et al., 2003) and stored at 4° C in the dark for up to 30 days prior to NOM characterizations and DBPFP tests.

2.4.2. DBPFP

The DBPFP of all batch samples was quantified using the method developed by Do et al. (2015) utilizing a 250 $mg \bullet L^{-1}$ as Cl_2 dose of preformed monochloramine at pH 7.0. Total trihalomethane formation potential (TTHMFP) and dihaloacetonitrile formation potential

(DHANFP) were measured using pentane extraction and gas chromatography (GC, Shimadzu 2010) as detailed in Needham et al. (2016). TONOFP was measured via solid phase extraction (SPE) with EPA Method 521 activated carbon cartridges followed by chemiluminescence detection as detailed in Needham et al. (2017).

2.4.3. Continuous Flow Experiments with CNT Mats

A polycarbonate flow-through cell was fabricated with a dropped chamber to hold a single CNT mat to which a syringe pump was used to continuously flow water over the topside of the mat (Figure 1E). CNT mats were rinsed by pumping Milli-Q water through the cell at flow rates ranging from 0.2-4 $mL \bullet hr^{-1}$, which corresponded to empty bed contact times between 0.4-7.5 hours, to remove impurities that could interfere with UV and fluorescence measurements prior to continuous flow experiments with WS-EFF. A full UV spectrum from 225-600 nm was measured for the flow-through cell effluent to confirm that CNT mats were sufficiently rinsed ($UV_{254} < 0.01$ a.u. with a 1-cm pathlength quartz cuvette) before switching the water source to WS-EFF. Preliminary experiments were conducted with CNT-Mat-1 to determine an appropriate flow rate for future tests, which was determined to be 0.2 $mL \bullet hr^{-1}$, a flow rate intended to balance the needs to achieve adsorption of TTHM and TONO precursors while facilitating sample collection in 24-hour intervals. Additional details regarding selection of this flow rate is provided in Section 3.3. Following tests with CNT-Mat-4 at 0.2 $mL \bullet hr^{-1}$, flow rates of 4, 40, and 400 $mL \bullet hr^{-1}$ were run in an attempt to assess rate-limiting sorption mechanisms.

2.4.4. AF4-FLD

A Postnova Analytics AF2000-MT AF4 system hyphenated with a dual monochromator fluorescence detector (Agilent Technologies) was used to collect AF4-FLD fractograms for samples from the batch and the continuous flow-through cell experiments. The AF4 system

eluent was 0.01 mM phosphate buffer at pH 7 and the separation channel was backed with a 10 kDa regenerated cellulose membrane. The AF4 method, which combines slot flow and high cross flow (Table S3), has been shown to separate humic and protein-like fluorophores in WWTP effluent. As in Needham et al. (2017), the AF4-FLD fractograms were collected at a fluorescence excitation-emission wavelength pair of 280 and 340 nm, respectively, as this pair is associated with protein-like fluorophores and maximizes the signal to noise ratio. Each fractogram was divided into three sections: Section 1 from 8.50-14.55 minutes elution time corresponding to NOM 10-445 kDa, Section 2 from 14.55-25.00 minutes corresponding to NOM 445-1,500 kDa, and Section 3 from 25.00 minutes to the end of the run at 37.00 minutes corresponding to NOM larger than 1,500 kDa (Needham et al., 2017). The area under the curves in Sections 1, 2, and 3 (*AUC1*, *AUC2*, and *AUC3*) were calculated as well as the maximum intensity in Sections 1 and 2 (*Max*) for use in developing numerical models of DBP precursor adsorption.

2.4.5. Fluorescence EEMs

Fluorescence EEMs were collected on all batch-treated samples and flow-through cell samples following filtration with pre-rinsed 0.45-micron PES membranes. EEMs were run on whole water samples that had not been fractionated following the methodology in Needham et al. (2016). The fluorescence intensity at an excitation wavelength of 225 nm and an emission wavelength of 310 nm ($I_{225/310}$) has been associated with protein-like fluorophores (Hudson et al., 2007) and was represented as the variable *Intensity* in subsequent models.

2.5. Data Modeling

Multivariate analysis was used to assess the physical and chemical characteristics controlling DBP precursor sorption using a similar statistical approach to Needham et al. (2016).

Samples varying sorbent dose and pH were modeled separately and, within each of those categories, individual models were developed for each DBP type (TTHM, DHAN and TONO). The independent variables used in models of dose-varying samples include CPV, S_{BET}, oxygen content, and the sorbent dose. Samples with varying pH were modeled against the same independent variables with the exception of adsorbent dose, as this was held constant at 20 mg•L^{-1}. To fairly compare models with differing numbers of variables, all R^2 values presented are adjusted for the number of independent variables (Montgomery, 2013).

Multivariate models were also generated from the dose-varying batch samples to identify potential TONOFP precursor surrogates describing changes in TONOFP due to sorption. To develop these models, TONOFP values of batch samples were correlated to all available combinations of independent variables derived from AF4-FLD fractograms and whole water fluorescence EEMs (*AUC1-3*, *Max*, and *Intensity*). Models with one, two, and three variables were explored and evaluated based on their significance (*p*-value) and correlation coefficient (adjusted R^2 value). Once significant models were elucidated, any containing the variable *Intensity* were rerun using all 57,750 wavelength pairs in the EEMs to determine the pair for which the best correlation coefficient existed (called *Intensity**).

3. Results and Discussion

3.1. Batch Adsorption Models

Figures 2A-C show the fractional removals of TTHM-, DHAN-, and TONOFP from WS-EFF at sorbent doses of 5-, 10-, 20-, 35-, and 50 mg•L^{-1} for three CNT types and PAC at an unadjusted pH of 8.0. Decreases in the DBPFP are attributed to adsorption of the DBP precursors. For TTHM precursors (Fig. 2A), CNT 3 and PAC performed similarly to one another and better than CNTs 1 and 2, with 0.04-0.23 more fractional removal. For the DHAN precursors (Fig. 2B),

CNT 3 outperformed PAC and CNT 2, which performed similarly to one another, but better than CNT 1. CNT 3 had 0.01-0.08 more fractional removal than CNT 2 or PAC and 0.08-0.19 more than CNT 1. For both TTHM and DHAN precursors, CNT 1 did not perform as well as the other three sorbents. In contrast, CNT 1 removed the greatest fractions of TONO precursors (Fig. 2C) and outperformed PAC at every sorbent dose. CNTs 2 and 3 also outperformed PAC in terms of TONO precursor removal at all doses except 35 $mg \bullet L^{-1}$. Taken together, the results in Figs. 2A-C suggest that TONO precursors have dissimilar sorbate characteristics compared to TTHM and DHAN precursors (together referred to as carbonaceous DBP precursors), and the sorbents tested have contrasting affinities for these differing precursor types. The physicochemical properties driving enhanced sorption of the various DBP precursors is explored below.

Figures 2D-F show the fractional removals of TTHM-, DHAN-, and TONOFP for each of the four sorbents at pH 4, 6, 8, and 10. In these experiments, the sorbent dose was 20 $mg \bullet L^{-1}$. For TTHM precursors (Fig. 2D), all CNT types performed the best at pH 4 and similarly to one another at pH 6, 8, and 10. For DHAN precursors (Fig. 2E), CNT types 1 and 3 performed best at pH 4. Of the oxygen-containing functional groups on the CNT surfaces, only carboxyl groups have a pKa (~5) (Suggs, 2002) within the pH range of these experiments. The samples at pH 4 are the only ones for which the pH is below the pKa of the carboxyl groups, which suggests that negatively charged carboxyl functional groups impaired removal of TTHM precursors, albeit only modestly (with a maximum of 0.15 more fractional removal at pH 4 compared to the other pH values), and DHAN precursors to a lesser extent. Removal of TTHMFP and DHANFP by PAC did not exhibit strong trends with pH, although the lowest removals were observed at pH 10. Fig. 2F shows TONO precursor removal as a function sorbent type at pH 4, 6, 8, and 10. However, aberrant trends are apparent, such as the three instances of negative fractional

removals (i.e., the TONOFP was up to 40% higher in the sorbent-treated samples compared to the untreated samples). It is possible that the pH perturbations interfered with the TONO measurement, and, as such, it was concluded that the data presented in Fig. 2F were unreliable. Importantly, however, these data point to the need for a robust study of the impact of pH and buffer type on TONO measurements by SPE followed by chemiluminescence.

The multivariate analysis of both dose-varying and pH-varying samples for each DBP type yielded models of each (Figures 3 and S1) with regression coefficients and *p*-values given in Table 2. Independent variables were assumed to be nonzero and to be significant in models of DBPFP if their *p*-value was less than 0.05, controlling for other variables in the model. For the models of DBPFP in which adsorbent dose was varied, strong correlations were found for TTHMFP ($R^2 = 0.92$, Figure 3A) and DHANFP ($R^2 = 0.88$, Figure 3B). As expected, sorbent dose was a significant variable controlling the DBPFP of the samples. Additionally, S_{BET} was significant ($p = 0.029$) in the model of TTHMFP and was nearly significant ($p = 0.079$) in the model of DHANFP, indicating the importance of sorbent surface area for removal of THM and DHAN precursors. In contrast, S_{BET} was insignificant in the model of TONOFP ($p = 0.667$). Only moderate correlations were found for the model of TONOFP ($R^2 = 0.65$, Figure 3C) and the surface oxygen content came close to significance ($p = 0.054$). Data regarding the removal of TONOFP in samples varying adsorbent dose showed a few samples that were not consistent with typical adsorption behavior thereby prompting the search for potential outliers in the TONOFP data set. Among all the samples ($n = 20$), only three had absolute errors larger than 1 nmol•L^{-1} as NDMA (noted by asterisks in Figure 2C). The model of TONOFP was recalculated without these samples and resulted in an R^2 of 0.91 and a model in which all of the independent variables were significant (Figure 3D and Table 2), particularly CPV ($p = 0.007$) and the surface oxygen content

(p = 0.000). Taken together, the results of the multivariate models of dose-varying samples indicate that S_{BET} controls the adsorption of TTHM and DHAN precursors while CPV and oxygen content control the adsorption of TONO precursors. This finding for TONO is similar to previous work indicating that CPV and negatively charged oxygen groups (such as carboxyl groups) control the adsorption of precursors (Needham et al., 2016), however the models in this study were developed with CNTs that spanned larger ranges of CPV, S_{BET}, and various types of surface oxygen (Table 1).

Of the models developed from samples in which the pH was varied (Figure S1A-C), only the model of TTHMFP was significant (R^2 = 0.58), indicating S_{BET} was again the physiochemical variable most strongly correlated to adsorption of TTHM precursors. Models of DHAN (Fig. S1B) and TONO (Fig. S1C) developed with the pH-varying samples were not significant and, as such, cannot be used to draw additional conclusions about factors controlling adsorption of their precursors.

3.2. TONO Precursor Surrogate Development

The recently developed precursor surrogate (R^2 = 0.996) for tracking formation and destruction of TONO precursors through various oxidation processes leveraged metrics from AF4-FLD fractograms and whole water fluorescence EEMs (Needham et al., 2017). Similar models were sought for a TONOFP precursor surrogate (also based on metrics from AF4-FLD fractograms, shown in Figure S2, and fluorescence EEMs) to describe the efficacy of sorption processes, rather than oxidation. An illustrative representation of the independent variables is shown in Figure S3 and the raw data used to generate the multivariate model are in Table S4. Of all the possible combinations of the five independent variables from AF4-FLD and fluorescence EEMs, the significant model with the best correlation coefficient (R^2 = 0.55) was a multivariate

model of *AUC1*, *AUC2*, and *Intensity*. All three variables were significant in addition to the model as a whole ($p = 0.001$). *AUC1* and *AUC2* are associated with protein-like organic matter measured by the AF4-FLD in the 10-445 kDa and 445-1,500 kDa ranges, respectively (Needham et al., 2017). *Intensity* ($I_{225/310}$) is based on a wavelength pair associated with the protein-like region of the whole water fluorescence EEMs. This model was then explored further to determine at which wavelength pair the best correlation coefficient existed (*Intensity**) by running multivariate models of TONOFP with *AUC1*, *AUC2*, along with each of the 57,750 wavelength pairs from the EEMs. *Intensity** was determined to be $I_{225/300}$ and the model of *AUC1*, *AUC2*, and *Intensity** had an improved adjusted R^2 value of 0.576. The moderate fit of the model (Figure 4) is based on TONOFP removal from sorption processes onto three types of CNTs and one activated carbon. While this model is not as strong as our previously developed model describing TONOFP oxidation ($R^2 = 0.996$) (Needham et al., 2017), its moderate fit facilitated estimation of TONO precursor breakthrough profiles in the continuous flow CNT mat testing.

3.3. Continuous Flow CNT Mat Testing

As the sample volumes generated from the CNT mat tests were small due to low flowrates (typically 0.05 to 4 $mL \bullet hr^{-1}$), breakthrough curves were generated using DBP precursor surrogates only. For TONO, the precursor surrogate discussed in Section 3.2 and Figure 4 was used, while for TTHM, UV_{254} was used (Do et al., 2015). Preliminary tests with CNT-Mat 1 used an initial flow rate of 4 $mL \bullet hr^{-1}$, and both the TTHM and TONO precursor surrogates stabilized at a C/C_0 of approximately 0.8 after 2.5 bed volumes (Figure 5A-B). During sample collection at 4 $mL \bullet hr^{-1}$, both surrogates increased indicating decreasing sorption of TTHM and TONO precursors. This result is proof-of-concept that the CNT mats can be used to sorb these precursors. Next, the flow rate was decreased to 0.2 $mL \bullet hr^{-1}$ at 2.5 bed volumes and

finally to 0.05 mL•hr^{-1} at 4.5 bed volumes, but the effluent profiles were unaffected, suggesting that film diffusion was not limiting (Fairey et al., 2010). Based on these results and as a matter of convenience, a flow rate of 0.2 mL•hr^{-1} was chosen for the subsequent CNT mat tests, as this flow rate facilitated collection of a larger number of samples prior to breakthrough.

Continuous flow tests with CNT-Mat-2 (Figure 5C-D) and CNT-Mat-3 (Figure 5E-F) revealed several notable trends. TONO precursors increased initially and then stabilized near breakthrough (C/C0 ≈ 1). Unexpectedly, TONO precursors surpassed a C/C_0 of 1 (i.e., the effluent exceeded the influent concentration), indicative of a chromatographic effect (Benjamin and Lawler, 2013), suggesting that sorbed TONO precursors were displaced by more strongly sorbing compounds and released into the effluent. It is unlikely that THM precursors were these preferentially sorbing compounds, given their rapid breakthrough (Figures 5D and F). This CNT-Mat-4 (Figure 5G-H) was run longer than the other three CNT Mats (~235 bed volumes) as the TONO precursor surrogate concentration did not stabilize, varying between C/C_0 values of 0.5-1.4. In contrast the TTHM precursor surrogate stabilized and achieved breakthrough after the first sample. This may be due to the smaller diameter of the CNT microstructures in CNT-Mat-4 compared to those of the other three CNT mats (see Figure 1). Additionally, the flow rate increases from 0.2 mL•hr^{-1} to 4 mL•hr^{-1} and then to 40 mL•hr^{-1} did not appear to impact the TONO precursor surrogate concentration, again indicating the lack of a film diffusion limitation. Assessing the importance of CNT surface chemistry is not possible in these experiments, given that SBET and pore volume distributions could not be measured. However, these data demonstrate a proof-of-concept for this novel sorption mode, making such measurements worthwhile in future studies. Importantly, visual assessment of effluent and SEM images of CNT mats after continuous flow experiments, indicate that vertically aligned freeform CNTs remained

attached to the substrate even under high surface loading rates. As a whole, continuous flow tests have revealed that attached growth CNTs have the ability to remove TONO precursors.

Future work with CNT mats would benefit from the ability to measure DBPFP of the samples directly, rather than relying on precursor surrogates. Under these flow conditions, we estimate the CNT mats would need to be approximately 100 times larger (~3125 mm^2) to obtain sufficient sample volumes in practical periods of time (24 hours or less). If physical characteristics could also be calculated despite the CNTs being attached to a substrate, numerical models similar to those used for batch adsorption studies could be generated to determine the importance of CNT physical and chemical characteristics for DBP precursor adsorption. These models should also include variables to quantify the shape of the CNT microstructures such as height, diameter, or microstructure spacing to determine if the adsorption of particular types of DBP precursors is impacted by these variables.

4. Conclusions

Modified CNTs were selected for their potential to remove DBP precursors, with an emphasis on TONO precursors. Batch experiments with modified CNTs and a PAC encompassing a wide range of physical and chemical characteristics were conducted with various sorbent doses and at a range of pH values. Multivariate models of TTHMFP, DHANFP, and TONOFP with physiochemical characteristics revealed that specific surface area controls the adsorption of TTHM and DHAN precursors, while CPV and surface oxygen content control the adsorption of TONO precursors. Additional models were generated for TONOFP with metrics from AF4-FLD fractograms and fluorescence EEMs. The best-fit model utilized intensity values at $I_{225/300}$ and had an adjusted R^2 value of 0.576 resulting in a usable TONO precursor surrogate. This surrogate, along with UV_{254}, which was used as TTHM precursor surrogate, was applied to

continuous-flow tests of CNT mats. These tests demonstrated that TONO precursors could be sorbed, providing a proof-of-concept for this novel method of application. CNT mats would benefit from future studies with larger sample volumes, physical property characterizations, and the development of numerical models to determine factors controlling DBP precursor adsorption.

5. Associated Content

Notes

The authors declare no competing financial interest.

Acknowledgements

The authors acknowledge Adrian Fernandez de Luis Maldonado for his assistance with the statistical analysis as well as Michael De Volder from the Institute of Manufacturing at the University of Cambridge for manufacturing the CNT mats. Financial support from the National Science Foundation (CBET #1254350 to JLF) and the University of Arkansas Doctoral Academy Fellowship (to EMN) is gratefully acknowledged.

6. Figures and Tables

Table 1. Physical and Chemical Characteristics of the Selected Carbons

Carbon Description from Supplier	Supplier	Physical Characteristics from SAA[a]		Relative Amount of Chemical Bonds from XPS[b]				Oxygen Content from XPS (%)
		CPV[c] ($cm^3 \cdot g^{-1}$)	S_{BET}[d] ($m^2 \cdot g^{-1}$)	C=C or C-C[e]	C-O[f]	C=O[g]	COO[h]	
P2	CS[i]	8.3	690	62.5	10.9	6.1	1.1	3.2
P3	CS	4.5	125	56.9	14.7	8.0	5.0	15
MW[j], COOH[k] functionalized	NAM[l]	1.2	131	65.8	13.2	5.4	0.7	0.9
MW, OH[m] functionalized	NAM	2.1	182	65.3	11.3	6.6	1.3	3.7
MW, large inner diameter	NAM	2.1	165	66.7	11.8	5.0	1.1	0.4
SW, COOH functionalized	NAM	5.4	435	67.4	10.8	6.8	1.2	3.9
SW, OH functionalized	NAM	5.9	488	62.1	12.2	6.3	2.0	4.2
MW, COOH functionalized	CT[n]	1.7	183	66.2	11.5	6.2	1.3	3.0
MW, OH functionalized	CT	1.7	153	67.9	9.6	6.2	0.7	5.4
MW, NH_2[o] functionalized	CT	2.3	238	67.0	9.6	6.2	1.3	1.3
SW, COOH functionalized	CT	5.5	435	66.9	10.9	6.1	1.4	3.3
SW, OH functionalized	CT	5.8	500	63.5	13.3	4.8	1.8	2.3
Filtrasorb 400	CC[p]	12.1	754	63.4	11.1	7.1	2.2	5.8
CNT-Mat-1	MDV[o]	-	-	59.0	14.0	12.1	3.0	2.0
CNT-Mat-2	MDV	-	-	54.5	18.8	11.4	2.6	2.9
CNT-Mat-3	MDV	-	-	53.1	25.2	10.1	3.0	35.2
CNT-Mat-4	MDV	-	-	67.0	12.8	11.1	9.1	1.0

[a] Quantachrome Nova 2200e surface area and pore size analyzer. [b] PHI 5000 VersaProbe X-ray photoelectron spectrometer, reported as the percent of total carbon bond types present and does not include shake-up features. [c] Cumulative pore volume. [d] Surface area calculated using the Brunauer-Emmett-Teller (BET) method. [e] Analyzed as total of C=C, C-C, and C-H bonds. [f] Alcohol bonds. [g] Carbonyl bonds. [h] Carboxyl bonds. [i] Carbon Solutions, Inc. [j] Multi-walled. [k] Carboxyl group. [l] Nanostructured Amorphous Materials, Inc. [m] Alcohol group. [n] Cheap Tubes, Inc. [o] Amino group. [p] Calgon carbons. [o] Michael De Volder, Institute for Manufacturing, University of Cambridge.

Table 2. Linear regression models of DBPFP for TTHM-, DHAN-, and TONOFP

	Independent Variables[a]	TTHMFP		DHANFP		TONOFP		TONOFP without Outliers	
		Coeff.[b]	**p-value**	**Coeff.**	**p-value**	**Coeff.**	**p-value**	**Coeff.**	**p-value**
Varying Dose	CPV[c]	0.0062	0.134	0.0035	0.111	0.2497	0.390	0.4943	0.007
	S_{BET}[d]	-0.0001	0.029	-0.0001	0.079	-0.0020	0.667	-0.0050	0.049
	Oxygen Content (%)[e]	-0.0002	0.880	0.0000	0.993	-0.1802	0.054	-0.2844	0.000
	Dose[f]	-0.0022	0.000	-0.0010	0.000	-0.0537	0.000	-0.0615	0.000
	Constant	0.2977	0.000	0.1077	0.000	7.0570	0.000	7.7792	0.000
Varying pH	CPV	-0.0073	0.235	-0.0069	0.348	0.0201	0.527	-	-
	S_{BET}	0.0003	0.003	0.0002	0.057	0.0001	0.738	-	-
	Oxygen Content (%)	0.0210	0.274	0.0195	0.398	-0.0394	0.692	-	-
	Constant	0.1642	0.000	0.2317	0.000	-0.0424	0.804	-	-

[a] Independent variables all represent terms in regression equations. [b] Regression coefficients. [c] Cumulative pore volume. [d] BET surface area. [e] Calculated as the percentage of total measured bonds on the surface. [f] Applied dose of adsorbent

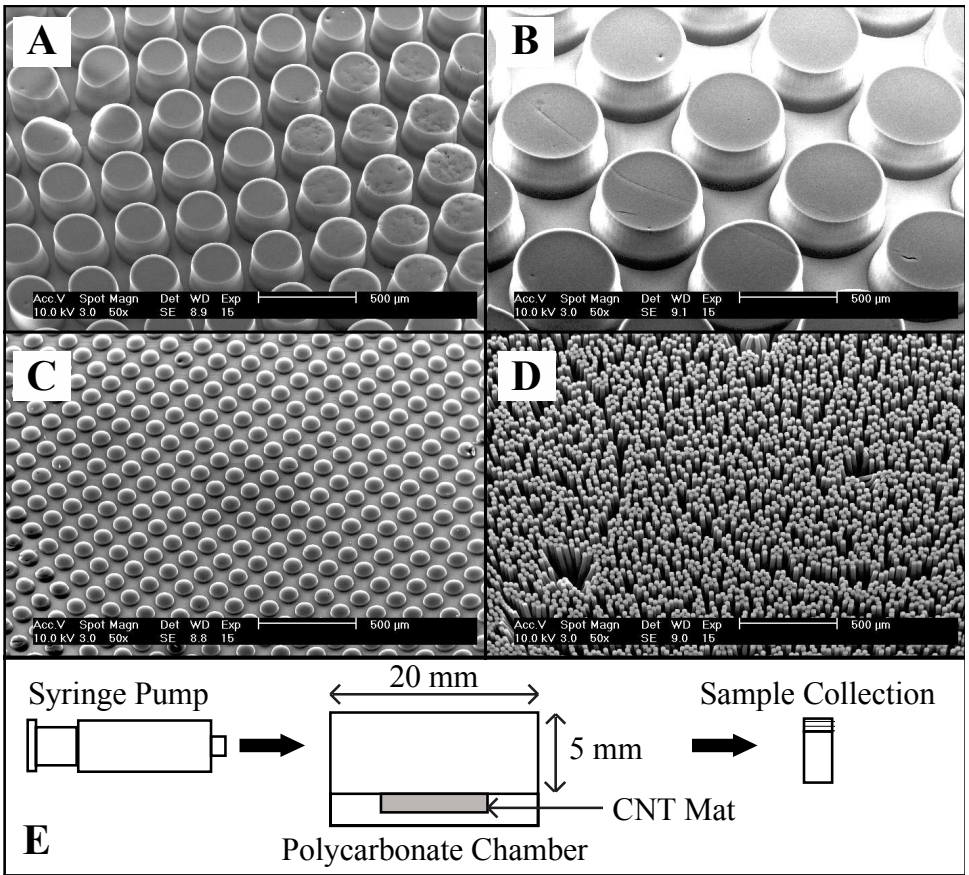

Figure 1. Scanning electron microscopy (SEM) images of CNT-Mats 1-4 (Panels A-D, respectively) at 50 times magnification and (E) a representation (not to scale) of the flow through cell experimental setup used for testing the CNT mats.

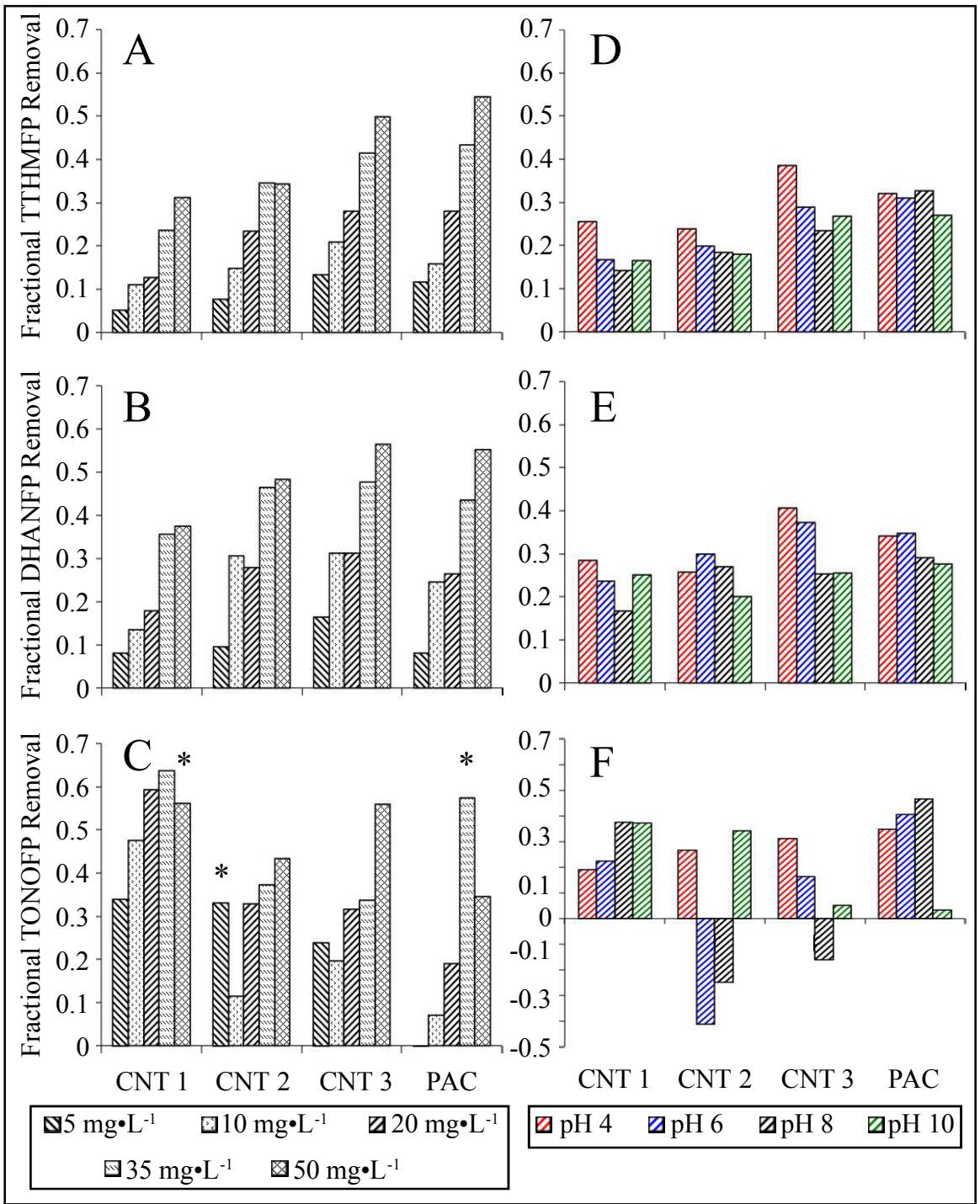

Figure 2. Batch removal of TTHMFP (Panels A and D), DHANFP (Panels B and E), and TONOFP (Panels C and F) by four sorbents, including three types of CNT s and one PAC. Samples in Panels A-C varied sorbent dose at an unadjusted pH of 8.0. Samples in Panels D-F varied pH at a sorbent dose of 20 mg•L $^{-1}$. Samples with an asterisk (*) in Panel C were identified as potential outliers as discussed in the text.

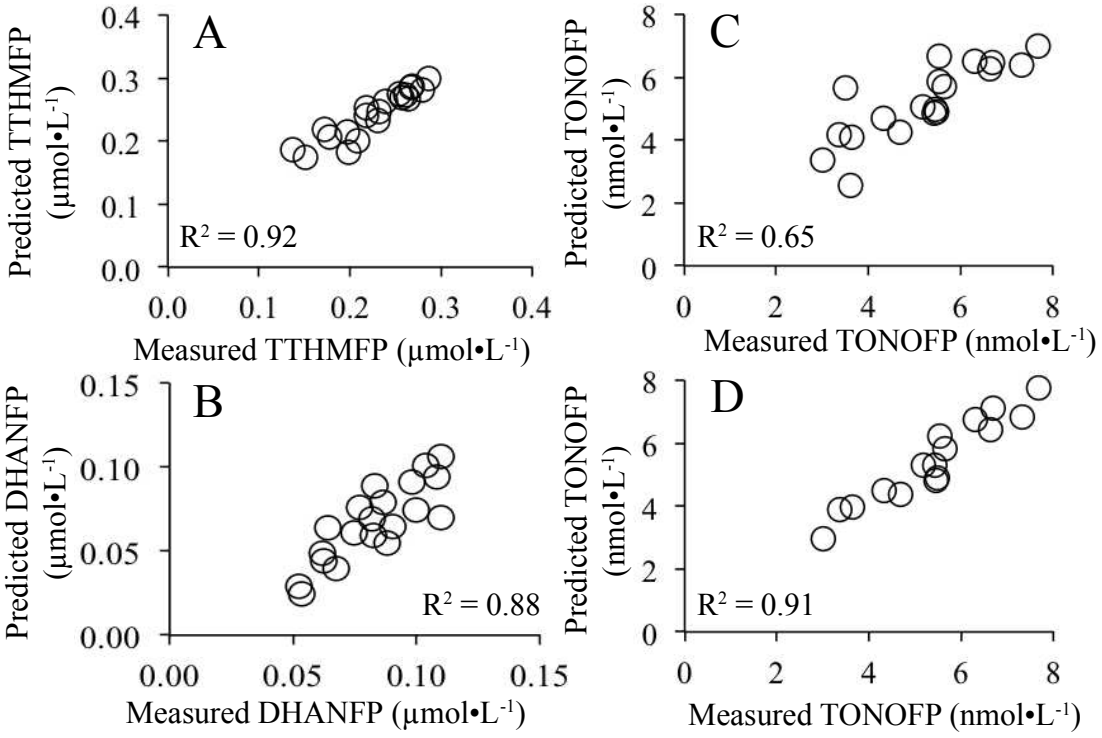

Figure 3. Multivariate models of dose-varying batch samples. Second model of TONOFP (Panel D) was generated without the three probable outliers. All R^2 values are adjusted for the number of independent variables. Model coef ficients and p-values can be found in Table 2.

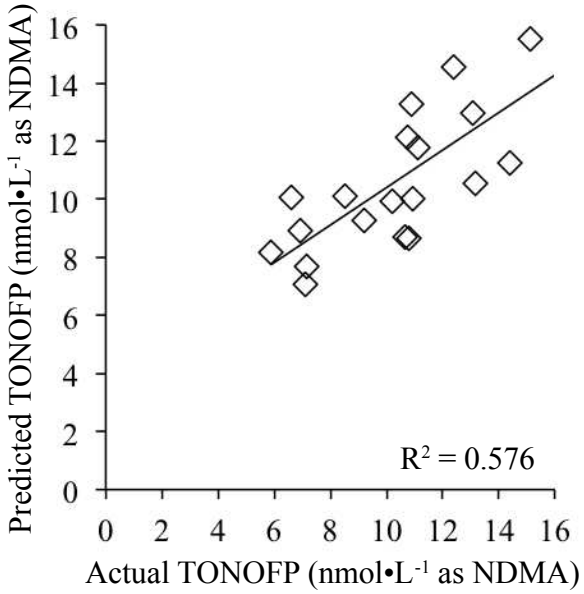

Figure 4. Multivariate model (p = 0.000) of TONOFP with independent variables *AUC1* (p = 0.035), *AUC2* (p = 0.015), and *Intensity* ($I_{225/300}$, p = 0.017). The model represents the following equation: TONOFP = 1.324 *AUC1* – 0.718 *AUC2* + 0.388 *Intensity* – 5.8. R^2 value is adjusted for the number of independent variables.

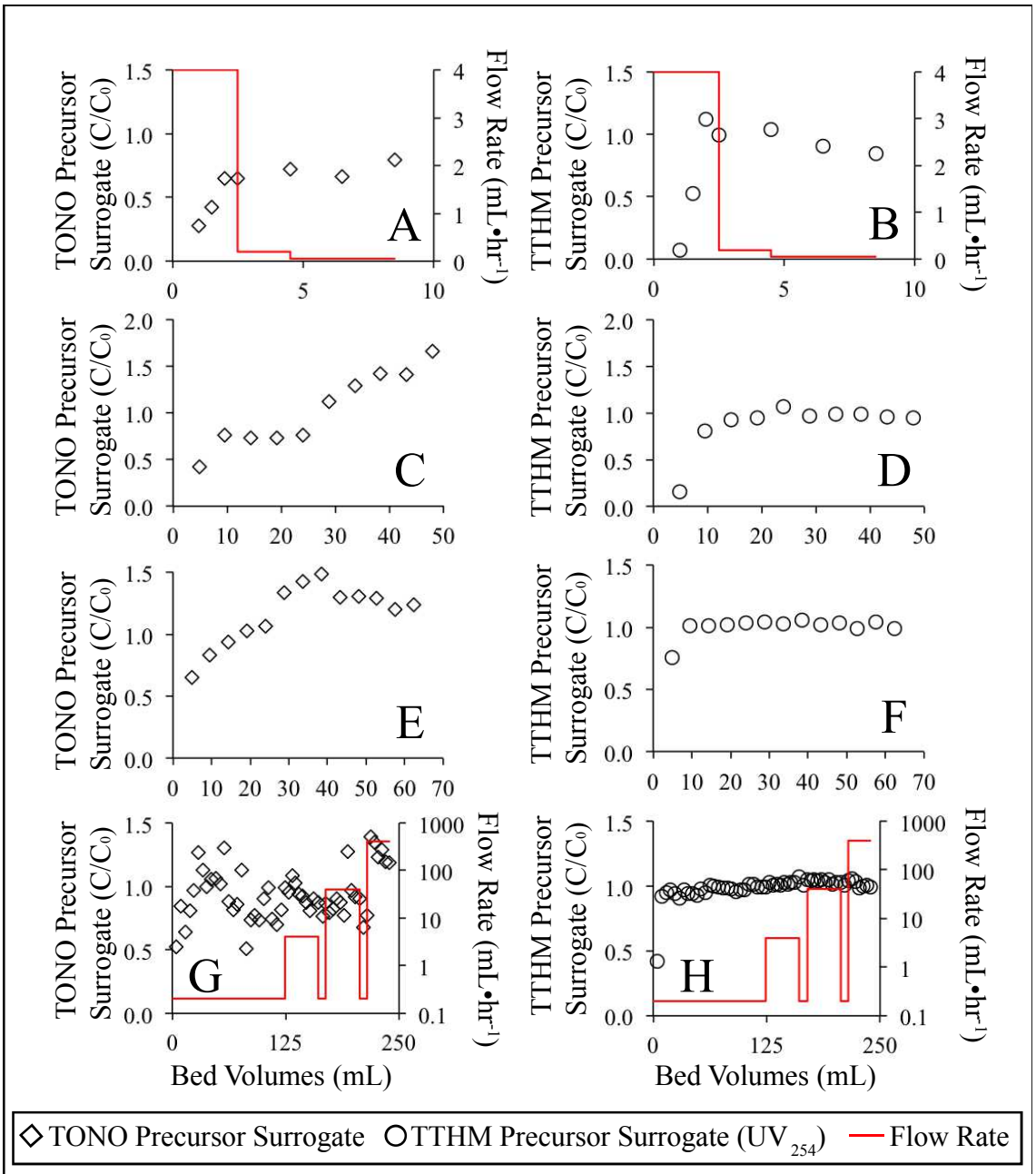

Figure 5. Influent-normalized concentrations of TONO and TTHM precursor surrogates for CNT-Mat-1 (Panels A and B), CNT-Mat-2 (Panels C and D), CNT-Mat-3 (Panels E and F), and CNT-Mat-4 (Panels G and H). For CNT-Mats 2 and 3, flow rate was constant at 0.2 mL•hr^{-1}.

7. References

Balasubramanian, K. and Burghard, M., 2005. Chemically functionalized carbon nanotubes. Small 1 (2), 180-192.

Benjamin, M. M. and Lawler, D. F., 2013. Water Quality Engineering: Physical/Chemical Treatment Processes, John Wiley & Sons, Inc., Hoboken, NJ.

Birch, M. E., Ruda-Eberenz, T. A., Chai, M., Andrews, R. and Hatfield, R. L., 2013. Properties that influence the specific surface areas of carbon nanotubes and nanofibers. Annals of Occupational Hygiene 57 (9), 1148-1166.

Cho, H.-H., Smith, B. A., Wnuk, J. D., Fairbrother, D. H. and Ball, W. P., 2008. Influence of surface oxides on the adsorption of naphthalene onto multiwalled carbon nanotubes. Environmental Science & Technology 42 (8), 2899-2905.

Dai, N. and Mitch, W. A., 2013. Relative importance of N-nitrosodimethylamine compared to total N-nitrosamines in drinking waters. Environmental Science & Technology 47 (8), 3648-3656.

Das, R., Hamid, S. B. A., Ali, M. E., Ismail, A. F., Annuar, M. S. M. and Ramakrishna, S., 2014. Multifunctional carbon nanotubes in water treatment: The present, past and future. Desalination 354, 160-179.

Dastgheib, S. A., Karanfil, T. and Cheng, W., 2004. Tailoring activated carbons for enhanced removal of natural organic matter from natural waters. Carbon 42 (3), 547-557.

De Volder, M., Park, S., Tawfick, S. and Hart, A. J., 2014. Strain-engineered manufacturing of freeform carbon nanotube microstructures. Nature Communications 5, 4512.

De Volder, M., Park, S., Tawfick, S. and Hart, A. J., 2014. Strain-engineered manufacturing of freeform carbon nanotube microstructures. Nature Communications 5.

Do, T. D., Chimka, J. R. and Fairey, J. L., 2015. Improved (and singular) disinfectant protocol for indirectly assessing organic precursor concentrations of trihalomethanes and dihaloacetonitriles. Environmental Science & Technology 49 (16), 9858-9865.

Fairey, J. L., Wahman, D. G. and Lowry, G. V., 2010. Effects of Natural Organic Matter on PCB-Activated Carbon Sorption Kinetics: Implications for Sediment Capping Applications. Journal of Environmental Quality 39 (4), 1359-1368.

Hrudey, S. E. and Charrois, J. W. A., Eds. (2012). Disinfection by-products and human health. IWA Publishing and Australian Water Association, London.

Hudson, N., Baker, A. and Reynolds, D., 2007. Fluorescence analysis of dissolved organic matter in natural, waste and polluted waters - A review. River Research and Applications 23 (6), 631-649.

Karanfil, T., Erdogan, I. and Schlautman, M. A., 2003. Selecting filter membranes for measuring DOC and UV_{254}. Journal American Water Works Association 95 (3), 86-100.

Krasner, S. W., Mitch, W. A., McCurry, D. L., Hanigan, D. and Westerhoff, P., 2013. Formation, precursors, control, and occurrence of nitrosamines in drinking water: A review. Water Research 47 (13), 4433-4450.

Krasner, S. W., Weinberg, H. S., Richardson, S. D., Pastor, S. J., Chinn, R., Sclimenti, M. J., Onstad, G. D. and Thruston, A. D., 2006. Occurrence of a new generation of disinfection byproducts. Environmental Science & Technology 40 (23), 7175-7185.

Liu, Y., Zhao, Y., Sun, B. and Chen, C., 2013. Understanding the toxicity of carbon nanotubes. Accounts of Chemical Research 46 (3), 702-713.

Mitch, W. A., Sharp, J. O., Trussell, R. R., Valentine, R. L., Alvarez-Cohen, L. and Sedlak, D. L., 2003. N-nitrosodimethylamine (NDMA) as a drinking water contaminant: A review. Environmental Engineering Science 20 (5), 389-404.

Montgomery, D. C., 2013. Applied Statistics and Probability for Engineers, 6th Edition, John Wiley & Sons.

Needham, E. M., Fernandez de Luis, A. M., Chimka, J. R. and Fairey, J. L., 2017. Revealing a size-resolved fluorescence-based metric to track oxidative treatment of total N-nitrosamine precursors in wastewater-derived waters. Environmental Science & Technology Letters In Revision.

Needham, E. M., Sidney, S. M., Chimka, J. R. and Fairey, J. L., 2016. Trihalomethane, dihaloacetonitrile, and total N-nitrosamine precursor adsorption by carbon nanotubes:

the importance of surface oxides and pore volume. Environmental Science: Water Research & Technology 2, 1004-1013.

Needham, E. M., Sidney, S. M., Chimka, J. R. and Fairey, J. L., 2016. Trihalomethane, dihaloacetonitrile, and total N-nitrosamine precursor adsorption by carbon nanotubes: the importance of surface oxides and pore volume. Environmental Science-Water Research & Technology 2 (6), 1004-1013.

Rook, J. J., 1976. Haloforms in drinking water. Journal American Water Works Association 68 (3), 168-172.

Russell, C. G., Blute, N. K., Via, S., Wu, X. and Chowdhury, Z., 2012. National assessment of nitrosamine occurrence and trends. Journal American Water Works Association 104 (3), E205-E217.

Suggs, J. W., 2002. Organic Chemistry, Barron's Educational Series.

Zeng, T., Plewa, M. J. and Mitch, W. A., 2016. N-Nitrosamines and halogenated disinfection byproducts in US Full Advanced Treatment trains for potable reuse. Water Research 101, 176-186.

Appendix 3

Supplementary Information for

"Trihalomethane, Dihaloacetonitrile, and Total *N*-nitrosamine Precursor Adsorption by Modified Carbon Nanotubes (CNTs) and Freeform CNT Microstructures"

List of Supporting Information

Carbon Spectra Deconvolution

Table S1. Raw Water Characteristics

Table S2. CNT Mat Dimensions

Table S3. AF4 Method

Figure S1. Multivariate Models of pH-Varying Batch Samples

Figure S2. AF4-FLD Fractograms for Dose-Varying Batch Samples

Figure S3. Illustration of Variables for TONO Surrogate Model

Table S4. AF4-FLD and Fluorescence EEM Data for TONOFP Surrogate Model

Carbon Spectra Deconvolution

Carbon spectra were deconvoluted using a similar method to Needham et al. (2016). The binding energy was charge corrected based on a C1s peak position of 284.4 eV, C1s peaks were deconvoluted with a Gaussian-Lorentzian mix function, and a Shirley background subtraction was applied. The peak corresponding to carbon-carbon bonds was modified with an asymmetry parameter of 0.19 and other peaks were assigned for alcohols (C-O), carbonyls (C=O), and carboxyls (COO) with a final peak corresponding to the shake-up features satellite in the higher binding energy region of the spectra. Carbon-carbon bonding was set to a binding energy of 284.4 eV. Alcohol, carbonyl, and carboxyl groups were represented by peaks located at 285.35, 286.84, and 288.58 eV, respectively. The peak associated with shake-up features was located at 290.4 eV.

Table S1. WS-EFF Raw Water Characteristics

WS-EFF[a] Collection Date	**Oct. 11, 2016**	**Jan. 5, 2017**
pH	8.0	7.8
DOC[b] ($mg \cdot L^{-1}$)	5.09	7.11
UV_{254} (cm^{-1})	0.55	0.12
Specific Conductivity ($\mu S \cdot cm^{-1}$)	523	524
Fluoride ($mg \cdot L^{-1}$)	ND[c]	ND
Chloride ($mg \cdot L^{-1}$)	47.73	42.40
Bromide ($mg \cdot L^{-1}$)	ND	ND
Nitrate ($mg \cdot L^{-1}$)	35.05	49.48
Phosphate ($mg \cdot L^{-1}$)	9.23	8.84
Sulfate ($mg \cdot L^{-1}$)	36.84	42.29
Nitrite ($mg \cdot L^{-1}$)	0.53	ND

[a]Effluent from the West Side Wastewater Treatment Plant
[b]Dissolved Organic Carbon
[c]Not detected

Table S2. CNT Mat Dimensions

CNT Mat	Length (mm)	Width (mm)	Area (mm^2)
CNT-Mat-1	6.27	5.92	37.12
CNT-Mat-2	4.59	4.88	22.40
CNT-Mat-3	4.23	5.99	25.34
CNT-Mat-4	5.16	4.66	24.05

Table S3. AF4 Method Details

Stage	Time (min)	Tip Flow (mL•min^{-1})	Focus Flow (mL•min^{-1})	Cross Flow (mL•min^{-1})	Slot Flow (mL•min^{-1})	Profile
Focusing	0	0.2	1.8	1.0	0.5	Constant
Transition	5	0.2	1.8	1.0	0.5	Linear
Elution	6	2.0	0	1.0	0.5	Constant
	8	2.0	0	1.0	0.5	Linear
	10	1.1	0	0.1	0.5	Constant
	25	1.1	0	0.1	0.5	Linear
	26	1.0	0	0	0.5	Constant
	36	1.0	0	0	0.5	-

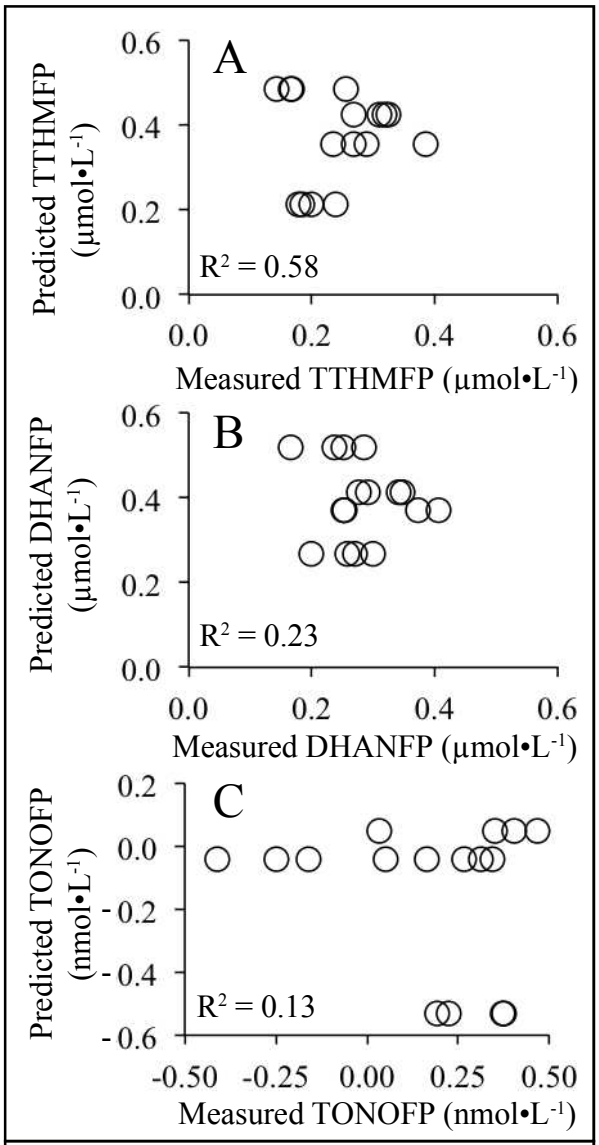

Figure S1. Multivariate models of pH-varying batch samples. All R^2 values are adjusted for the number of independent variables. Model coefficients and p-values can be found in Table 2.

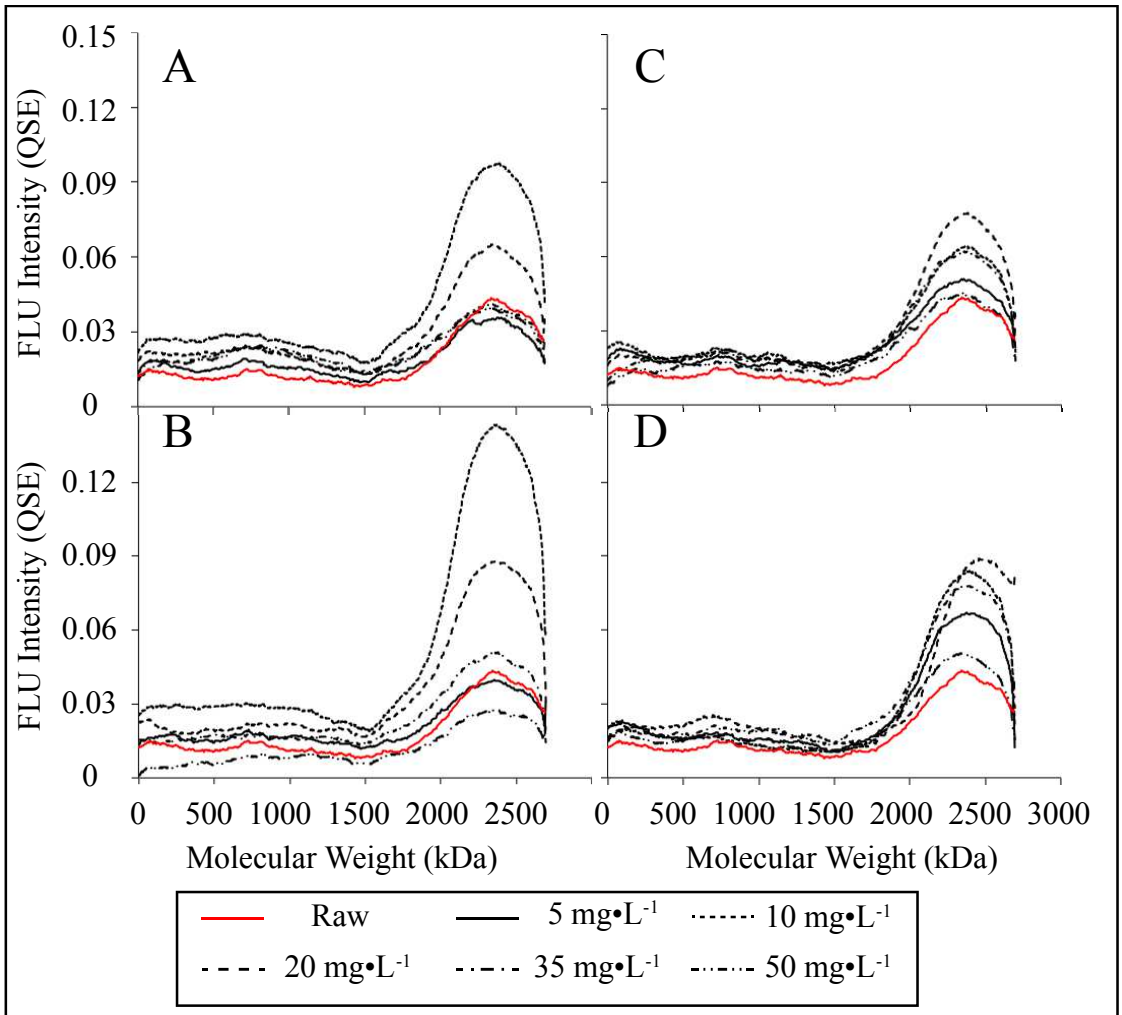

Figure S2. AF4-FLD fractograms for dose-varying batch samples with CNT 1 (Panel A), CNT 2 (Panel B), CNT 3 (Panel C), and PAC (Panel D). Raw samples (—) were not dosed with any sorbent.

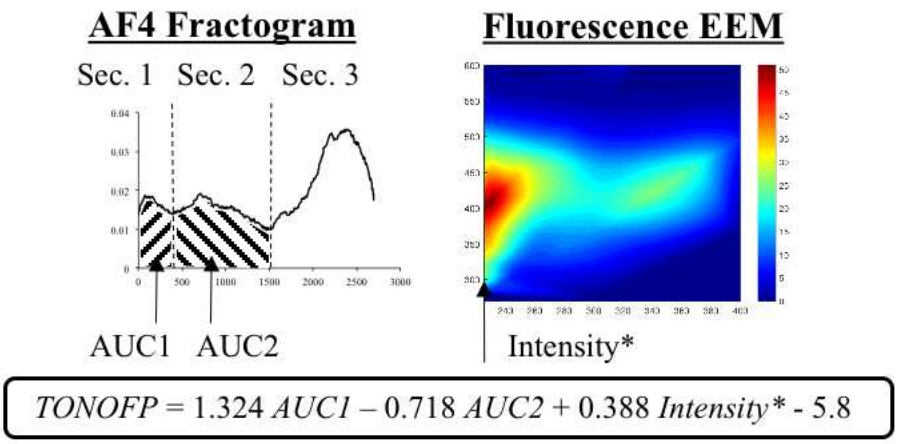

Figure S3. Representation of the origin of variables used in the TONO precursor surrogate multivariate model. AUC1 and AUC2 correspond the the area under the curve of Sections 1 and 2 of the AF4 fractograms, respectively, and Intensity* is the intensity of the fluorescence excitation-emission matrices at an excitation wavelength of 225 nm and an emission wavelength of 300 nm.

Table S4. AF4-FLD and Fluorescence EEM Data for TONOFP Surrogate Model

Sample Name	Carbon Type	Dose ($mg \cdot L^{-1}$)	AUC1[a]	AUC2[a]	Intensity*[b]
Raw	-	0	5.67	12.02	22.78
C1-5	CNT 1	5	7.20	15.73	20.86
C1-10	CNT 1	10	11.72	26.49	20.09
C1-20	CNT 1	20	9.38	20.76	17.42
C1-35	CNT 1	35	7.99	21.57	18.78
C1-50	CNT 1	50	7.50	20.82	16.20
C2-5	CNT 2	5	7.14	16.60	25.68
C2-10	CNT 2	10	12.75	28.38	23.04
C2-20	CNT 2	20	8.86	21.30	20.13
C2-35	CNT 2	35	6.85	17.15	18.99
C2-50	CNT 2	50	2.06	8.27	17.23
C3-5	CNT 3	5	8.75	17.84	25.72
C3-10	CNT 3	10	9.69	20.53	23.35
C3-20	CNT 3	20	8.40	19.50	22.87
C3-35	CNT 3	35	7.11	18.91	18.07
C3-50	CNT 3	50	5.72	15.64	14.25
C4-5	PAC	5	8.64	16.09	25.45
C4-10	PAC	10	8.35	14.37	23.19
C4-20	PAC	20	8.89	21.13	21.01
C4-35	PAC	35	8.25	19.05	15.08
C4-50	PAC	50	7.01	15.45	12.11

[a] For a description of the variables *AUC1* and *AUC2*, see Section 2.4.4 of the manuscript. [b] Fluorescence intensity at $I_{225/300}$ detailed in Section 2.5 of the manuscript.

References

Needham, E. M., Sidney, S. M., Chimka, J. R. and Fairey, J. L., 2016. Trihalomethane, dihaloacetonitrile, and total N-nitrosamine precursor adsorption by carbon nanotubes: the importance of surface oxides and pore volume. Environmental Science-Water Research & Technology 2 (6), 1004-1013.

Chapter 5

Conclusion

1. Summary

Chapter 2 utilized batch application of CNTs to demonstrate their efficacy to remove precursors of TTHMs, DHANs, and TONO, thereby addressing Objective 1. Additionally, numerical modeling of adsorption of DBP precursors from multiple water types indicated that carboxyl functional groups on the CNT surfaces led to increased cumulative pore volume, which resulted in enhanced DBP precursor adsorption. These conclusions informed the experimental design of the adsorption studies in Chapter 4.

Chapter 3 addressed Objective 2 through the development of an AF4-FLD method to characterize protein-like NOM in EfOM-enriched samples from local WWTPs. QA/QC practices for TONO measurement were further developed through the use of SPE standard curves and an adjustment to account for TONO chamber degradation. The TONO precursor surrogate developed based on metrics from fluorescence EEMs and the AF4-FLD method is capable of tracking changes in TONOFP from oxidative treatment processes ($R^2 = 0.996$). Beyond this research effort, this TONO precursor surrogate is transformational for the future development of strategies to curb TONO formation.

Objective 3 was addressed in Chapter 4 in which physical and chemical CNT characteristics identified in Chapter 2 informed the selection of 12 CNT types for screening and ultimately three CNTs for use in batch adsorption studies to assess removal of TONO, TTHM, and DHAN precursors. Numerical modeling of batch adsorption data yielded information about physiochemical properties controlling DBP precursor adsorption. Primarily, specific surface area controlled the adsorption of TTHM and DHAN precursors while cumulative pore volume and surface oxygen content controlled the adsorption of TONO precursors. Batch sorption data was also used to successfully develop a TONO precursor surrogate based on metrics from AF4-FLD

and fluorescence EEMs that describe TONO precursor removal through sorption processes (R^2 = 0.576). This TONO precursor surrogate was utilized to determine that CNT mats – consisting of freeform CNT microstructures affixed to a silicon substrate – can sorb TONO precursors in continuous flow through mode, providing a proof-of-concept for this novel application.

2. Significance and Future Work

The findings from this work provide mechanistic insights into DBP precursor adsorption by CNTs, and reveal the importance of tuning surface chemistry differently for TONO as compared to TTHMs and DHANs. As CNTs have not yet been considered for use in drinking water treatment plants, this work demonstrates their potential for DBP precursor adsorption and the need for their continued development, particularly in applications in which they are affixed to substrates to minimize fate and toxicity concerns. The use of numerical modeling to understand the experimental data collected in this study highlighted physical and chemical properties of CNTs that should be modified to enhance DBP precursor adsorption. Future work should include adsorption studies with freeform CNTs, with surface chemistries specifically designed to target particular types of DBP precursors.

A novel AF4-FLD method was developed that, in combination with metrics from whole water fluorescence EEMs, can predict changes in TONO precursors from oxidative treatment processes. A similar metric was developed to assess adsorption of TONO precursors with CNTs. Future studies should be completed with an extensive suite of waters (i.e., varying DBP precursor concentrations) that have been subjected to a diverse array of treatment processes to further develop and refine TONO precursor surrogates. Insights from the development of such surrogates can also be used in future work to explore the physicochemical properties of TONO

precursors, to help optimize treatment processes and curb formation of *N*-Nitrosamines in drinking water systems.